IMPROVING LAYER-BY-LAYER ASSEMBLY FOR SUPERIOR FLAME RETARDANT AND GAS BARRIER THIN FILMS

A Dissertation

by

TYLER C GUIN

Submitted to the Office of Graduate and Professional Studies of
Texas A&M University
in partial fulfillment of the requirements for the degree of

DOCTOR OF PHILOSOPHY

Chair of Committee,	Jaime Grunlan
Committee Members,	James Batteas
	Jodie Lutkenhaus
	Perla Balbuena
Head of Department,	Nazmul Karim

December 2015

Major Subject: Chemical Engineering

ABSTRACT

Layer-by-layer (LbL) assembly is a promising technique for depositing multi-functional thin films from dilute aqueous solutions. These films have found use as environmentally-benign flame retardants, replacing halogenated flame retardants, and as flexible gas barrier thin films, replacing vacuum-deposited inorganic oxide thin films. Unfortunately, LbL assembly has drawbacks that have not been adequately addressed, such as stiffening of coated substrates and the high number of deposition steps required.

Thin films of chitosan and poly(sodium phosphate) were deposited on cotton fabric via LbL assembly to reduce flammability. The fabric was rinsed in an ultrasonication bath between deposition steps to improve the softness (i.e., hand) of the coated fabric. Ultrasonication is believed to remove weakly adhered polyelectrolyte and eliminate bridging of individual fibers, preventing the fabric from becoming stiff while improving the flame retardant behavior.

Incorporating amine salts into the cationic polyelectrolyte and its associated rinse enables LbL clay-containing films to achieve large thickness (>1 μm) with relatively few deposition steps. This technique is potentially universal, exhibiting thick growth with multiple types of nanoclay, including montmorillonite and vermiculite, a variety of amine salts (e.g., hexylamine and tris), and a host of cationic polyelectrolytes, such as poly(allylamine) and chitosan. The characteristic ordered structure found in LbL-assembled films is maintained despite the increased thickness. These films display extraordinary gas barrier and flame resistance with fewer than 8 deposition cycles.

DEDICATION

To Tara and my parents, who offered me unconditional love, support, advice, and encouragement throughout my graduate studies.

ACKNOWLEDGEMENTS

First and foremost, I would like to thank Dr. Jaime Grunlan, who made all of this research possible through his guidance, financial support, and encouragement. I want to thank him for teaching me what it takes to be a scientist. I would like to thank my committee members, Dr. James Batteas, Dr. Jodie Lutkenhaus, and Dr. Perla Balbuena for all of their advice and insight.

I would like to thank the group members of the Polymer Nanocomposites Lab for all the great discussions, advice, and ideas over the years. This work would not have been possible without the amazing contributions of my undergraduate assistants, Michelle Krecker, Aaron Milhorn, and John D'Angelo. I would also like to acknowledge the former and present students and post-doctoral workers of the Polymer Nanocomposites Lab, Dr. Morgan Priolo, Dr. Galina Laufer, Dr. Bart Stevens, Dr. David Hagen, Dr. Amanda Cain, Dr. Fangming Xiang, Dr. Ping Tzeng, Kevin Holder, Merid Haile, Dr. Marcus Leistner, Dr. Chungyeon Cho, Ryan Smith, and Yixuan Song.

Finally, I would like to thank my parents for their incredible support and advice. My deepest gratitude goes to my wife, Tara, who always believed in me, for her unconditional love.

NOMENCLATURE

AFM	Atomic force microscope
ASTM	American Society for Testing and Materials
BL	Bilayer
CH	Chitosan
DI	Deionized
DMSO	Dimethyl sulfoxide
FR	Flame retardant
GO	Graphene oxide
HRR	Heat release rate
KES	Kawabata Evaluation System
LbL	Layer-by-layer
LG	Laevoglucosan
MCC	Microcombustion calorimetry
Mel	Synthetic eumelanin
MMT	Montmorillonite clay
NCHS	U.S. National Center for Health Statistics
OSHA	Occupational Safety and Health Administration
OTR	Oxygen transmission rate
PAA	Poly(acrylic acid)
PAH	Poly(allylamine hydrochloride)

PDDA	Poly(diallyldimethylammonium chloride)
PEDOT	Poly(3,4-ethylenedioxythiophene)
PEI	Polyethylenimine
PET	Poly(ethylene terephthalate)
PP	Polypropylene
PS	Polystyrene
PSP	Poly(sodium phosphate)
PSS	Poly(styrene sulfonate)
PU	Polyurethane
PVAm	Poly(vinylamine)
QCM	Quartz Crystal microbalance
rGO	Reduced graphene oxide
RH	Relative humidity
SEM	Scanning electron microscopy
TEM	Transmission electron microscopy
TGA	Thermogravimetric analysis
tris	Trizma base
VFT	Vertical flame test
VMT	Vermiculite clay
XPS	X-ray photoelectronic spectroscopy

TABLE OF CONTENTS

Page

LIST OF FIGURES

LIST OF TABLES

1. INTRODUCTION

1.1 Background

Layer-by-layer (LbL) assembly is a promising technique for depositing multi-functional thin films from dilute aqueous solutions.[1] LbL assembly is a simple technique in which a charged substrate (e.g., glass,[2] silicon,[3] cotton[4]) is alternately exposed to solutions containing oppositely charged polyelectrolytes, inducing the polyelectrolytes to deposit as alternating thin layers, a pair of which is referred to as a bilayer (BL).[1, 5] A schematic of the LbL deposition process is shown in Figure 1.1. This is a quickly expanding field with an exponentially growing body of literature.[6] LbL assembly has been successfully used to fabricate thin films under ambient conditions with flame retardant,[7] gas barrier,[8] gas separation,[9] anti-microbial,[10] UV-protective,[11] anti-reflective,[12] super hydrophilic,[13] and a multitude of other behaviors.[5]

LbL-assembled thin films are an exciting frontier of research due to their incredible properties and ease of fabrication.[1] For example, multilayer films composed of reduced graphene oxide (rGO) and polyaniline have the largest capacitive energy storage of any organic material.[14] LbL thin films composed of vermiculite nanoclay (VMT), polyethyleneimine (PEI), and polyacrylic acid (PAA) have oxygen permeability orders of magnitude lower than vacuum-deposited SiO_x and yet remain transparent and flexible.[15] The simplicity of fabrication has encouraged the development of industrially viable methods of producing these films. Running the substrate through subsequent baths of polyelectrolyte solutions[16] or spraying a moving substrate with alternating

solutions[17] are both simple methods to apply these coatings in a scalable, steady-state process.

Unfortunately, LbL assembly has found only limited commercial use, primarily due to the large number of processing steps required.[18] For example, flame retardant (FR) LbL films for cotton fabric can take over 80 processing steps to pass industry-standard FR requirements.[19] More than 80 processing steps are needed to produce super-hydrophilic surfaces for anti-fogging applications.[13] This is in contrast to current commercial processes, such as Proban, which require only 5 processing steps for adequate flame retardance,[20] or Lexan Anti-Fogging thin films which require only two processing steps.[21] LbL thin films have only found practical use in applications where a relatively small number of deposition steps will suffice, such as for hydrophobic coatings,[22] or where there is no current commercial alternative, such as flexible anti-reflection films for flat panel mobile displays.[23]

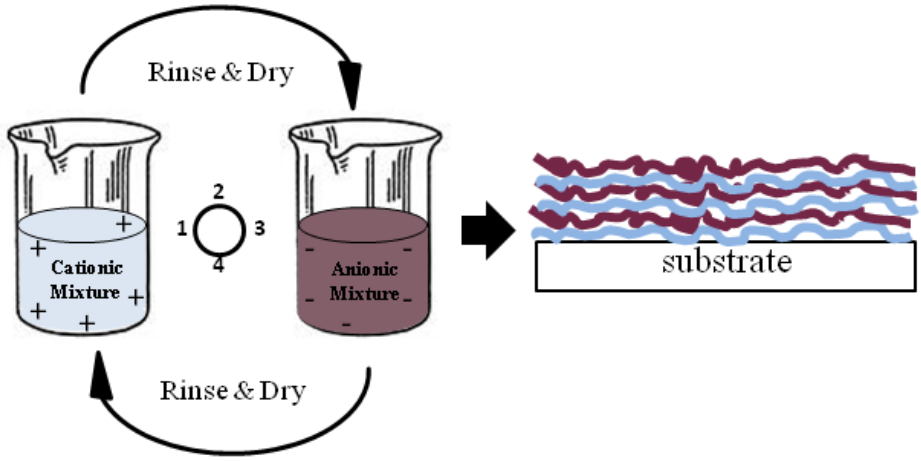

Figure 1.1. Layer-by-layer deposition process used to prepare functional thin films from aqueous mixtures. Steps 1 – 4 are repeated until the desired number of cationic/anionic bilayers are deposited on a substrate.

1.2 Objectives and Dissertation Outline

The purpose of this research is to explore the multifunctional nature of polyelectrolyte multilayer assemblies, specifically oxygen barrier and flame retardant assemblies, and to optimize their deposition. This research is important for food packaging,[24] flexible electronics,[25] and textiles,[26] which are in need of gas impermeable and/or antiflammable thin films. This work presents proof-of-concept for multilayer films that render polyethylene terephthalate thick films impermeable to oxygen, polystyrene plates flame resistant, and cotton fabric self-extinguishing in a more efficient manner than earlier multilayer assemblies and competing technologies.

Section 2 presents a review of layer-by-layer assembly, gas barrier in polymers and nanocomposites, and flammability of cellulosic materials. Layer-by-layer assembly is a processing technique that deposits multifunctional thin films from dilute aqueous

solutions and is the focus of every study in this dissertation. A brief synopsis and some background theories describing how gas molecules permeate polymers and nanocomposites are presented. Cellulose is a highly flammable, ubiquitous material, and the mechanism of its flammability is presented along with its interactions with phosphate-containing flame retardants.

Section 3 describes a novel technique to create softer, more effective flame retardant cotton fabric using layer-by-layer assembly. In this study, the fabric is rinsed with ultrasonication between polyelectrolyte deposition steps, preventing bridging of the fabric fibers. Flammability of the coated and uncoated fabric was analyzed using vertical flame testing, thermogravimetric analysis (TGA), and microcombustion calorimetry. The softness, or hand, of the fabric was determined using the Kawabata Evaluation System. Rinsing with ultrasonication increased contact between the flame retardant film and fabric, reducing the amount of flame retardant required for the fabric to pass a vertical flame test (VFT) by nearly 50%. The reduction in aggregations and bridging greatly improved the hand of the fabric, improving or maintaining it in every measured way.

Section 4 describes how tris buffer greatly increases the thickness of layer-by-layer assembly clay nanocomposite films. The increase in thickness is far greater than what would be expected from an increase in solution ionic strength. These “super thick” thin films are able to achieve extreme oxygen impermeability with very few bilayers, and contain a very high concentration of clay compared to traditional clay nanocomposites. The films were analyzed with transmission electron microscopy (TEM), TGA, profilometry, and quartz crystal microbalance (QCM). It was shown that

the characteristic order found in layer-by-layer assembled films was maintained despite the increased thickness.

Section 5 explores the “super thick” layer-by-layer phenomenon in depth, and applies the principles to flame resistance. The thickening mechanism occurred with a number of amine-containing salts aside from tris, such a hexylamine, and the phenomenon applied to both strong and weak cationic polyelectrolytes, demonstrating its applicability to a wide range of known systems. The increase in thickness was dependent on the type of nanoclay deposited and the concentration of the amine salt. It was found that films containing both montmorillonite and vermiculite nanoclay were able to achieve incredible thickness and still maintain excellent clay ordering. Polystyrene plates coated with “super thick” films were able to become self-extinguishing in a flame-through test with very few bilayers. The films themselves were analyzed using TEM, X-ray photoelectron spectroscopy (XPS), TGA, profilometry and QCM.

Section 6 looks at the overall impact of this work and possible future directions. To further improve the layer-by-layer technique, large-scale machines capable of coating complex 3-dimensional substrates will need to be devised. A method to detect flaws in these films would also improve the commercial viability of the layer-by-layer technique, allowing for quick detection and correction of ultra-high gas barrier films. Finally, incorporating amine salts in graphene oxide-based films would allow for free-standing layer-by-layer based composites to be produced on an industrial scale.

2. LITERATURE REVIEW

2.1 Layer-by-Layer Assembly

2.1.1 Layer-by-Layer Assembly History

In 1966, Iler at DuPont de Nemours & Co. discovered that that colloidal silica and alumina fibrils could be alternately adsorbed on an anionic black glass surface, creating thin films which were electrostatically adsorbed.[27] The deposited layers were not easily rinsed off with water in between depositions, and the process could be repeated as many times as desired. Each deposition increased the thickness of the resultant film by a proportional amount, which led Iler to believe that a layer of either silica or alumina was being deposited with each dip. Iler explored a variety of other particles, such as boehmite, polystyrene micelles, and albumin and was able to fabricate films nearly 1 mm thick by increasing the particle size.[27]

This technique received little attention until 1992, when Decher reintroduced the subject by incorporating polymer polyelectrolytes.[2] He found that by using polyelectrolyte polymers with alternate charges, he could mimic the charge reversal displayed by Iler's colloidal silica and alumina fibril system and deposit thin, durable polymer films from water. Each deposition of a cationic and anionic polyelectrolyte was called a "bilayer" (BL). The process is shown in Figure 2.1. This technique was found to work with a variety of cationic and anion polyelectrolytes, including polystyrenesulfonate sodium salt (PSS) and poly(allylamine hydrochloride) (PAH). As the thickness and light absorbance of the deposited film was directly proportional to the

number of depositions, Decher hypothesized that the film was being assembled “layer by layer” (LbL). Decher also found that the surface charge of the film reversed with each deposition into the alternately charged solutions, indicating that the film surface was composed primarily of the last deposited species.[2] Since then, LbL assembly has been used to deposit films for an incredible variety of purposes, including but not limited to flame retardance,[7] gas barrier,[8] gas separation,[9] anti-microbial,[10] UV-protective,[11] anti-reflective,[12] super hydrophilicity,[13] color,[28] controllable drug release,[29] hydrophobicity,[30] anti-static,[16] catalsysis,[31] among many others.[1]

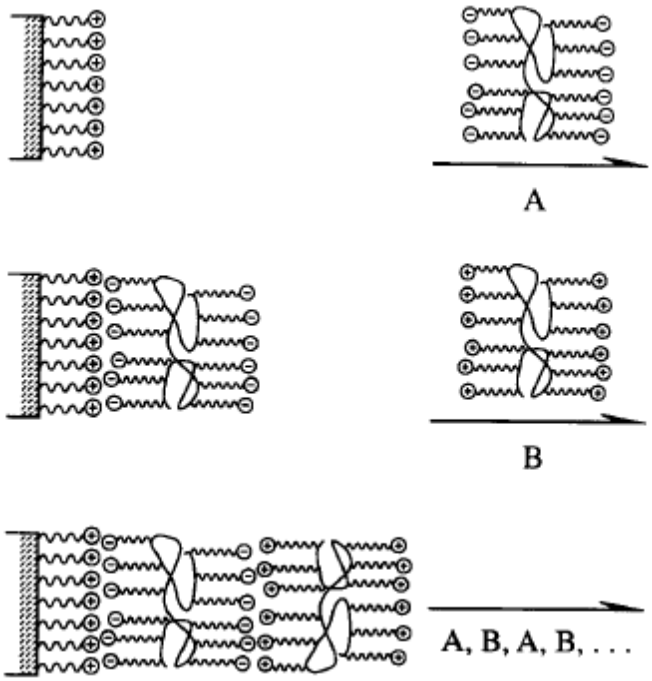

Figure 2.1. Schematic for the buildup of multilayer assemblies by consecutive adsorption of anionic and cationic polyelectrolytes. Reprinted with permission from Elsevier.[2]

2.1.2 Layer-by-Layer Assembly Fundamentals

The dominant method of depositing LbL films has been through electrostatic self-assembly.[18] The negatively charged functional groups of the anionic polyelectrolyte attract the positively charged groups of the cationic polyelectrolyte, resulting in a very strong pseudo-ionic bond and a surface charge reversal.[32] The properties of electrostatic self-assembled films are dependent on a number of solution parameters,[32] including pH,[33] ionic strength,[34] and temperature,[35] and also on the deposition time,[36] humidity,[37] and drying.[38] The pH of the solutions has a dramatic effect on the properties of the resultant films, as shown in Figure 2.2, due to the polyacid or polybase interactions with solution pH.[18, 39] Weak polyelectrolytes change their charge and conformation characteristics in response to pH changes, oftentimes reconfiguring from coiled to uncoiled and vice-versa.[39] At low pH values, polyacids become more coiled as their charge density is reduced due to the increased protonation. During LbL deposition, when a polybase surface is immersed into a polyacid solution at low pH, more polyacid will be deposited than if the polyacid solution was at a higher pH, due to the lower charge density of the polyacid.[18] Ionic strength performs a similar role to pH, effectively screening electrostatic charges and increasing the amount of each polyelectrolyte deposited.[40] The increase in film thickness is proportional to ionic strength as I^a, where I is the ionic strength and a ranges from 0.5 to 1.[40] However, due to the more coiled nature of the polymer, the roughness of the resultant film is increased as well.[18, 34] Increased temperature of the solutions will also increase the thickness of the assembled films, as increased temperature encourages diffusion of the polyelectrolytes into the film.[35]

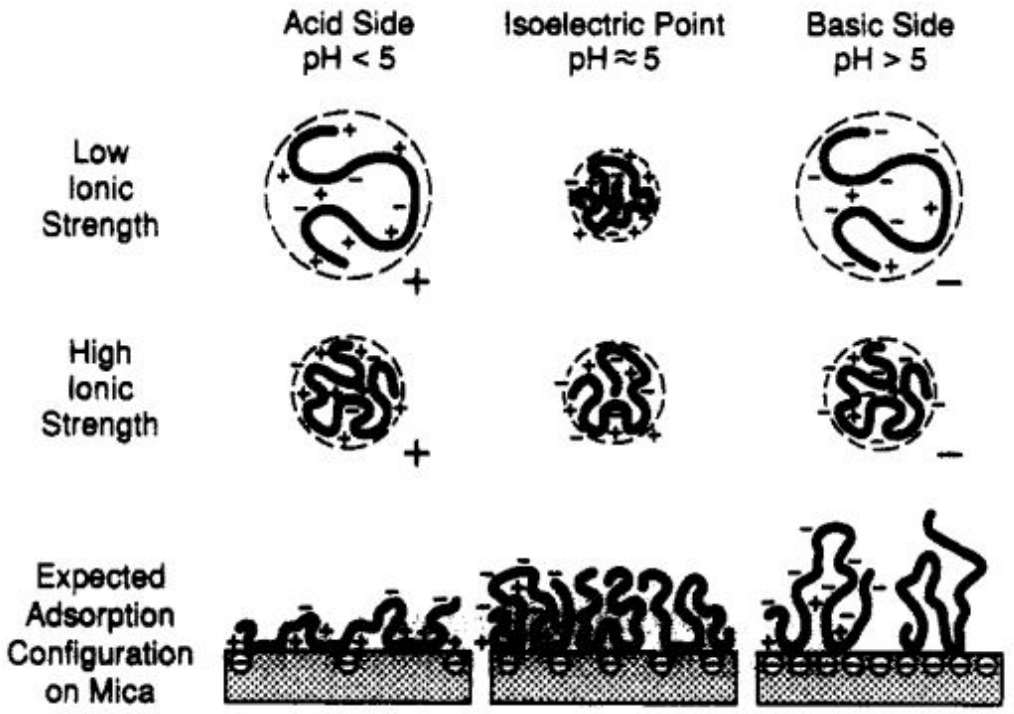

Figure 2.2. Proposed coil configurations of amphoteric polyelectrolyte and its adsorption on a charged substrate as a function of pH and ionic strength. Reprinted with permission from the American Chemical Society.[39]

Since 1992, numerous other methods of depositing films in a layer-by-layer fashion have emerged, many of which are shown in Figure 2.3. These alternative LbL assembly methods include hydrogen[41] and covalent bonding,[42] as well as charge-transfer,[43] coordination,[44] and biological interactions.[18] Film deposition via hydrogen bonding utilizes proton donor/accepting pairs rather than electrostatic pairs. For example, a fully protonated polyacid, such as poly(acrylic acid) at low pH, acts as a hydrogen bond donor, while a macromolecule with many lone electron pairs, such as poly(ethylene oxide), can act as a hydrogen bond acceptor.[45] These films have lower

moduli, lower thermal stability, and higher sensitivity to pH than electrostatically assembled films,[6, 18, 45-46] which make them ideal for applications such as stretchable gas barriers[45] and biomedical capsules.[47] It should be noted that films deposited using traditional electrostatic interactions oftentimes display hydrogen bonding as well.[1] Covalent LbL assembly utilizes self-limiting surface reactions to deposit a single monolayer with each deposition,[42] oftentimes through "click chemistry."[48] These films are remarkably durable,[1] as the covalent linkages are nominally irreversible,[48] and can withstand extreme ranges of pH[42] and temperature.[48] Covalent-bonded LbL films show promise for organic semiconduction,[42] biosensing,[49] and catalysis.[42] Unfortunately, one of the primary advantages of LbL assembly is the ambient, aqueous processing conditions, which are unfavorable to most covalent LbL assembly to date.[18]

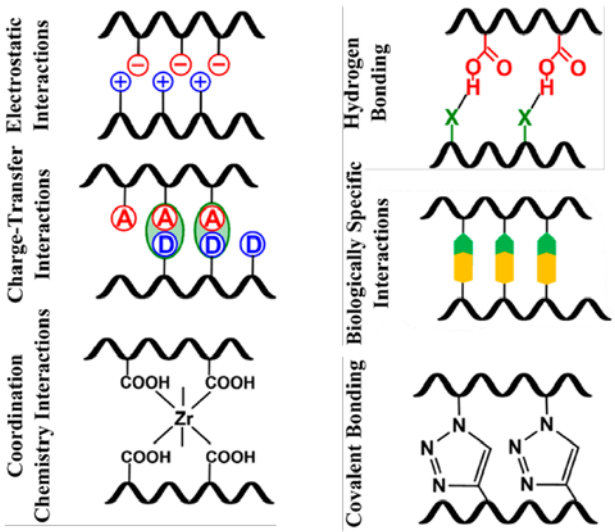

Figure 2.3. Commonly studied interactions for producing layer-by-layer films. Reprinted with permission from the American Chemical Society.[18]

2.1.3 Improving Layer-by-Layer Assembly

Layer by layer assembly benefits from its ability to be effectively processed in ambient aqueous conditions with very dilute solutions, but suffers from a number of disadvantages that have limited its commercial significance. LbL films often require a large number of processing steps,[1, 3, 5, 18] are vulnerable to a variety of chemical attacks,[6, 13] and require expensive specialty polyelectrolytes.[50] In order to achieve useful properties, such as high gas barrier, LbL films can require over 16 deposition steps with rinsing and drying in between each one (64 processing steps),[15] as opposed to commercial SiO_x films which require a single deposition step.[51] While covalent crosslinking has shown promise to reduce the vulnerability of LbL films to chemical attacks,[52] most LbL films can be removed through extreme ionic strength, shown in Figure 2.4, surfactants, or strong bases.[18] These attacks inhibit electrostatic interactions through charge screening or neutralization, dissolving the film completely.[32, 52] While some work has been done to utilize inexpensive polyelectrolytes, such as chitosan (CH),[53] most LbL films in literature are composed of specialty polyelectrolytes such as poly(diallyldimethylammonium chloride) (PDDA),[12] polethyleneimine (PEI),[25] and poly(allylamine hydrochloride) (PAH).[54]

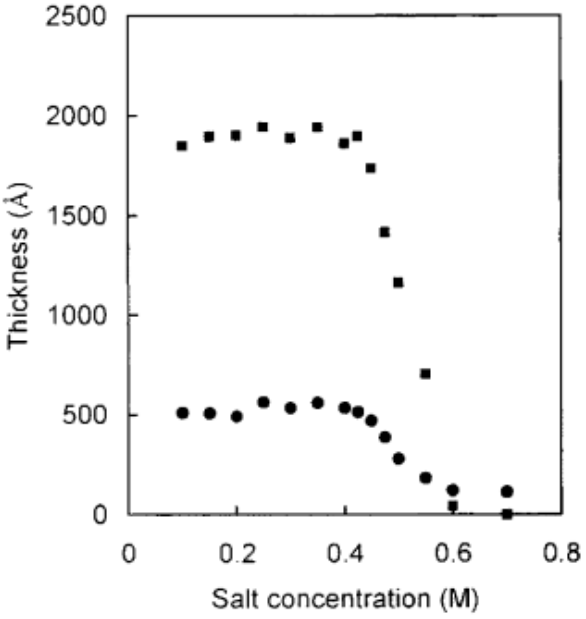

Figure 2.4. Film thickness as a function of NaCl concentration of a 10 bilayer PDDA/PAA film. Squares represent higher molecular weight PAA, circles represent lower molecular weight PAA. At high ionic strength, the polyelectrolyte charges are completely screened, and the film is removed. Reprinted with permission from the American Chemical Society.[32]

Since Decher's seminal work in 1992, the number of deposition steps to achieve useful LbL films has been gradually declining. The first LbL clay-based oxygen barrier films, reported by Jang, et. al. in 2008, required over 60 depositions to achieve an oxygen barrier below the detection limit of commercial equipment (<0.005 $cc/m^2 \cdot day \cdot atm$).[55] However, by 2010, Priolo et. al. showed that by using a quadlayer approach (four polyelectrolytes in series) with nanoclay, an undetectable oxygen transmission could be achieved with only 16 depositions, shown in Figure 2.5.[15] The increase in gas barrier was due to the increased thickness of the polymer film between

clay stacks due to the interdiffusing components of the quadlayer.[56] The interdiffused polyelectrolytes composed a highly electrostatically crosslinked "tortuous path," which increased the effective path length of permeating gas molecules.[57]

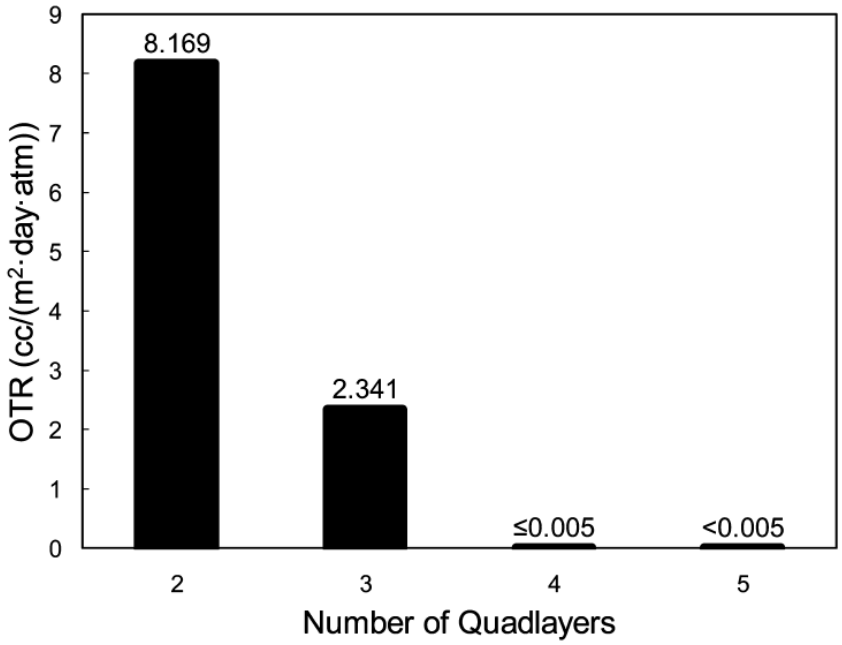

Figure 2.5. Oxygen transmission rate (OTR) of a PEI/PAA/PEI/MMT quadlayer LbL film as a function of bilayers. Reprinted with permission from the American Chemical Society.[15]

In 2014, Hagen et. al. showed that some LbL films deposit very quickly with shorter deposition times in the first few bilayers, but that with increasing bilayers the films deposit more thickly with longer deposition times.[58] This phenomenon was exploited to create thicker and more impermeable gas barrier films with fewer and shorter depositions. This technique is referred to as "shift-time deposition," and is shown in Figure 2.6. This marked a huge reduction in the necessary fabrication time for gas

barrier LbL films, reducing it by 73% to achieve undetectable oxygen transmission.[58] Simultaneously, in 2015, Cui et. al. found that complimentary polyelectrolyte complexes could be deposited with one deposition, creating very thick films with few bilayers.[59] These films displayed excellent electrochromic properties with only 30 bilayers, while similar films grown with the individual components as separate layers displayed only half the electrochromic potential at 30 bilayers. While these films displayed a higher porosity than normal LbL films, this porosity actually increased the effective surface area of the films, increasing the electrical potential.[59] In 2013, Apaydin et. al. discovered a method to create super-thick clay-based LbL films that achieved a thickness of over 5 μm with only 20 bilayers.[54] The researchers used these films to render polyamide-6 char-forming, as the clay-filled film was able to suffocate fire. Polyamide-6 is extremely difficult to flame retard due to its melt-dripping and complicated pyrolysis behavior, but the extreme thickness of these films allowed for such a difficult substrate to be rendered flame retardant. Unfortunately, these researchers did not postulate a reason or mechanism for the thick-growing polymer-clay LbL film.[54]

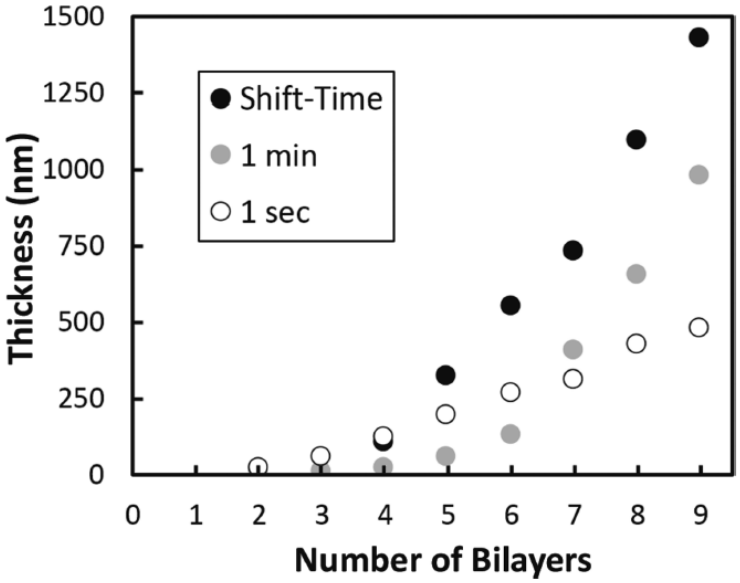

Figure 2.6. "Shift-time" LbL deposition compared to 1 min and 1 sec depositions. By increasing the deposition time from 1 sec to 1 min after 3 bilayers, a thicker film can be deposited with fewer bilayers in a shorter total amount of time. Reprinted with permission from the American Chemical Society.[58]

2.2 Gas Barrier of Films

2.2.1 Gas Diffusion Fundamentals

Gas barrier materials are used for a myriad of applications, such food packaging, liquid crystal displays, and vacuum insulation. Traditionally, glass and metal have been employed for gas barrier applications due to their impermeability, but these materials are relatively heavy and expensive compared to polymers.[60] Polymeric materials have been developed which display extremely low permeabilities, but none have been developed which can be used for ultra-high barrier applications, such as organic light emitting diode (OLED) protection.[61] Polymeric films which are capable of replacing ceramic and

metal barriers would allow for gas sensitive products to protected with lower cost and lower weight, and can potentially reduce their carbon footprint due to lessened transportation requirements.

Permeation through a dense polymer membrane occurs in five stages, as shown in Figure 2.7. Gasses must diffuse through the upstream film boundary layer (1), adsorb to the surface of the film (2), diffuse through the membrane (3), desorb into the downstream side (4), and then diffuse through the downstream boundary layer (5).[62]

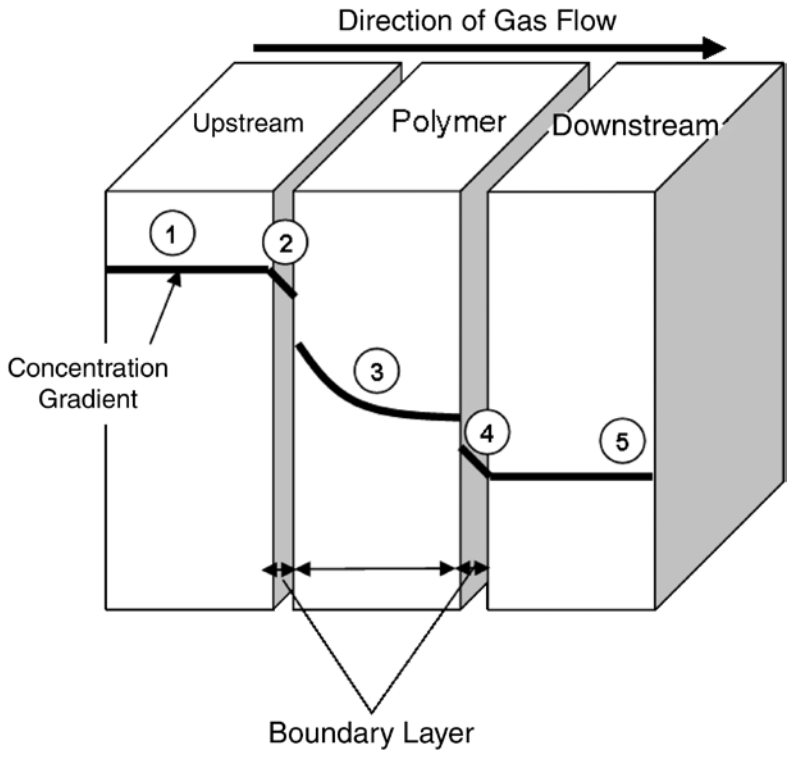

Figure 2.7. Schematic presentation of gas permeation steps across polymer membranes according to the solution-diffusion mechanism. Reprinted with permission from Wiley-VCH.[62]

In most polymer films, the dominate term (the slowest rate) is typically step 3, which is diffusion through the polymer membrane.[62] Fick in 1855 is credited with deriving the first model for diffusion, famously through Fick's first law, Equation 2.1.[63]

$$J = -\frac{DC}{RT}\Delta(\mu) \tag{2.1}$$

where J is the diffusion flux, D is the diffusivity, C is the concentration of the permeant, R is the ideal gas constant, T is temperature, and μ is the chemical potential of the permeant. In a one-dimensional, planar system at steady state, Fick's first law simplifies to

$$J = -\frac{DC}{RT}\frac{d\mu}{dx} \tag{2.2}$$

This simple result signifies that the permeation of a gas through a material is directly proportional to the diffusivity coefficient, D and the concentration differential of the permeant. If the permeant is an ideal solution at constant temperature,[64] then the equation can be simplified further to

$$J = -D\frac{dC}{dx} \tag{2.3}$$

Taking the integral of Equation 2.3 at steady state, knowing the thickness of the membrane, L, and the concentration on both sides of the membrane, C_f and C_o, the diffusivity constant can be found.

$$D = \frac{JL}{C_o - C_f} \tag{2.4}$$

Determining the concentration at the surfaces of the membrane is very difficult,[65-66] and it is more common to monitor the concentration of the permeate in the gas phase on both sides of the membrane.[66-67] The concentration at the surface of the membrane can be determined from

$$C_i = Sp_i \tag{2.5}$$

where S is the sorption equilibrium constant and p is the partial pressure of the gas.[64] This leads to Equations 2.6, which combined the sorption equilibrium constant and the diffusivity constant as a permeability constant, P, and Equation 2.7 which is the permeability equation for a one-dimensional planar system.

$$P = DS \tag{2.6}$$

$$P = \frac{JL}{p_o - p_f} \tag{2.7}$$

This modified form of Fick's first law allows for experimental determination of a film's permeability, but it does not provide any fundamental reason for why some materials are more diffusive than others. In 1861, Graham explored the various diffusivity parameters of polymer membranes and found that most polymers were diffusive, following Graham's law of diffusion:[68-69]

$$J \propto M^{-1/2} \tag{2.8}$$

where M is the molecular weight of the permeating gas. Graham's law is followed for any polymer in which the mean free path of the gas molecules is smaller than the pores of the material.[64, 70] When this is the case, the permeation of the gas is dominated by

Knudsen diffusion.[71-72] However, when the membrane pore size is less than mean free path of the diffusing gas (~10 nm, typically), gasses permeate via molecular sieving, which is a combination of surface diffusion and solution diffusion.[73-74] As dense polymer membranes (pore size < 10 nm) have lower diffusion rates than more porous membranes, the majority of ultra-high gas barrier polymer films are dense membranes.[72, 74-76] In dense polymer films, the diffusivity term can be defined by the free volume theory:[64]

$$D = A\exp\left(-\frac{B}{F}\right) \tag{2.9}$$

where *A* and *B* are constants of the system and F represents the fractional free volume, which is defined by

$$F = \frac{V_{total} - V_{occupied}}{V_{total}} \tag{2.10}$$

where V_{total} is the total volume of the polymer and $V_{occupied}$ is the volume occupied by the polymer chains themselves. As the free volume of the system increases, gasses are more able to permeate the membrane.[64, 76] Therefore, increasing the density will decrease the diffusivity of the system.

The sorption characteristic of the systems, *S*, affects permeability as well. Sorption is a thermodynamic quantity related to the liquid-vapor properties of the gas (boiling point, enthalpy of vaporization, vapor pressure, etc.) and the interactions between the gas and the polymer film.[75] Sorption is primarily defined by the Gibb's free energy of the sorption given by Equations 2.11-2.14.[75]

$$S = \exp\left(-\frac{\Delta G}{RT}\right) \tag{2.11}$$

$$\Delta G = \Delta H - T\Delta S \tag{2.12}$$

$$S = \exp\left(\frac{\Delta S}{R}\right)\exp\left(-\frac{\Delta H}{RT}\right) \tag{2.13}$$

$$\ln(S) = \frac{\Delta S}{R} - \frac{\Delta H}{RT} \tag{2.14}$$

where ΔG is the Gibb's free energy, ΔH is the enthalpy, and ΔS is the entropy of sorption. The enthalpic term is a function of temperature, and follows a logarithmic correlation with permeability, as shown in Figure 2.8.[77] In most situations, the enthalpic term is the dominant term, as the migrating gas has enough thermal energy to move through vacant sites (free volume) in the polymeric material.[77-79] However, at very high temperature or in separation membranes when both gasses have similar ΔH terms, the entropic term can become dominant. In order to minimize the permeability of a polymer film, the diffusion and sorption terms should be minimized.[75, 80] Commonly, the diffusion term is dominant, and the overall permeability can be decreased by decreasing the free volume (i.e., increasing the density) of the polymer.[77, 80-82] By incorporating a dense filler, the overall free volume of the polymeric system can be decreased.[83-84]

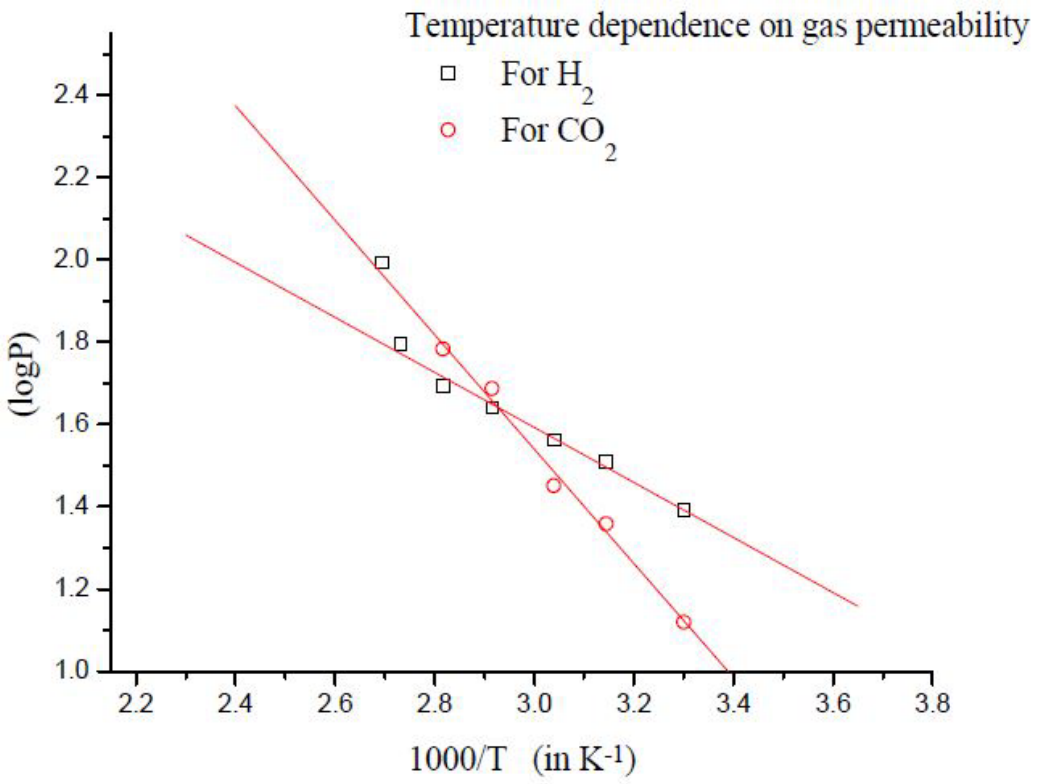

Figure 2.8. Log hydrogen and carbon dioxide permeability as a function of inverse temperature for a polycarbonate film. The fitted curve models Equation 2.14 when sorption is dominant. Reprinted with permission from CS&IR.[77]

2.2.2 Gas Diffusion in Nanocomposites

Nanocomposites are a novel class of polymeric materials containing a particulate filler with a characteristic length less than 100 nm.[85-87] These materials can be composed of elastomers,[86] thermoplastics,[88] or thermosets[89] along with a wide variety of nanoscale organic or inorganic platelets,[85, 90] rods,[91-92] or spheres.[93] Nanocomposites show a wide array of beneficial properties over their base polymer component, including enhanced modulus,[94-95] thermal stability,[90, 96] electrical conductivity,[97] and gas barrier.[98-99] Clay-

based nanocomposites have already found commercial use in gas barrier thin films as food packaging[100] or in the automotive industry as sealant layers.[101] Nanocomposites rely on the relatively large combined surface area of the nanoparticles, which creates a very high amount of interfaces between the polymer and the nanoparticle, as shown in Figure 2.9.[98, 102] By incorporating impermeable nanoparticles, such as clay platelets, the diffusion of a film is greatly reduced, as the free volume is reduced and the path length of the diffusing gas molecule is increased.[94, 100, 103] This is due to the "tortuous path" phenomenon, which predicts that a diffusing gas molecule will have to diffuse through the polymer matrix perpendicular to the normal direction of the film in order to find areas between the impermeable nanoparticles which it can diffuse through.[57, 104]

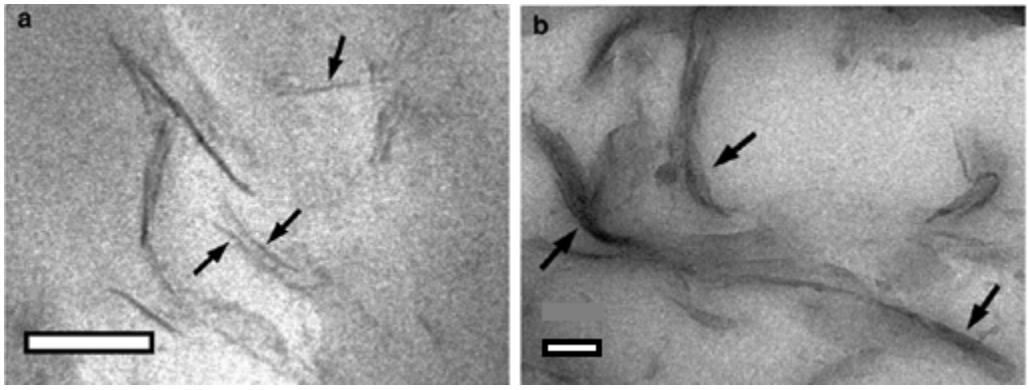

Figure 2.9. TEM images of poly(3-hydroxybutyrate) nanocomposite with a) 1 wt% and b) 5 wt% montmorillonite (MMT).The scale bar is 100 nm. Reprinted with permission from Wiley-VCH.[94]

Gas diffusion through nanocomposites can also be viewed as a sorption-diffusion process.[69] Assuming no interaction between the nanoparticle and the permeate, the

sorption of the composite can be simply expressed in terms of the volume fraction of the polymer matrix.[105]

$$S = S_o(1 - \varphi) \tag{2.15}$$

where S_o is the sorption of the polymer and φ is the volume fraction of the filler. Simply put, the total sorption of the system is just the sorption of the polymer in the system. By increasing the amount of filler, the sorption is proportionally decreased. The diffusivity of the system, however, is highly dependent on the properties of nanoparticle filler.[105] [106]As the permeating gas cannot diffuse through the nanoparticle, it must take a longer, tortuous, path around it.[100, 106] The tortuous path of a flake-filled polymer composite was first described by Nielson in 1967,[107] which predicted the permeability as shown in Equation 2.16 (Figure 2.10).

$$\frac{P}{P_o} = \frac{1-\varphi}{1+\frac{\Phi\alpha}{2}} \tag{2.16}$$

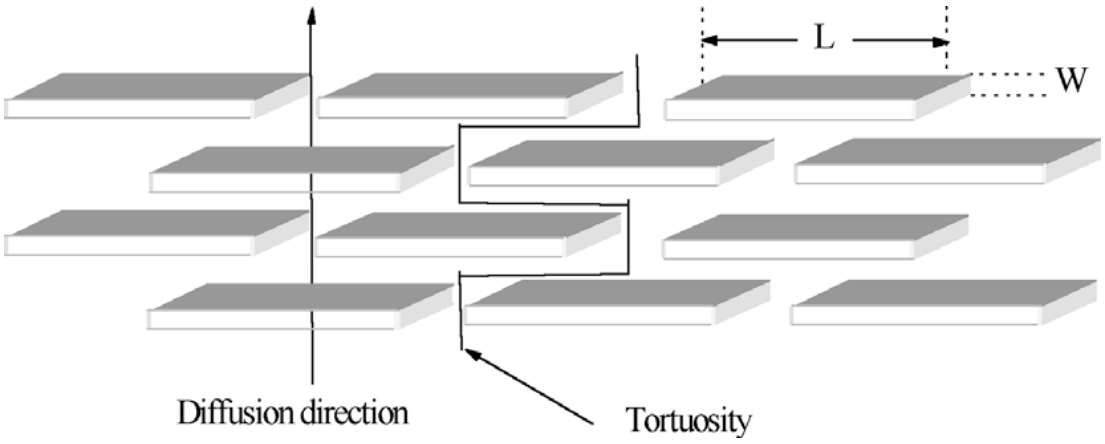

Figure 2.10. Schematic for the Nielson model of gas diffusion through a polymer/platelet composite. Reprinted with permission from Taylor and Francis.[107]

where P_o is the permeability of the polymer and α is the aspect ratio of the filler. In 1988, Cussler proposed a model which refined the Nielson model, allowing for various filler shapes to be accounted for.[57]

$$\frac{P}{P_o} = \left(1 + \frac{\alpha\varphi}{\sigma} + \frac{\alpha^2\varphi^2}{1-\varphi}\right)^{-1} \tag{2.17}$$

where σ is the regular array spacing. In 2004, Cussler's model was modified to account for irregularly-spaced arrays of 2-dimensional platelets which are parallel to the surface,[108] shown in Equation 2.18.[109] From this equation, it is apparent that nanoplatelet-based layer-by-layer assembled composites, which display high degrees of orientation and filler contents will have extremely low permeability.[108-109]

$$\frac{P}{P_o} = \left(\frac{\left(1 + \frac{2}{3}\alpha\varphi^2\right)}{1-\varphi}\right)^{-1} \tag{2.18}$$

2.2.3 Layer-by-Layer Gas Barrier

Utilizing the advancements in nanocomposite barrier technology, layer-by-layer assembly has achieved incredibly impermeable polymer nanocomposite films.[104] The first LbL nanoclay-based gas barrier film was demonstrated by Avery Dennison in 2004,[110] and was composed of polyacrylamine and montmorillonite clay (MMT). This technology was inspired by the original polymer-based gas barrier LbL film first demonstrated by Levälsmi et. al. in 1996.[111] Since 2003, a myriad of gas barrier nanocomposite LbL films have been explored by researchers which were able to prevent the permeation of oxygen,[53, 112] carbon dioxide,[9] helium,[113] and even hydrogen.[113] In 2010, Priolo et. al. were able to achieve an undetectable oxygen barrier with just 4 quadlayers by increasing the spacing between clay layers, increasing the tortuous path.[15] By 2014, Stevens et. al. were able to achieve an equivalent oxygen barrier using reduced graphene oxide (rGO) platelets with 20 bilayers, demonstrating the first flexible, conductive, ultra-high gas barrier LbL thin film.[114] In 2012, Laufer et. al. were able to demonstrate an impressive oxygen barrier using chitosan (CH) and MMT,[53] showing the broad applicability of this technology for environmentally-friendly and inexpensive materials.[24]

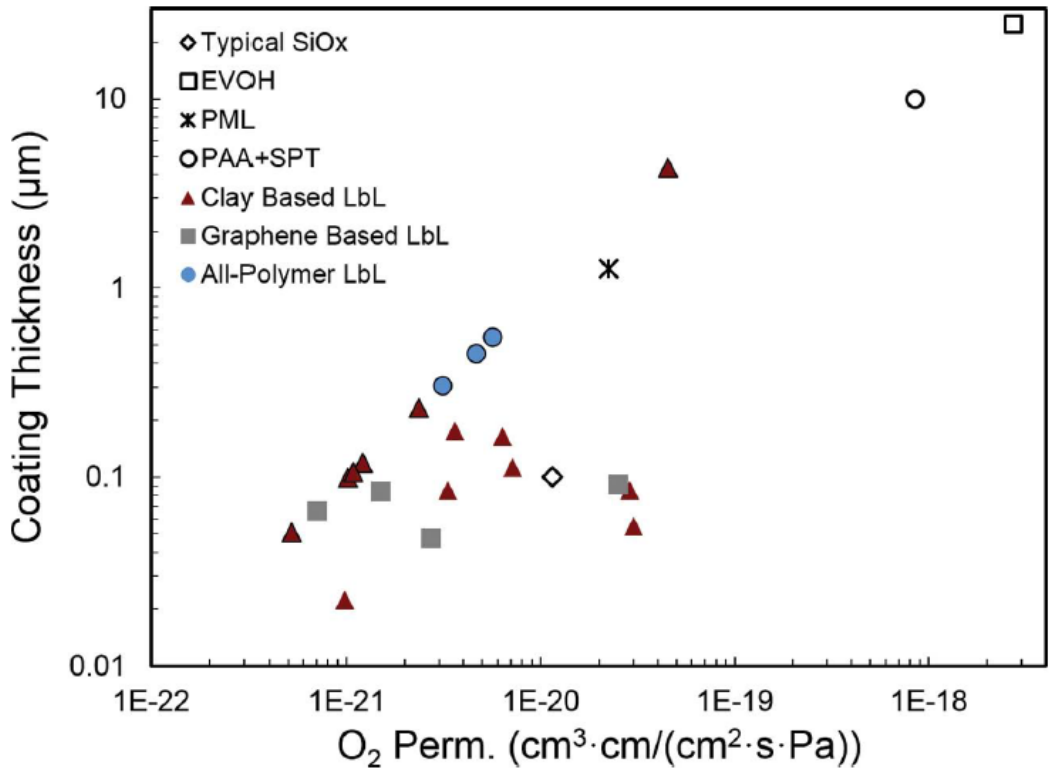

Figure 2.11. Coating thickness as a function of oxygen permeability. LbL data points with an outline, as well as PML, represent a permeability value calculated from an OTR below the detection limit of the measurement used. Reprinted with permission from the American Chemical Society.[104]

The extreme impermeability of these films, demonstrated in Figure 2.11, is tied to the well-ordered polymer and nanoplatelet layers.[56] These layers also have well-defined thicknesses, making them ideal for gas selective membranes.[56, 104] In 1996, Stroeve et. al. showed that a LbL film of PAH and PSS was able to separate nitrogen and carbon dioxide with a separation factor of 23.8.[115] Yang et. al. created multilayer nanocomposite thin films in 2013 from PEI and graphene oxide (GO) which were able to separate hydrogen from carbon dioxide with a separation factor of 383.[9] In 2014, Kim et.

al. were able to separate nitrogen and hydrogen using a film of PEI and poly(acrylic acid) (PAA) that broke the upper bound of the Robeson plot (Figure 2.12), a commonly used plot which shows maximum separation capacity.[116] The extreme tunability of LbL films makes them an exciting frontier in gas separations work, allowing for size-selecting sieving to be constructed easily and repeatedly.[116-117]

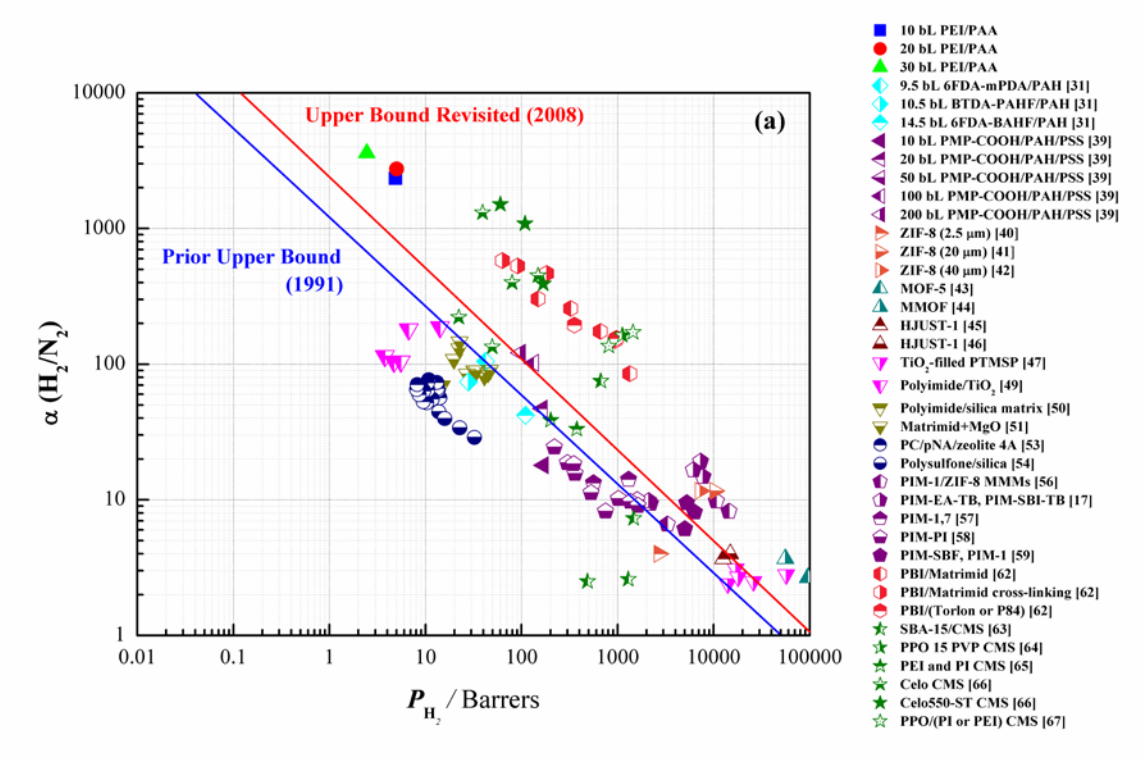

Figure 2.12. Robeson's upper bound plots of H2/N2 separation systems with 10, 20, and 30 bilayer PEI/PAA polymer films and various other polymer and inorganic (or mixed matrix) membranes. Reprinted with permission from Wiley-VCH.[116]

2.3 Flame Retardance

2.3.1 Combustion Fundamentals

Fire is the exothermic process by which materials exothermically decompose and oxidize in a positive feedback loop.[118] A material first degrades, then decomposes into the material's constituent parts and radicals, which combust in the vapor phase by reacting with oxygen.[118-119] This vapor-phase combustion is exothermic, which thermally decomposes the underlying material, feeding the combustion zone with fuel.[119-120] This process is represented in Figure 2.13.

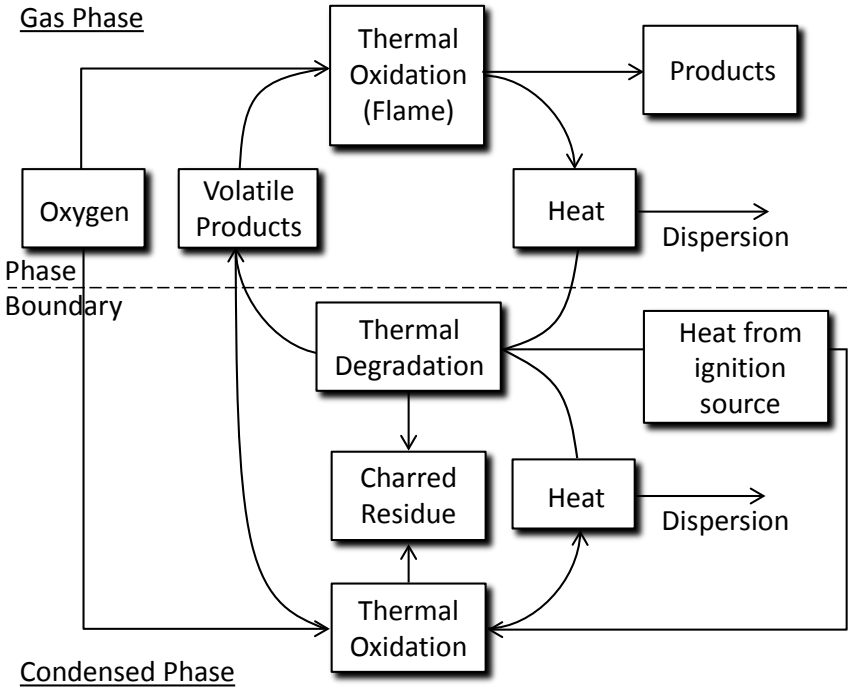

Figure 2.13. Diagram of the polymer degradation and combustion feedback cycle. Reprinted with permission from Elsevier.[119]

Bolland and Gee in 1945 proposed a series of reactions that polymers undergo for combustion, where the polymer breaks down into alkyl radicals which react exothermically with oxygen, as shown in Equations 2.19-2.25.[121-122] First, the radical reaction must be initiated (2.19) by heat or light, which leads to propagation through a reaction with oxygen and surrounding polymer (2.20, 2.21). The radical can terminate by reaction with other polymer radicals (2.22, 2.23) or by reacting with other oxygen containing radicals (2.24). The polymer can also have a chain branching mechanism (2.25).

$$H + Heat \rightarrow ROOH + R\bullet \quad (2.19)$$

$$R\bullet + O_2 \rightarrow RO_2\bullet \quad (2.20)$$

$$RO_2\bullet + RH \rightarrow ROOH + R\bullet \quad (2.21)$$

$$R\bullet + R\bullet \rightarrow R - R \quad (2.22)$$

$$RO_2\bullet + R\bullet \rightarrow ROOR \quad (2.23)$$

$$RO_2\bullet + RO_2\bullet \rightarrow Combustion\ Products \quad (2.24)$$

$$ROOH \rightarrow RO\bullet + OH\bullet \quad (2.25)$$

Table 2.1. Structural groups and their molar contribution to heat release capacity. Reprinted with permission from Wiley-VCH.[123]

Structural group	Contribution (kJ/mol K)	Structural group	Contribution (kJ/mol K)	Structural group	Contribution (kJ/mol K)
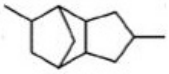	118[a]	—H	8.1	—OH	−19.8
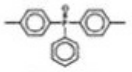	77.0		7.6	—Br	−22.0
	69.5	—CH_2—O—	4.18		−22.0
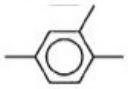	30.6		1.8	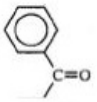	−23.2[a]
	29.5		0.1	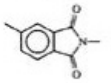	−25.5
	28.8	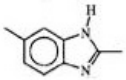	−8.8	—Cl	−34.7
	28.3	—S—	−10.9[a]	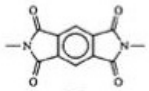	−36.4[a]
	26.6	—O—	−11.6	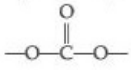	Pendant: −39.5 Backbone: −13.7
—CH_3	22.5		−13.8		−43.0[a]
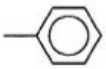	19.0	—NH_2	−13.9[a]	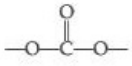	−49.0
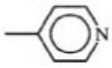	18.7	—CF_3	−14.8		−53.5[a]
	16.7	—C≡N	−17.6		−66.7
	15.1	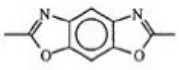	−18.9[a]		−74.5
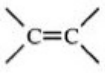	9.7		−19.2		−76.7

As the polymer breaks down into radicals due to heat and radical self-propagation, more fuel is fed to the combustion zone, which increases the amount of radicals that are formed by the heat.[118, 122] Polymer chemical structure greatly affects the combustion behavior of a polymer.[123-124] For example, polymers that favorably crosslink by reacting in the solid, or condensed phase, during degradation form a carbonaceous char that hinders the feedback-driven reaction.[86, 125-126] Table 2.1 gives examples of different polymer chemicals and their contribution to heat release capacity, which is a measurement of flammability.[123-124] Halogens frequently have negative contributions to a polymer's heat release capacity due to their vapor-phase flame retardant mechanism, in which free halogen radicals will quench the combustion reaction.[118, 124] Phosphates are a promising flame retardant for a wide variety of applications due to their extremely low heat release contribution (Table 2.1)[123] and relatively low toxicity.[19, 103, 125, 127]

2.3.2 Cellulose Flame Chemistry

In the United States, preventable household fires resulted in 1900 deaths and $3.6 billion in property damage from 1998 to 2008,[128] and cellulosic materials contribute the largest household fuel load.[125, 128] Rendering cellulosic materials, such as wood and cotton, flame retardant has been an historical problem,[128] and there is evidence from 450 BC that the ancient Egyptians were rendering wooden beams flame retardant using potassium alum and vinegar,[129] which catalyze the dehydration of cellulose to nonflammable char by lowering the pyrolysis temperature.[125, 130-131] Figure 2.14 shows the degradation mechanism of cellulose. At lower temperatures (<300 ˚C), cellulose

preferentially dehydrates, forming water, carbon dioxide, and char.[132-133] Acid sources, especially phosphoric acid, catalyze this lower temperature reaction, rendering cellulose charring.[125] At higher temperatures, cellulose decomposes into laevoglucosan (tar) (LG),[125, 132-133] which volatilizes into combustible vapor. The conversion to LG is the primary mechanism of cellulose degradation without added flame retardants.[125, 132]

While cotton fabric comprises the majority of clothing,[125, 133-134] very little of it is rendered flame retardant, making it a ubiquitous energetic ignition source.[125] Current flame retardant solutions for cotton use either toxic chemicals,[119-120] such as halogenated hydrocarbons, or require expensive processing conditions, such as high pressure.[20] There is still a need for a soft, inexpensive, environmentally-benign, nontoxic flame retardant solution for cellulosic materials.[125, 133 135]

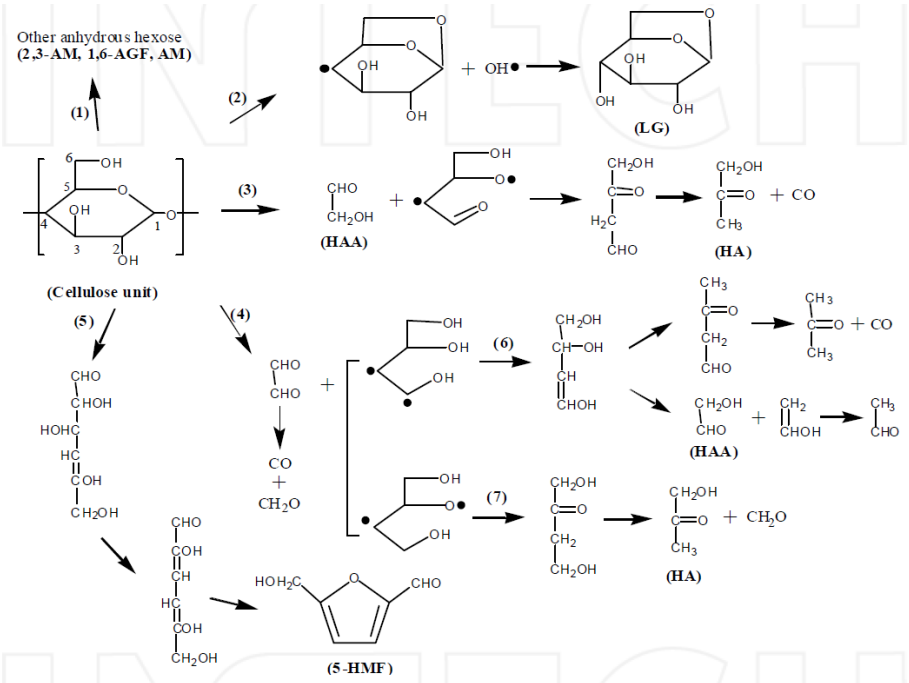

Figure 2.14. Proposed degradation pathway of cellulose. Reprinted with permission from Elsevier.[133]

2.3.3 Phosphorous Flame Retardants

Phosphorous-based flame retardants are an excellent alternative to traditional halogenated flame retardants due to their low environmental toxicity and nontoxic flame retardant mechanism.[19, 119-120, 125, 128, 135] Phosphate catalyzes the degradation of cellulose to char by dehydrating the cellulose during pyrolysis, as shown in Figure 2.15.[125, 136] Phosphoric acid reacts with the cellulose, forming phosphorylated cellulose,[136] which form conjugated double bonds in the glucopyranose rings during degradation.[125, 136] The conjugated double bonds encourage char formation and prevent the formation of laevoglucosan.[125, 132-133, 136]

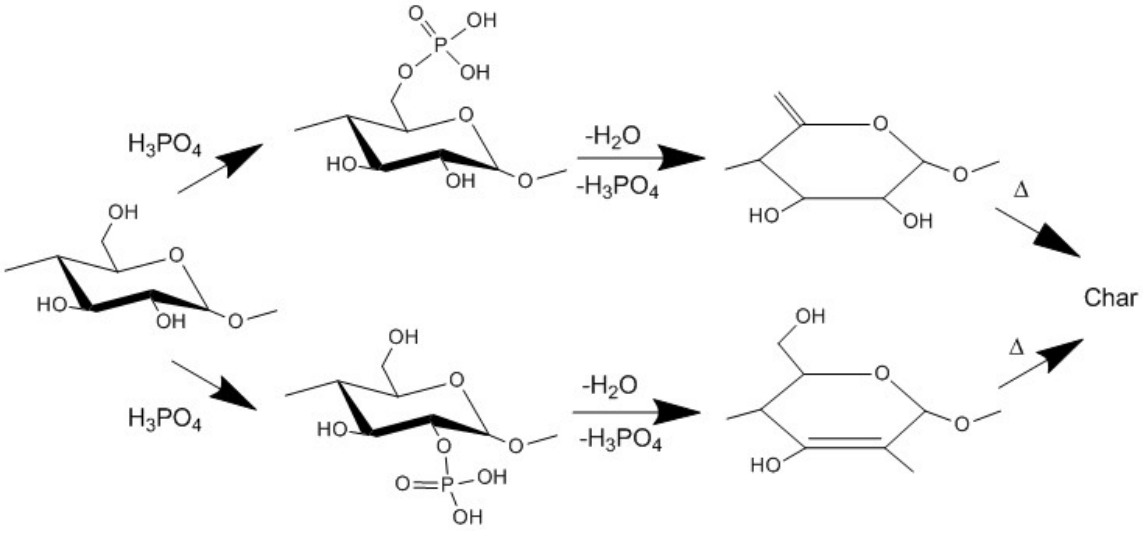

Figure 2.15. Cellulose degradation pathway in the presence of a phosphate catalyst. Reprinted with permission from Elsevier.[137]

Phosphate flame retardants, while highly effective for cellulose, suffer from poor washfastness[138] and must be fixed to the substrate, often through crosslinking with toxic formaldehyde-based chemistries.[20, 139] While these crosslinked polymeric phosphate flame retardants are effective, it is difficult to apply them in a uniform and soft manner to fabric.[20, 125, 127, 140-141]

2.3.4 Layer-by-Layer Flame Retardants

Layer-by-layer nanofilms are able to conformably coat complex substrates with ease,[1] and a variety of substrates such as polyurethane foam,[7] nylon,[54] and cotton fabric[19] have been rendered flame retardant with LbL films. Cotton fabric has a very high surface area to volume ratio,[125] and is an ideal substrate for flame retardant LbL films.

In 2009, Li et. al. published the first work on flame retardant layer-by-layer assembled films for fabric, rendering cotton fabric mildly charring with 10 bilayers of PEI and laponite clay.[142] In 2010, Li et. al. greatly improved on this work replacing laponite with MMT clay, which has a much higher aspect ratio. The nanoclay in the system acted as a thermal barrier, but was not charring enough to render the fabric self-extinguishing.[126] This work was inspired by the increase in thermal stability of LbL-coated cellulose fibers reported by Lin et. al. in 2007.[143] In 2011, Li et. al. found that a phosphate-based LbL film was able to render cotton fabric self-extinguishing, passing the vertical flame test (ASTM D6413) with 20 bilayers added (Figure 2.16).[19] Since then, several researchers have demonstrated the efficacy of LbL films to render various fabrics self-extinguishing.[16, 26, 135] The ability of LbL films to incorporate normally

water-soluble phosphate salts allows for environmentally-friendly coatings that can survive aqueous conditions, though these films still suffer from a lack of washfastness and a moderate stiffening of the fabric.[16, 19, 26, 126, 142]

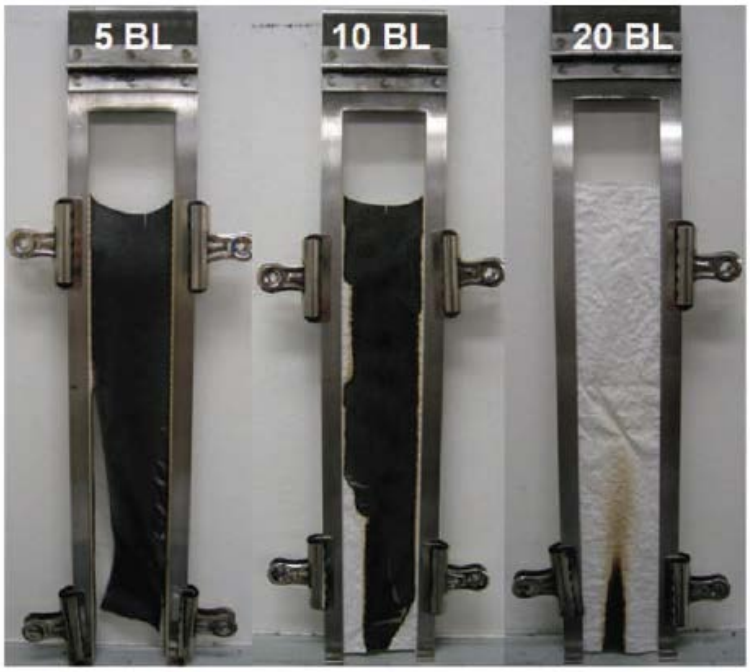

Figure 2.16. Vertical flame test aftermath of cotton fabric coated with poly(allylamine) / poly(sodium phosphate) (PSP) LbL films. Reprinted with permission from Wiley-VCH.[19]

3. MAINTAINING HAND AND IMPROVING FIRE RESISTANCE OF COTTON FABRIC THROUGH ULTRASONICATION RINSING OF MULTILAYER NANOCOATING[1]

3.1 Introduction

The U.S. National Center for Health Statistics (NCHS) estimates that over 4,300 people are injured each year in the United States due to clothing-related burn injuries, and that this is a worldwide problem. Many of these injuries (20-30%) are due to workplace exposures, causing numerous guidelines to be put into place, such as OSHA guideline 29 CFR 1910.132, that requires all workers in oil and gas operations to wear flame retardant clothing. In 2000, the Industrial Fabric Association International estimated the market size for flame retardant protective apparel to be over $800 million/year worldwide. This growing market segment is driving the development of new FR treatments that protect workers, while maintaining comfort, but any new flame retardants have to meet various safety, health, and environmental standards. Specifically, there remains a need for low cost, environmentally benign, durable, and comfortable flame retardant treatment for fabric.[125] Numerous strategies are currently used to render textiles flame retardant: surface treatments, additives or co-monomers in synthetic fibers, nanocomposite technology, inherently heat resistant fibers, and fiber blending.[127] More

[1] Reprinted with permission from "Maintaining Hand And Improving Fire Resistance Of Cotton Fabric Through Ultrasonication Rinsing Of Multilayer Nanocoating" by Guin, et. al, 2014. *Cellulose*, 4, 3023-3030, Copyright 2014 by Springer.

recently, layer-by-layer (LbL) assembly has been shown to impart flame retardance to cotton fabric by conformally coating each individual fiber with an intumescent multilayer thin film,[19, 135, 144-146] but the comfort, or "hand," of the coated cotton fabric was not adequately addressed.

In the present study, an intumescent nanocoating was prepared with chitosan (CH) and poly(sodium phosphate) (PSP), alternately deposited on cotton fabric. Ultrasonication was applied to the aqueous rinse step between deposition steps to improve the hand and FR behavior of the coated fabric. CH/PSP is an intumescent system in which chitosan and cotton act as a carbon source and blowing agent, while PSP acts as an acid source. In the presence of this acid, cotton preferentially dehydrates[137], generating water vapor and forming char. This mechanism significantly enhances the cotton's resistance to combustion[128]. The sonication more effectively removes excess coating material and prevents "bridging" of the cotton fibers, which appears to be the primary cause of fabric stiffening. When compared to the same coated fabric prepared without sonication rinsing, it is shown that ultrasonicated fabric exhibits a softer hand and the ability to pass vertical burn testing with lower weight gain. This is a tremendous breakthrough that is expected to make LbL-based fire protection more appealing to the apparel industry, potentially creating more markets for cotton.

3.2 Experimental

3.2.1 Materials

Chitosan (CH) (Mw ~60,000 g/mol, G.T.C. Bio Corporation, Qingdao, China), sodium hexametaphosphate (PSP) (crystalline, +80 mesh, 96%, Sigma Aldrich, Milwaukee, WI), branched polyethylenimine (PEI) (Mw ~25,000 g/mol, Aldrich), hydrochloric acid (HCl) (ACS reagent 37%, Aldrich), and sodium hydroxide (NaOH) (ACS reagent >97.0%, Aldrich) were used as received. Silicon wafers (single-side-polished (1 0 0), University Wafer, South Boston, MA) and polished Ti/Au crystals with a resonance frequency of 5 MHz (Maxtek, Inc., Cypress, CA) were used for characterization of film growth. Desized, scoured, and bleach plain-woven cotton fabric (with a weight of 100 g/m2) was purchased from Testfabrics, Inc. (West Pittston, PA).

3.2.2 Layer-by-Layer Deposition and Film Growth

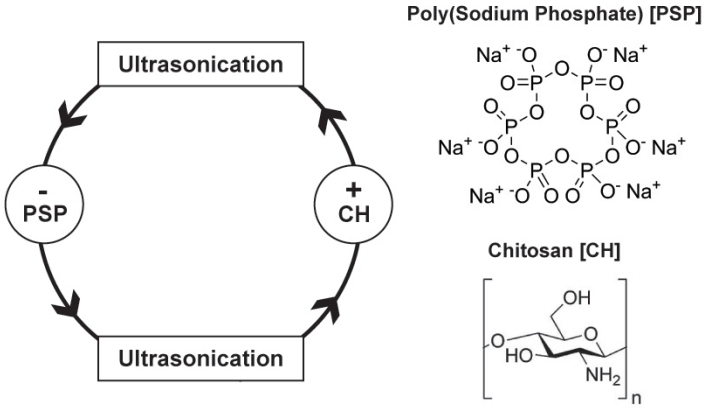

Figure 3.1. Schematic of layer-by-layer assembly using ultrasonication during the rinse steps, along with chemical structures of the polyelectrolytes deposited.

Separate 2 wt% PSP (pH 4) and 1 wt% BPEI (natural pH) solutions were prepared in deionized water (18.2 MΩ). 0.5 wt% CH solution was prepared in pH 1.5 HCl and then adjusted to pH 4 using 1M NaOH. A 30 min piranha treatment was used to clean silicon wafers. Caution! Piranha solution reacts violently with organic materials and should be handled with extreme care. A 5 min plasma cleaning treatment, using a PDC-32G plasma cleaner (Harrick Plasma, Ithaca, NY), was performed on QCM crystals prior to deposition. All film growth began with a 5 minute deposition of BPEI solution in order to improve adhesion to the substrates. Films were then alternately dipped between the anionic PSP and cationic CH solutions, beginning with PSP, as shown in Figure 3.1. The first dip into PSP was 5 minutes, while the rest of the deposition steps were one minute. Between every deposition the substrate was rinsed in DI water for one minute. The fabric was wringed by hand after each deposition and rinse step to remove excess liquid. After the desired number of bilayers was deposited, samples were dried in a 70˚C oven for 2 hours. Ti/Au crystals were dried using a stream of dry air after each rinse step to minimize moisture uptake. For the sonication procedure, fabric and silicon wafer samples were rinsed for one minute in a 10L Branson 5510 ultrasonic cleaner (Branson Ultrasonics Corporation, Danbury, CT). Rinse water was replaced after every 5 bilayers. Film thickness was measured on silicon wafers using an alpha-SE elliposometer (J.A. Woollam Co., Inc., Licoln, NE). Mass deposited was measured on Ti/Au crystals using a Maxtek Research Quartz Crystal Microbalance (QCM) from Infinicon (East Syracuse, NY), with a frequency range of 3.8-6 MHz.

Surface images of coated fabric, burned and unburned, were taken with a Quanta 600 (FEI Company, Hillsboro, OR) or a Model JSM-7500F (JEOL; Tokyo, Japan) FE-SEM.

3.2.3 Thermal Stability, Flammability and Combustibility of Fabric

The thermal stability, degradation temperature, and pyrolysis behavior of cotton was measured with a Q50 Thermogravimetric Analyzer (TA Instruments, New Castle, DE). Each sample was approximately 20 mg and tests were conducted in air, from room temperature to 650˚C, with a heating rate of 10˚C/minute. All tests were conducted in triplicate. Vertical flame testing was performed on five 3.3 x 12 in. fabric samples according to ASTM D6413, using a VC-2 automatic vertical flammability cabinet (Govmark, Farmingdale, NY). Microscale combustibility experiments were conducted with a Govmark MCC-1 Microscale Combustion Calorimeter, according to ASTM D7309 method A. The sample size for microscale combustion was 15 mg and samples were tested with a 1˚C/sec heating rate under nitrogen, from 150˚C to 550˚C. All MCC testing was performed by the University of Dayton Research Institute (UDRI, Dayton, OH).

3.2.4 Mechanical Properties

Tensile, shear, bending, compression, and surface properties were measured using the Kawabata Evaluation System (KES). Tests were performed in triplicate in weft and warp directions at 21 ˚C and 65% RH. Tensile and shear testing was performed with a KES-FB1 Tensile-Shear Tester (Kato Tech Co., Kyoto, Japan). The maximum load for

tensile testing was 50 gf/cm, and the maximum offset angle for shear testing was 8˚. Bend testing was performed using a KES-FB2 Bending Tester and was measured to 150˚. Compression testing was performed using a KES-FB3 Compression Tester from 0 to 50 gf/cm2. Surface testing was performed using a KES-FB4 Surface Tester, and a 20 gf/cm tension was applied. All KES testing was performed by the Textile Protection and Comfort Center at North Carolina State University (Raleigh, NC).

3.3 Results and Discussion

3.3.1 Film Growth

Figure 3.2 shows thickness and mass growth of chitosan/poly(sodium phosphate) assemblies monitored using ellipsometry and quartz crystal microbalance (QCM), respectively. The film thickness increases linearly up to 10 BL, but transitions to thicker growth with additional bilayer deposition. The mass deposition shows a similar growth trend (Figure 3.2(b)). It has been theorized that this growth transition is due to the deposition process transitioning from one dominated by surface kinetics to a diffusion dominated regime.[147] As the CH in the film swells, it is able to absorb more PSP from the solution during each deposition step, as the relatively small PSP molecules are able to diffuse into the swollen film. QCM was also used to determine composition of the film, which reveals PSP content increasing with bilayers deposited (25 wt% PSP at 3 BL and leveling off to 46 wt% by 30 BL). It is likely that the appearance of exponential growth occurring near 10 BL is really a transition to second linear regime with a steeper

slope, known as supralinear growth.[148] Either way, this growth trend is indicative of an interdiffusing polyelectrolyte system.

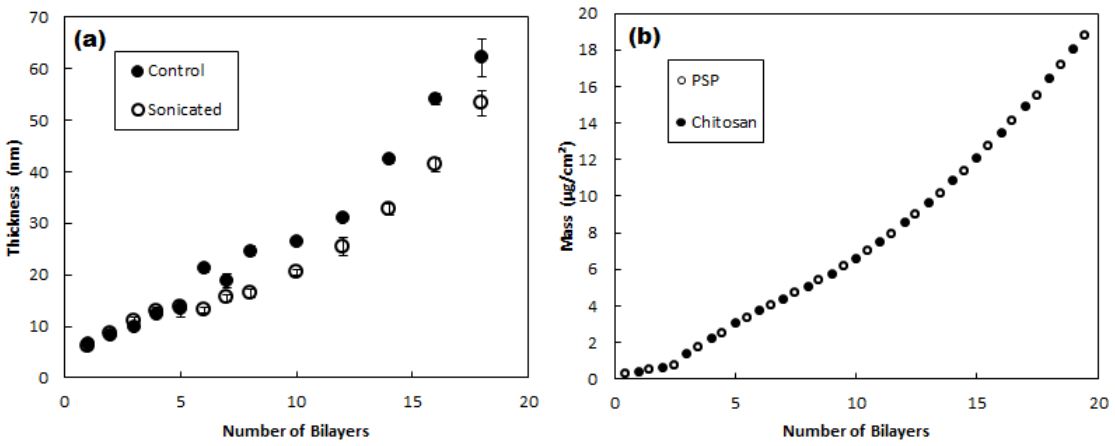

Figure 3.2. Thickness as a function of CH/PSP bilayers deposited on silicon wafers (a), rinsed in either still water or an ultrasonic bath, and mass deposited as a function CH and PSP deposited on a Ti/Au quartz crystal (b).

During deposition, wafers were rinsed either in an ultrasonic bath, referred to as "sonication," or undisturbed water for one minute between layers. There is no appreciable difference in the thickness between these two rinsing methods prior to five bilayers being deposited (Figure 3.2(a)). Beyond 10 BL, the assemblies that were not sonicated were significantly thicker. For example, a non-sonicated 14 BL film is 42 nm, while sonication results in a 33 nm film. It is believed that sonication more effectively removes weakly adhered polyelectrolyte from the film. In the surface kinetics regime (i.e., the initial layers), the polyelectrolytes layer more thinly.[147] In the diffusion regime

(i.e., beyond 10 BL), the polyelectrolyte layer more thickly, with some of the material bound with weaker interactions, which can be overcome through sonication.

The CH/PSP system was also deposited on cotton fabric using the same general procedure as silicon wafers. In this case, nanocoating growth is measured by weight gain of the fabric. Sonicating the cotton between depositions steps decreased the mass deposited by 48% relative to cotton coated without sonication. Without sonication, the fabric's weight gain necessary to achieve passing flame retardant behavior is comparable to most intumescent LbL FR systems reported in the literature.[19, 135, 146] Sonication results in excellent FR behavior with weight gain that is far less than any other LbL systems that pass vertical flame testing (VFT). This reduced weight gain also results in improved hand (softness).

3.3.2 Flame Retardant Behavior

The CH/PSP nanocoating promotes a dehydration reaction in conjuction with the cotton (i.e., cellulose), which generates an intumescent effect on the surface of the individual fibers. Acidic phosphate groups are known to catalyze such reactions.[127] When heat is applied, the cotton preferentially chars and releases water, creating pockets of insulating gasses trapped by the char and extinguishing the flame.[128] To better understand the nature of this coating and its FR mechanism, the fabric was imaged pre and post-burn using scanning electron microscopy (SEM), as shown in Figure 3.3. These micrographs show a stark difference between the control and sonicated fabric. While the weave structure is still visible in the control sample, it is clear that the coating has

bridged the majority of the fibers. In the sonicated sample, individual fibers are much more visible because there is very little bridging. It should be noted that 17 CH/PSP bilayers added 9.1 wt% to sonicated fabric while 17 CH/PSP bilayers added 17.6 wt% to fabric without ultrasonication. In the post burn images (right side of Figure 3.3), there is clear evidence of intumescence in the form of bubbles. This raised topography is the result of gas being trapped by char during burning. Despite having a thicker intumescent char, the control fabric did not exhibit improved FR performance.

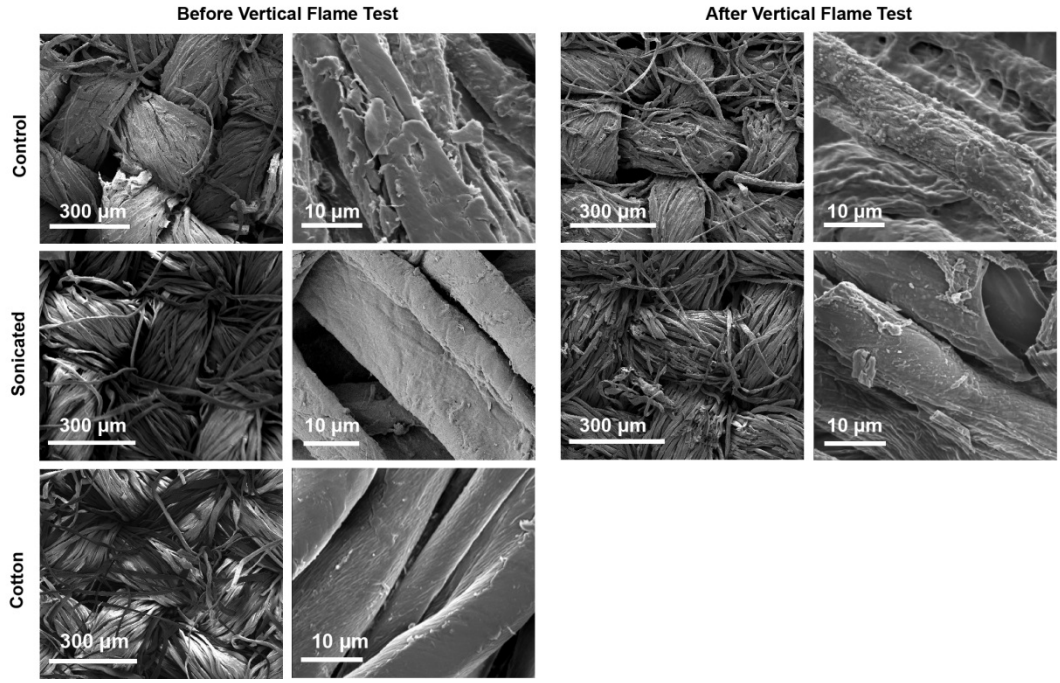

Figure 3.3. SEM images of uncoated cotton fabric and fabric coated with 17 BL of CH/PSP, with and without (i.e., control) sonication rinsing, before and after burning.

The flame retardant behavior of the coated cotton fabric was evaluated using vertical flame testing (VFT), thermogravimetric analysis (TGA), and micro cone calorimetry (MCC). VFT was used to determine the self-extinguishing behavior of the fabric (residues shown in Figure 3.4). Uncoated cotton underwent complete combustion, leaving virtually no residue, while the coated samples ignited initially, but self-extinguished immediately upon removal of the flame. While the char left behind was brittle, the weave structure was maintained, and the burned sample could be handled without flaking. Height of the sonicated fabric char was shorter and more consistent than the control fabric's char. Both coated samples experienced no afterglow, while the afterglow for uncoated cotton persisted for 21 seconds.

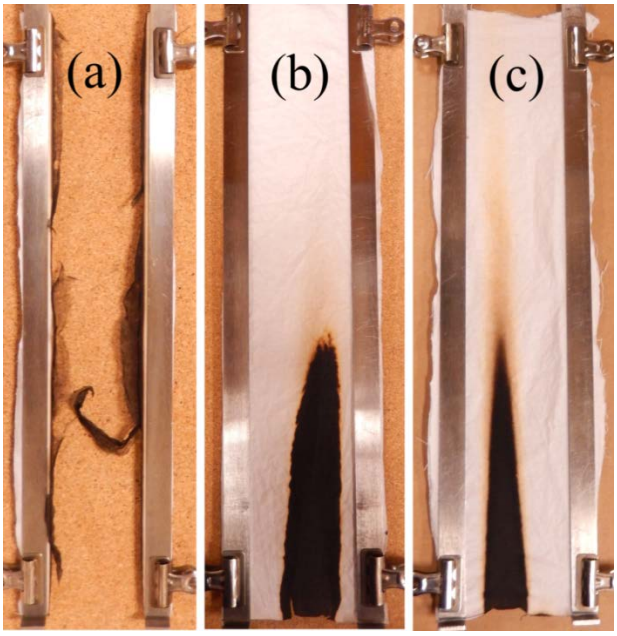

Figure 3.4. Post-vertical flame test images of cotton fabric (a), control coated fabric (b), sonicated coated fabric (c).

Table 3.1. Post burn residue and char dimensions of 17 CH/PSP BL coated fabric.

	% Residue (wt/wt)	Height (in)	Width (in)
Control	88.3 ± 5.4	6.2 ± 1.25	1.1 ± 0.2
Sonicated	92.0 ± 2.9	5.1 ± 0.3	1.1 ± 0.2

TGA was used to characterize the pyrolysis behavior of the fabric, as shown in Figure 3.5(a).The coating decreased the degradation temperature of the cotton fabric from 344˚C to 292 ˚C, for both control and sonicated samples. Cotton burned completely in the absence of a coating, leaving almost no residue, while the coated cotton left behind a large residue that slowly decomposed. Cellulosic materials will preferentially dehydrate if a condensed phase acid catalyst, such as poly(sodium phosphate), is present to prevent decomposition into volatile combustible gasses.[127] Although seemingly counterintuitive, it is desirable for the flame retardant mechanism to begin before the substrate begins to degrade in order to maximize protection.

MCC was used to analyze the combustion behavior of the fabric. The coated fabric experienced a large reduction in peak heat release rate (HRR peak) and total heat release (THR), as shown in Figure 3.5(b) and Table 3.2. Both the HRR peak and the THR reduction for the control are the best reported for an LbL fabric FR system, and sonication improves it even further. The HRR peak for the sonicated sample was 10% less than the coated control (both were less than 70% of the uncoated cotton). The THR for the sonicated sample was 15% less than the control sample, demonstrating that sonication provided superior FR behavior with lower coating weight.

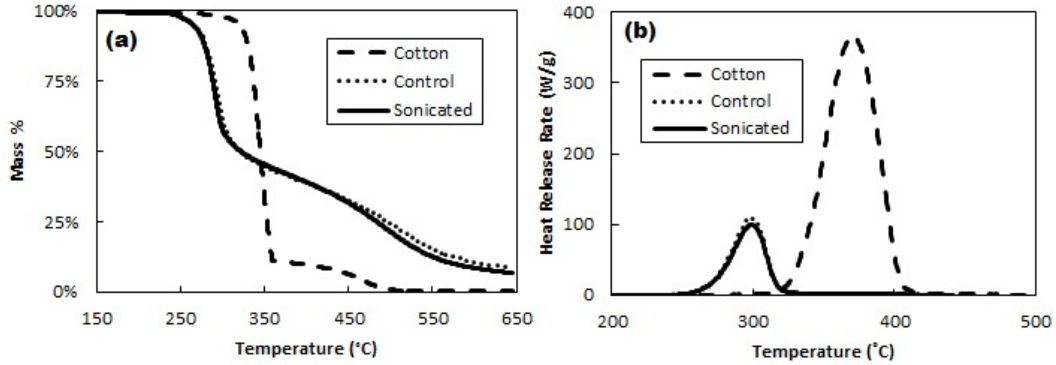

Figure 3.5. Weight loss as a function of temperature for uncoated fabric, and fabric coated with 17 bilayers of CH/PSP (a), and heat release rate as a function of temperature for uncoated cotton fabric and fabric coated with 17 CH/PSP bilayers (b).

Table 2.2. Microscale calorimetry measurements of uncoated cotton fabric and 17 CH/PSP BL coated fabric.

	Char Yield (wt%)	HRR Peak (W/g)	HRR Peak Reduction	THR (kJ/g)	THR Reduction
Cotton	4.06	370.83	N/A	13.47	N/A
Control	35.25	110.26	70%	2.97	78%
Sonicated	35.4	99.55	73%	2.53	81%

3.3.3 Mechanical Properties

The mechanical properties of uncoated cotton, coated control, and fabric prepared with sonicated rinsing were determined with a Kawabata Evaluation System (KES).[149] A KES is comprised of five testing instruments that measure the shearing, surface, bending, compression, and tensile properties of fabric. These mechanical properties, are important factors in determining a fabric's hand,[150] which is the

subjective assessment of a textile obtained from the sense of touch.[151] Sonication during the rinse step dramatically improves most of the mechanical properties measured by the KES. While both the control and sonicated cotton have a worse hand than the uncoated fabric, sonication greatly improves the properties relative to the control. Table 3.3 summarizes the key properties related to hand.

Shear stiffness is associated with the ability of a fabric to "drape" and its softness.[152] When cotton fibers are bridged during the LbL coating process (see SEM images of control fabric in Figure 3.3), it becomes difficult for them to slide past each other, which is a necessary condition for a fabric to drape. Coated control fabric exhibited much greater shear stiffness than uncoated cotton, but sonication reduced the increase in stiffness by a factor of 5, nearly matching the untreated cotton (see Table 3.3). Imperfections and aggregates in the nanocoating, which can be seen in Figure 3.3, increased the roughness of the fabric. As with the shear stiffness, sonication improved this property by reducing the increase in roughness by 58% relative to the control. Toughening and bridging the fibers with a polymer coating was shown to reduce the fabric's ability to bend, resulting in a very stiff fabric.[153] Control fabric showed an extremely large 720% increase in bending rigidity relative to uncoated cotton, but the minimized bridging in sonicated fabric reduced this rigidity by a factor of two, resulting in a much softer fabric.

Table 3.3. Representative KES measurements of 17 CH/PSP BL coated fabric.

	Cotton	Control	Sonicated
Shear Stiffness (gf/cm·deg)	0.95	6.49	1.28
Geometric Roughness (micron)	3.26	4.47	3.77
Bending Rigidity (gf·cm²/cm)	0.07	0.58	0.27

3.4 Conclusions

Sonication was employed during the rinsing step of layer-by-layer deposition in an effort to produce soft, flame retardant cotton fabric. This multilayer nanocoating of chitosan and poly(sodium phosphate) was applied to cotton fabric and acted as an intumescent flame retardant. By rinsing the fabric in an ultrasonic bath between deposition steps, less mass was deposited on the fabric and fiber bridging was largely eliminated. Cotton fabric gained 9.1 wt% when 17 CH/PSP bilayers were deposited, which was nearly half of the weight gain of the same coating deposited without sonication rinsing. The low coating weight of the sonicated cotton still resulted in a pass of vertical flame testing and a hand that was much more comparable to uncoated cotton. Incorporating sonication into layer-by-layer assembly is a simple modification that improves the FR performance of fabric, while sacrificing none of its desirable qualities (e.g., soft hand). It is believed that this procedure could be used with any type of fabric (e.g., nylon, polyester, etc.) to achieve similar improvement, making this a commercially viable treatment.

4. THICK GROWING MULTILAYER NANOBRICK WALL THIN FILMS: SUPER GAS BARRIER WITH VERY FEW LAYERS[2]

4.1 Introduction

Thin films that are impermeable to oxygen are required for a wide variety of applications, such as food and microelectronics packaging.[154] Highly oxygen sensitive food packaging (e.g., coffee and high fat snacks) requires an oxygen transmission rate (OTR) of less than 1 cc/m^2·day·atm,[155] while flexible organic light emitting devices require an OTR below 10^{-5} cc/m^2·day·atm.[61] Monolithic inorganic oxide thin films, such as SiO_x, are commonly used as transparent high barrier layers, but are frequently unable to meet these requirements.[51] These inorganic layers are prone to defect formation, poor substrate adhesion, failure upon flexure, and they require expensive ultrahigh vacuum processing conditions.[156] Many alternative gas barrier layers have been explored, such as polymer-inorganic nanocomposites.[57] In particular, polymer-clay nanocomposite films produced via layer-by-layer (LbL) assembly have shown promise due to their high transparency, ambient processing conditions, and extremely high oxygen barrier (<0.005 cc/m^2·day·atm at a thickness < 100 nm),[15, 53-54] but these films typically require many layers (≥16) to achieve such low oxygen transmission. Reducing the number of processing steps required to achieve a high gas barrier remains an important issue for commercial use of this nanocoating technology.

---

[2] Reprinted with permission from "Thick Growing Multilayer Nanobrick Wall Thin Films: Super Gas Barrier With Very Few Layers" by Guin, et. al, 2014. *Langmuir*, 30, 7057-7060, Copyright 2014 by ACS.

In this study, relatively thick growing super gas barrier LbL films, produced from environmentally-benign polyelectrolytes and few deposition steps, were prepared by buffering the polyelectrolyte and rinse solutions with tris buffer. It has been observed that increasing the ionic strength of the polyelectrolyte solutions results in increased film thickness,[32] but buffered solutions have only recently been reported.[54] The rinse water plays an especially crucial role, allowing for relatively thick films (> 1 μm) to be produced with few layers. This simple modification to the layer-by-layer assembly process facilitates achieving desirable properties, like oxygen barrier, with fewer bilayers.

4.2 Experimental

4.2.1 Materials and Film Growth

Cationic solutions contained 0.1 wt% chitosan (CH) (MW 60,000 g/mol, G.T.C. Bio Corp., Qingdao, China) and 0-100 mM Trizma Base (tris) (Sigma Aldrich, Milwaukee, WI), adjusted to pH 6 with 1M NaOH and 5M HCl (Sigma) using a previously described method. A 1 wt% vermiculite suspension (Microlite 963++, Specialty Vermiculite Corp), prepared in 18 MΩ deionized (DI) water, and adjusted to pH 10 with 1M NaOH, acted as the anionic component. Assembling these films began with dipping the substrate into the CH solution for 1 min, then dipping for 1 min in an equivalent concentration of tris at pH 6, dipping into the VMT solution for 1 min, and finally dipping in a pH 10 NaOH solution for 1 min to complete one bilayer, and a schematic is shown in Figure 4.1. The films were not dried in between depositions. It is

important to note that the pH of the polyelectrolyte solutions, and their associated rinses, were kept identical. After all the layers were deposited, the films were rinsed thoroughly in DI water and dried at 70˚C for 24 hours.

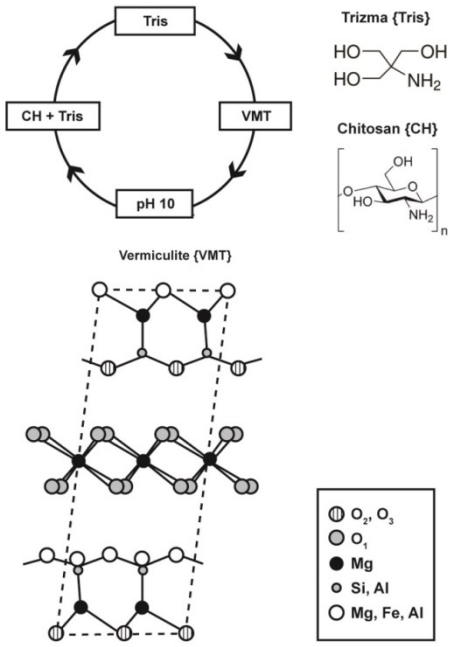

Figure 4.1. Schematic of layer-by-layer assembly using buffered chitosan solution and rinse. Chemical structures of the polyelectrolytes deposited are shown, along with a representation of the vermiculite structure.[157]

4.2.2 Film Characterization

Thickness of the films was measured on (1 0 0) silicon wafers with a P-6 profilometer (KLA-Tencor, Milpitas, CA). Silicon wafers were pretreated with a 3:1 concentrated sulfuric acid (Sigma) to 30% hydrogen peroxide (Sigma) piranha solution

(Caution! Piranha solution is very corrosive.) for 30 min, and the average thickness of the film was determined from five 0.2 mm cuts across the silicon wafer. Mass of the films was measured using a research quartz crystal microbalance (QCM) (Inficon, East Syracuse, NY) on polished Ti/Au crystals with a 5 MHz resonance frequency (Maxtek, Inc., Cypress, CA). A 5 min plasma cleaning treatment, using a PDC-32G plasma cleaner (Harrick Plasma, Ithaca, NY) was performed on QCM crystals prior to deposition. Films for oxygen transmission testing were deposited on 179 μm thick polyethylene terephthalate (PET) film (ST505, Dupont-Teijin), purchased from Tekra (New Berlin, WI). Films for thermogravimetric analysis were deposited on 1.6 mm thick polypropylene sheets (VWR International, Radnor, PA) and later detached and ground using a mortar and pestle. Cleaned PET and PP substrates were corona treated with a BD-20C Corona Treater (Electro-Technic Products Inc., Chicago, IL) to improve the adhesion of the first polyelectrolyte layer. The clay composition of freestanding films was measured with a Q50 Thermogravimetric Analyzer (TA Instruments, New Castle, DE). Samples were heated to 950˚C at 20˚/min, and held for 2 hours. A dry weight baseline was determined by heating the sample to 120˚C for 30 minutes.

Samples for optical microscopy and transmission electron microscopy (TEM) were prepared by embedding the film in Epofix (EMS, Hatfield, PA) resin overnight and cutting cross sections, using an Ultra 45° diamond knife (Diatome, Hatfield, PA), onto 300 mesh copper grids. Optical micrographs of the sections (~90 nm thick) were imaged using a Zeis Axiophot (Zeiss Microimaging, Thornwood, NY) microscope equipped with a 40x/0.75 Plan Neofluar objective and a Cool Snap CF (Photometrics, Tucson,

AZ) CCD camera controlled by Metaview software (Media Cybernetics, Rockville, MD). TEM micrographs of the sections (~90 nm thick) were imaged using a Tecnai G2 F20 (FEI, Hillsboro, OR) at an accelerating voltage of 200kV. Oxygen transmission rate (OTR) of the CH+tris/VMT films was measured on 179 μm PET and performed by MOCON (Minneapolis, MN) using an Oxtran 2/21 oxygen permeability instrument (using the procedure outlined in ASTM D-3985) at 23 ˚C and 0% RH. Permeability of the films was determined by assuming ideal laminate theory.[51]

4.3 Results and Discussion

4.3.1 Film Growth

Thick growing CH+tris/VMT multilayer films were initially grown on silicon wafers and their thickness was measured using profilometry, as shown in Figure 4.2. The influence of tris concentration was evaluated on 8 bilayer (BL) films. Due to diminishing improvement in thickness beyond 50 mM tris, this concentration became the baseline for the rest of the study. A thickness of 4.3 μm is achieved at 8 BL, which is among the thickest LbL films reported.[54] The mass of these films was also relatively large (Fig. 2(c)), reaching 1200 μg/cm^2 at 8 bilayers. Figure 4.2(b) shows the supralinear growth of thickness with increasing bilayers, while the mass increases linearly (Figure 4.2(c)). These observations indicate that film density decreases with increasing bilayers, but the net amount of material added was increased with the presence of tris.

CH+tris/VMT film thickness increased nonlinearly with increasing tris concentration, contradicting a previous study that showed a linear increase with

increasing salt concentration.[32] This previous study rinsed in DI water rather than using buffered solutions, which is the source of the discrepancy. When films were grown with 50 mM tris added to the chitosan solution, but not the rinse, the films reached a thickness of 1.7 μm. The thickness of this film was five times thicker than one grown without tris, but less than half the thickness of a film rinsed in tris solution. The thickness of an eight bilayer film ranges from 300 nm (no tris) to 5 μm (100 mM tris), demonstrating a high level of tailorability with tris concentration. The clay concentration of these thick-growing films was determined using TGA. Independent of the number of bilayers, the dry films were composed of 87 wt% vermiculite, which is comparable to other clay-containing LbL films.[53, 56] This high clay concentration has a significant influence on the behavior of the multilayer film. The films had a hazy, colored appearance that is believed to be due to poor ordering in the initial bilayers.

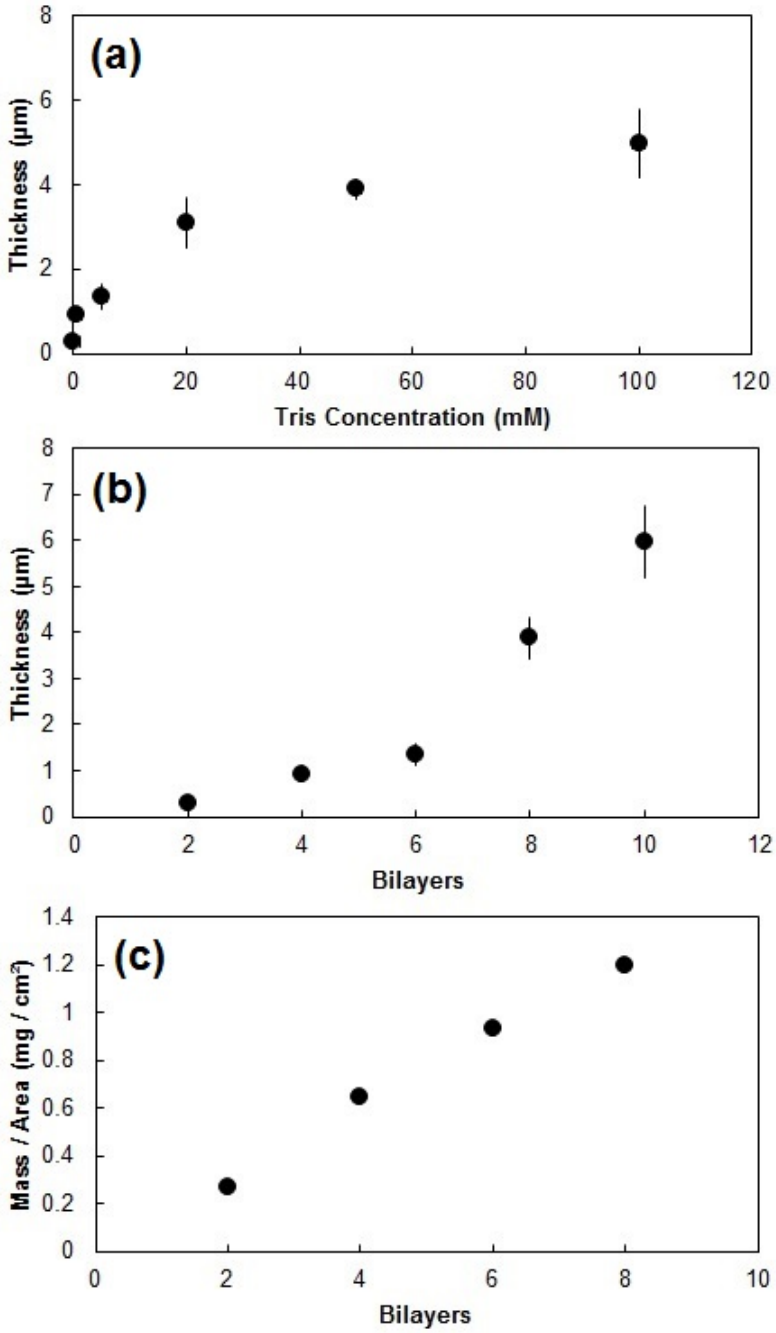

Figure 4.2. Thickness as a function of tris concentration for 8 BL CH+tris/VMT assemblies deposited on silicon wafers (a). Thickness as a function of bilayers deposited with 50mM tris in the CH solution and rinse on silicon wafers (b). Mass added as a function of bilayers deposited with 50mM tris in the CH solution and rinse (c), measured by a quartz crystal microbalance.

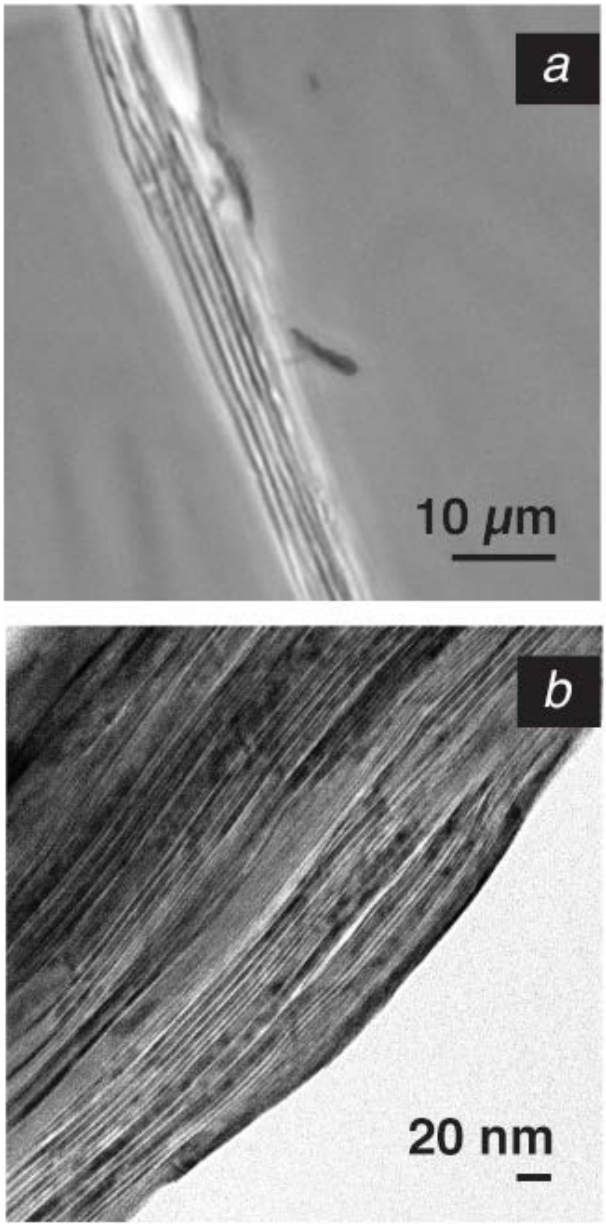

Figure 4.3. Optical micrograph of the cross-section of an eight bilayer CH+tris/VMT film, deposited on PET and embedded in epoxy taken in phase contrast mode (a) and TEM micrograph of outermost edge (b).

4.3.2 Microscopy

Optical and TEM micrographs of the CH+tris/VMT multilayer films on PET were used to qualitatively determine structural characteristics. Dark and light bands are visible in an optical micrograph (Figure 4.3(a)), indicating that the film is composed of large bands of varying composition. The dark bands indicate clay-rich regions while the light bands indicate regions composed primarily of chitosan. The outermost layer is sometimes seen removed from the surface, which is most likely the result of damage due to microtoming. The TEM micrograph (Figure 4.3(b)) shows individually aligned clay platelets at the outermost surface. It seems that these well-ordered clay platelets contribute to the extremely high oxygen barrier of the films. Previous studies have shown that polymer-clay multilayer films, with highly aligned clay platelets, exhibit very low oxygen transmission rates.[15, 53, 56]

4.3.3 Barrier Properties

Thin films grown on PET displayed a very high oxygen barrier and correspondingly low permeability, as shown in Table 1. At only 8 BL, the OTR of these films was below detection (<0.005 $cc/m^2 \cdot day \cdot atm$), while 6 BL was 0.009 $cc/m^2 \cdot day \cdot atm$. This is the lowest 6-bilayer oxygen transmission ever reported. The impressive oxygen barrier of these films is due to the extremely tortuous path taken by an oxygen molecule between clay platelets.[57] Despite the somewhat disordered nature of these films,[15, 53, 56] the permeability decoupled from the PET substrate is very low due to

the high clay concentration. The 6 BL film has a permeability that is comparable to a typical SiO_x layer.[156]

Table 4.1. Properties of CH+tris/VMT thin film assemblies.

Bilayer	Oxygen Transmission Rate (cc/m²·atm·day)	Thickness (μm)	Permeability (10^{-20} cc·cm/cm²·Pa·sec)
2	1.221	0.6 ± 0.2	194
4	0.122	1.0 ± 0.2	28.4
6	0.009	1.6 ± 0.2	3.4
8	0.005	4.3 ± 0.7	4.57

4.4 Conclusions

A new method to create a thick-growing polymer-clay layer-by-layer assembly was demonstrated, using a buffered rinse step. These somewhat low density nanobrick wall films contained over 87 wt% clay and could have their thickness tailored with tris concentration. TEM micrographs reveal that these films were disordered in the first few bilayers, before displaying a more ordered structure. The barrier of these films was extremely high despite depositing very few bilayers, achieving an OTR of 0.009 cc/m^2·day·atm with only 6 bilayers. With a minimum number of bilayers and excellent gas barrier properties, these multilayer nanocomposites provide an inexpensive, environmentally-benign alternative to current barrier layers. It is likely this same buffered rinsing concept can be used to increase thickness per bilayer of many types of

LbL assemblies. Reducing layers will result in faster deposition that should make this technique more appealing for commercial applications.

5. EXCEPTIONAL FLAME RESISTANCE AND GAS BARRIER OF THICK MULTILAYER NANOBRICK WALL THIN FILMS[3]

5.1 Introduction

Clay nanocomposite films are an attractive alternative to traditional bulk polymer films due to their enhanced mechanical strength,[158] thermal stability,[94] and gas barrier.[100] These nanocomposites have already found commercial use in food packaging[99] and in the automotive industry as sealant layers.[101] Clay nanocomposites are traditionally prepared either by melt-mixing or by in-situ polymerization of the polymer between nanoclay stacks.[102] Melt-mixing can be challenging, as the incorporation of clay platelets increases the viscosity of the melt during extrusion,[95] making it very difficult to minimize clay aggregation,[102, 116] which results in a hazy film.[25] In-situ polymerization between the nanoclay stacks reduces these drawbacks, but current technology yields nanocomposites with low clay content,[102] and the nanoclays often interfere with the polymerization.[159] Recently, layer-by-layer (LbL) assembly has proven to be a promising alternative to traditional bulk clay nanocomposites due to its ability to produce thin films with very high clay content (> 70%) and orientation.[25, 54, 160] Despite their promise, the high number of deposition steps required to produce a useful film is a significant drawback.[25, 54, 161] Recent work has focused on reducing the number of deposition steps required for desirable properties.[59] Incorporating tris buffer into the

[3] Reprinted with permission from "Exceptional Flame Resistance And Gas Barrier Of Thick Multilayer Nanobrick Wall Thin Films" by Guin, et. al, 2015. Advanced Materials Interfaces, 2, 11, Copyright 2015 by Wiley-VCH.

cationic solution promotes thicker growth with fewer bilayers,[3, 54] but a mechanism was never proposed. This is an ideal method for decreasing the number of deposition steps, as tris buffer is non-toxic and inexpensive. If the mechanism of thickening was determined, a variety of super-thick clay-based LbL films could be produced with fewer processing steps, while maintaining important properties (e.g., fire resistance, etc.).

In this work, the use of amine salts to create relatively thick LbL-assembled films, with few bilayers, was explored. Just 50 mM of tris buffer (a common amine salt) added to the cationic solution and its rinse increases the thickness of an 8 BL chitosan/clay film by an order of magnitude, while maintaining excellent clay orientation. The thickness of the film is easily modified by adjusting the amount of tris in the cationic solution, and the desirable properties of the film are maintained or improved. The amine salt in the cationic solution interacts with the dispersed anionic nanoclay,[162] encouraging stacks of clay to be deposited with each deposition. This phenomenon is independent of the cationic polyelectrolyte, so it is widely applicable to weak and strong polyelectrolytes alike. Furthermore, this tris addition is applicable to various silicate clay types, including vermiculite (VMT) and montmorillonite (MMT). Gas impermeable and flame resistant films were assembled with very few bilayers as a result of this thickening technique. For example, a 6 BL chitosan/vermiculite film assembled in 50 mM tris buffer has an oxygen permeability equivalent to SiOx[51] and has an undetectable oxygen transmission rate with 8 bilayers. A 2 BL film renders a 3.2 mm thick polystyrene sheet self-extinguishing in a flame-through test, while an 8 BL film is able to completely prevent ignition. This simple modification to the layer-by-layer

assembly process is applicable to a wide array of clay-containing systems and can make LbL processing more commercially amenable.

5.2 Experimental

5.2.1 Materials and Film Growth

Tris buffer (tris(hydroxymethyl) aminomethane), sodium chloride, hydrochloric acid, sodium hydroxide, polyethylenimine (25 kDa), poly(diallyldimethylammonium chloride) (200-350 kDa), hexylamine, methylamine, ethanolamine, diethanolamine, triethanolamine, glucose (Sigma Aldrich, St. Louis, MO), and poly(allylamine hydrochloride) (120-200 kDa, Polysciences, Inc., Warrington, PA) were all used as received. Solutions were prepared in 18 MΩ deionized (DI) water and stirred for 24 hr. Vermiculite (Microlite 630++, Specialty Vermiculite Corp., Phoenix, AZ) was diluted to a 1 wt% suspension and allowed to settle for 72 hours, and the supernatant was used for deposition. Montmorillonite (Southern Clay Products, Inc., Gonzales, TX) suspension was prepared by adding 1 wt% MMT to DI water and stirring for 24 hours. Clay suspensions were adjusted to pH 10 using 1 M NaOH prior to deposition. Chitosan (CH) (Mw ~60 kDa, G.T.C. Bio Corporation, Quingdao, China) solution was prepared by dissolving 0.1 wt% in tris buffer or DI water which was previously adjusted to pH 2 using HCl, and then adjusted to pH 6 using 1 M NaOH. Silicon wafers (single-side polished (1 0 0), University Wafer, South Boston, MA) and polished Ti/Au crystals with a resonance frequency of 5 MHz (Maxtek, Inc., Cypress, CA) were used for characterization of film growth. Films for oxygen transmission testing were deposited on

179 μm thick polyethylene terephthalate (PET) film (ST505, Dupoint-Teijin), purchased from Tekra (New Berlin, WI). Films for thermogravimetric analysis were deposited on 1.6 mm thick polypropylene (PP) sheets (VWR International, Radnor, PA) and later detached and ground using a mortar and pestle. Films for burn through testing were deposited on 3.2 mm thick polystyrene (PS) sheets (McMaster-Carr, Atlanta, GA). Cleaned PET, PP, and PS were corona treated with a BD-20C Corona Treater (Electro-Technic Products, Inc. Chicago, IL) to improve the adhesion of the first polyelectrolyte layer.

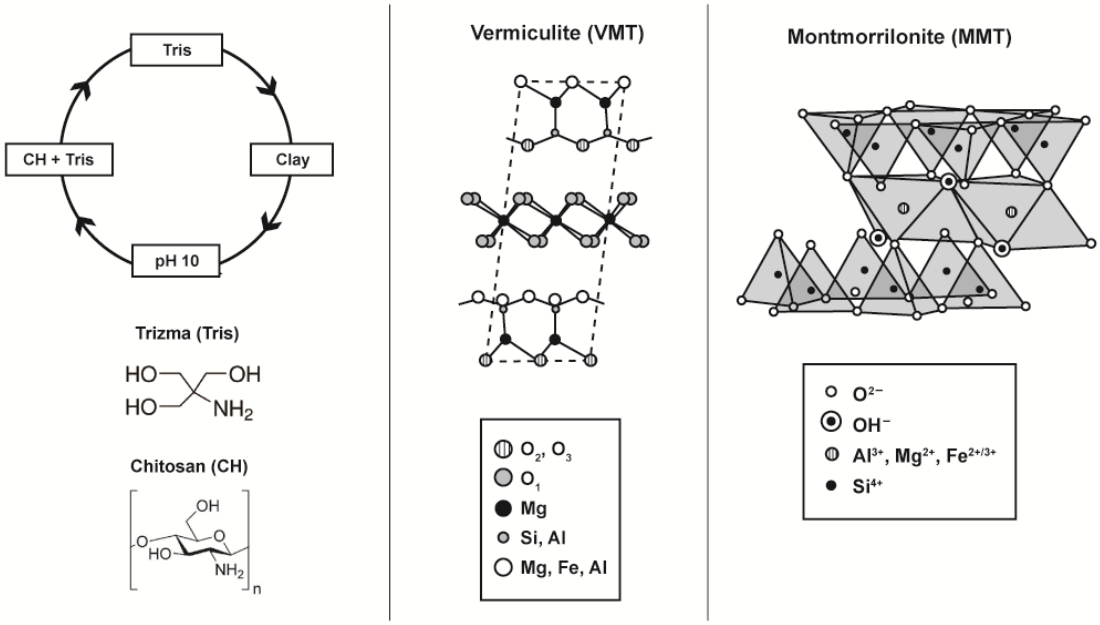

Figure 5.1. Schematic of layer-by-layer assembly using buffered cationic solution and rinse. Chemical structures of chitosan, tris buffer, vermiculite[163] and montmorillonite.[164]

Assembling these films began with dipping the substrate into the polycation solution for 1 min, then dipping for 1 min in a solution with an equivalent concentration of buffer, then dipping into the clay solution for 1 min, and finally dipping in a pH 10 NaOH solution for 1 min to complete one bilayer. It is important to note that the pH of the polyelectrolyte solutions and their associated rinses were kept identical. After all the layers were deposited, the films were rinsed thoroughly with DI water and dried at 70˚C for 24 hours. Figure 5.1 shows the LbL process and the chemical structures of the deposited components.

5.2.2 Film Characterization

Thickness of the films was measured using a P-6 profilometer (KLA-Tencor, Milpitas, CA). Silicon wafers were pretreated with a 3:1 piranha solution (Caution! Piranha solution is very corrosive) for 30 minutes, and the average thickness of the film was determined from five 0.2 mm cuts across the silicon wafer. Mass of the films was measured using a research quartz crystal microbalance (QCM) (Inficon, East Syracuse, NY). A 5 min plasma cleaning treatment using a PDC-32G plasma cleaner (Harrick Plasma, Ithaca, NY) was performed on QCM crystals prior to deposition. The clay composition of freestanding films was measured with a Q50 Thermogravimetric Analyzer (TA Instruments, New Castle, DE). Samples were heated to 950˚C at 20˚/min and held for 2 hours. A dry weight baseline was determined by heating the sample to 120˚C for 30 minutes. Samples for optical microscopy and transmission electron microscopy (TEM) were prepared by embedding the film in Epofix (EMS, Hatfield, PA)

resin overnight and cutting cross sections, using an Ultra 45° diamond knife (Diatome, Hatfield, PA), onto 300 mesh copper grids. Optical micrographs of the sections (~90 nm thick) were imaged using a Zeis Axiophot (Zeiss Microimaging, Thrnwood, NJ) microscope equipped with a 40x/0.75 Plan Neofluar objective and a Cool Snap CF (Photometrics, Tucson, AZ) CCD camera controlled by Metaview software (Media Cybernetics, Rockville, MD). TEM micrographs of the sections (~90 nm thick) were imaged using a Tecnai G2 F20 (FEI, Hillsboro, OR) at an accelerating voltage of 200kV. Samples for X-ray photoelectron spectroscopy (XPS) were prepared by mixing the buffer and clay suspension for 30 minutes, then rinsing the particles with DI water and centrifuging the suspension at 6000 RPM for 30 minutes three times. XPS spectra were taken on an ESCA+ XPS system (Oxford Instruments, Abingdon, Oxfordshire, UK) equipped with a hemispherical analyzer and 1253.6 Mg Kα source. Samples were sputtered with Ar before XPS analysis to ensure the removal of surface contaminants. N 1s scans were taken in 0.1 eV increments with 0.05 s dwell time and passing energy of 30 eV. Scans were taken 10 times and averaged. Oxygen transmission rate (OTR) of the CH+tris/VMT films was measured on 179 μm PET and performed by MOCON (Minneapolis, MN) using an Oxtran 2/21 oxygen permeability instrument (in accordance with ASTM D-3985) at 23˚C and 0% RH. Permeability of the films was determined by assuming ideal laminate theory.[51] Flame resistance (FR) of the films on 3.2 mm polystyrene sheeting was determined with a homemade flame-through test using a butane micro torch (Model ST2200, Benzomatic, Huntersville, NC).

5.3 Results and Discussion

5.3.1 Influence of Amine Salts on Growth of LbL Films

Thick growing multilayer films of chitosan and clay were initially grown on silicon wafers, and their thickness was measured using profilometry, as shown in Figure 5.2. Chitosan/clay films display a supralinear growth pattern, and the films containing vermiculite clay are thicker than films containing montmorillonite clay. This result is consistent with previous studies comparing MMT and VMT LbL films, as the higher aspect ratio VMT preferentially deposits more stacked platelets with every deposition.[25] The thickness of the chitosan/clay assembly increases further with increasing buffer concentration, irrespective of clay type, and displays a greater thickness than films deposited from solutions with equivalent concentrations of added sodium chloride. Eight bilayer MMT and VMT-containing films achieve a thickness of 2.0 and 4.3 μm with 50 mM tris added, which is over an order of magnitude greater than equivalent films deposited with no tris added. The increase in mass of these films with 50 mM added tris is also large, showing a 2000% increase in mass/area for the MMT films and a 2600% increase for the VMT films. This increase in mass confirms that more film is deposited and not that the film is simply less dense. Film thickness increases superlinearly with increasing bilayers, while the mass grows linearly, so the density of the tris-containing films decreases modestly with increasing bilayers. The clay concentration of the films was determined through thermogravimetric analysis (TGA). The clay concentration of all films is between 82 and 87 wt% clay, irrespective of the number of bilayers

deposited, which is comparable to other clay-containing LbL films. This high clay concentration is crucial for gas barrier[161] and flame resistance.[86]

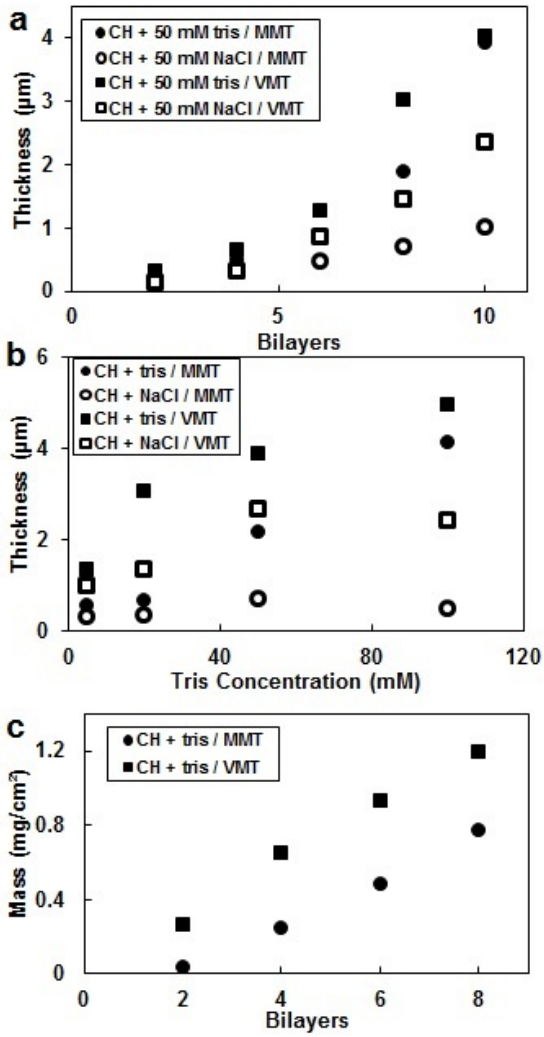

Figure 5.2. Film thickness as a function chitosan (CH) and montmorillonite (MMT) or vermiculite (VMT) bilayers deposited with 50 mM of tris buffer or sodium chloride added (a). Film thickness as a function of added tris buffer or sodium chloride for an eight bilayer chitosan/nanoclay film (b), and mass/area of CH+tris/nanoclay films as a function of bilayers deposited with 50 mM tris added (c).

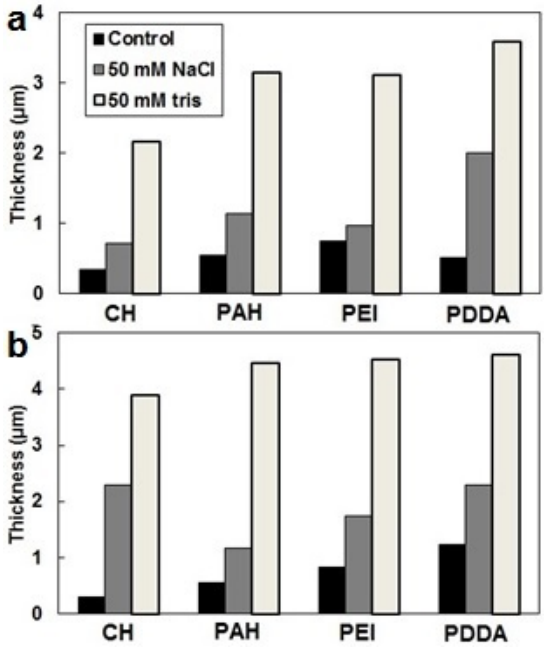

Figure 5.3. Thickness of films assembled from chitosan [CH], poly(allylamine hydrochloride) [PAH], polyethylenimine [PEI], or poly(diallyldimethyl ammonium chloride) [PDDA] and montmorillonite (a) or vermiculite clay (b).

To better understand the thickening mechanism of tris, three cationic polyelectrolytes were evaluated: poly(allylamine hydrochloride) (PAH), polyethylenimine (PEI), or poly(diallyl dimethyl ammonium chloride) (PDDA). The thickness of films deposited from each of these polymers with 50 mM tris added, and either MMT or VMT, at 8 bilayers is shown in Figure 5.3. For all tested polycations and clay types explored, tris shows a significant thickening effect, even when compared to sodium chloride. Added sodium chloride is known to produce thicker films, primarily due to charge screening.[18] Despite the tested polycations having vastly different deposition thicknesses, added tris markedly increased the film thickness. As the increase

in thickness appears to be independent of cationic polylectrolyte, it is likely that the tris is interacting with the nanoclay.

In an effort to confirm that the thickening phenomenon is dependent on the identity of the added salt, 8 BL chitosan/clay films were grown with a variety of potential thickeners, as shown in Table 5.1. The differences in film thickness with the various thickening agents are extreme, and are highly dependent on the nanoclay. While sodium chloride produced thicker films as expected, several amine salts had a much greater thickening effect, similar to tris. The thickest films containing MMT or VMT were deposited from solutions containing hexylamine. Previous studies have shown that akylamines, such as hexylamine, interact with the surface of nanoclays,[162, 165] increasing the spacing between the nanoclay stacks. This phenomenon has been shown to facilitate intercalation of polymer between dispersed nanoclay,[166-167] enabling more interactions between clay stacks. It is likely that during the layer-by-layer deposition process, the thickening agent interacts with the nanoclay, allowing cationic polyelectrolyte from the preceding layer to diffuse between the nanoclay, causing multiple stacks of clay to be deposited in a single deposition.

The nature of the interaction between tris and the nanoclay platelets was evaluated using X-ray photoelectron spectroscopy (XPS) to determine if tris was bound to the surface of the clay platelets after clay and tris buffer were mixed and rinsed thoroughly with DI water using centrifugation. The tris buffer was prepared as if to dissolve chitosan, so it contained hydrochloric acid and sodium hydroxide. Neat MMT clay is composed primarily of silicon, oxygen, and magnesium, and the surface is

sodium.[165-166] When MMT clay is mixed with tris buffer and rinsed, nitrogen and carbon appear on the surface of the clay, and sodium disappears, suggesting that there is surface-bound tris. Primary amine salts are known to bind to the surface of MMT clays, usually exchanging cations with the clay.[165] Neat VMT clay showed no nitrogen on the surface. Vermiculite is primarily composed of magnesium, aluminum, oxygen, and silicon, with a potassium surface.[163] When tris is added to the dispersed VMT, no nitrogen is found on the surface of the clay, indicating that there was no detectable surface-bound tris, but sodium appears when tris is added (most likely from the sodium hydroxide used to adjust the tris buffer), and the potassium signal decreases slightly, which indicates a possible cation exchange. Previous studies report that VMT clay preferentially exchanges potassium with sodium,[165] so it is possible that the sodium preferentially exchanges with the surface charge sites over the tris. This may explain the large increase in film thickness of VMT films deposited with sodium chloride.

Table 5.1. Thickness of 8 BL CH/MMT or CH/VMT films assembled with 50 mM of various thickening agents.

	Thickness (nm)	
Thickening Agent	MMT	VMT
Control	350	290
Glucose	340	270
Ammonium Chloride	540	1430
Sodium Chloride	720	2300
Methylamine	830	1000
Ethanolamine	910	2640
Triethanolamine	950	5900
Diethanolamine	2050	3210
Tris	2170	3900
Hexylamine	5190	10660

5.3.2 Structure of Thick Nanobrick Wall Thin Films

Optical and TEM micrographs of the multilayer nanobrick wall thin films on PET were used to clarify their structure. Dark and light bands are visible in the optical micrographs, as shown in Figure 5.4, indicating that the films are composed of large bands of varying composition. The light bands are layers of primarily chitosan, and the dark bands are layers of primarily clay. The thickness of the bands roughly corresponds to the thickness of the bilayers measured by profilometry, suggesting that the bands are most likely individually deposited layers. Typical nanobrick wall films contain mostly single layers of nanoclay separated by polymer,[56] but the addition of tris causes hundreds of clay platelet layers to be deposited with each bilayer. The TEM micrograph of the outermost surface shows well-aligned clay platelets (Figure 5.4b). Even though hundreds

of nanoplatlets are deposited with each deposition, the nanoclay stacks orient themselves parallel to the surface. A single bilayer of CH+tris/VMT appears to be comprised of many polymer/clay bilayers (Figure 5.4d). These well-aligned clay platelets contribute to the extremely high gas barrier and flame resistance exhibited by these thin films.[25, 54]

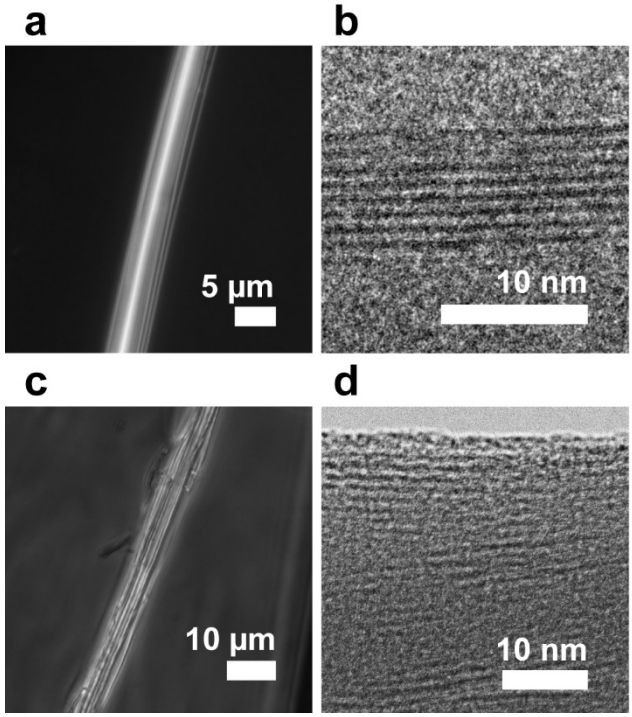

Figure 5.4. Phase contrast optical micrograph (a) and outside edge TEM micrograph of the cross-section of an 8 BL CH+tris/MMT film deposited on PET (b). Optical micrograph of the cross-section of an 8 BL CH+tris/VMT film on PET (c), and TEM micrograph of a 1 BL film (d).

5.3.3 Oxygen Barrier of Thick Nanobrick Wall Thin Films

Polymer/clay films deposited on PET exhibit a very high oxygen barrier and correspondingly low permeability, as shown in Figure 5.5. An 8 BL CH+tris/VMT film has an oxygen transmission rate (OTR) below the detection limit of the instrument (0.005 cc/m^2·day·atm). The high oxygen barrier of these films is due to the tortuous path taken by oxygen molecules between the highly-aligned clay platelets.[25, 56] High clay concentration in these nanocomposites results in a low gas permeability, as there is very little polymer for the oxygen to permeate through. A 6 BL CH+tris/MMT film, decoupled from its PET substrate, has an oxygen permeability of 4.0 x 10^{-20} cc·cm/cm^2·Pa·sec. With VMT replacing MMT, the same 6 BL film has an oxygen permeability of 2.7 x 10^{-20} cc·cm/cm^2·Pa·sec, both of which are comparable to the permeability of an SiO_x thin film.[156]

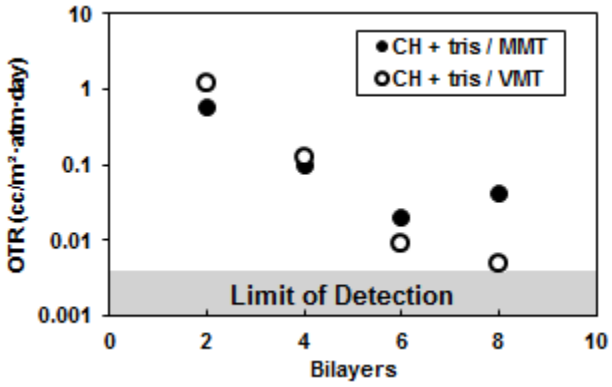

Figure 5.5. Oxygen transmission rate of chitosan/nanoclay films assembled in 50 mM tris

5.3.4 Flame Resistance of Thick Nanobrick Wall Thin Films

The thick growing nanobrick wall thin films display excellent fire resistance, completely preventing a 3.2 mm polystyrene (PS) plate from igniting in a flame-through test with an 8 BL CH+tris/MMT or CH+tris/VMT coating. A small black char is observed where the flame of the torch touched the PS plate, but the substrate underneath did not ignite, as shown in Figure 5.6. The flame-through test aggressively attacks a small area of the substrate, igniting polystyrene in less than 2 sec and ultimately consuming the uncoated substrate completely. With just 2 BL of CH+tris/VMT, or 3 BL CH+tris/MMT, the PS plate self-extinguishes when the torch is removed. Polystyrene produces thick black smoke when burned, and a single bilayer of the thick-growing nanobrick wall thin film dramatically reduces the smoke produced. As the flame from the torch melts the PS underneath the nanocoating, the nanobrick wall collapses and chars, creating a shield that smothers the fire.[86] The excellent fire resistance of nanobrick wall multilayer thin films is partly linked to their extremely high gas barrier. The clay stacks are intercalated with chitosan, which preferentially chars,[168] and the resulting clay-filled char prevents pyrolysis gases from escaping and oxygen from entering.[86, 96] Additionally, the high clay loading of the films acts as thermal insulation, preventing the heat of the fire from igniting the underlying substrate.[86] Due to the thickness of these layers, low surface area substrates can be effectively rendered flame retardant with thick-growing layer-by-layer assembly, when conventional LbL assembly would not be effective without a prohibitive number of layers.

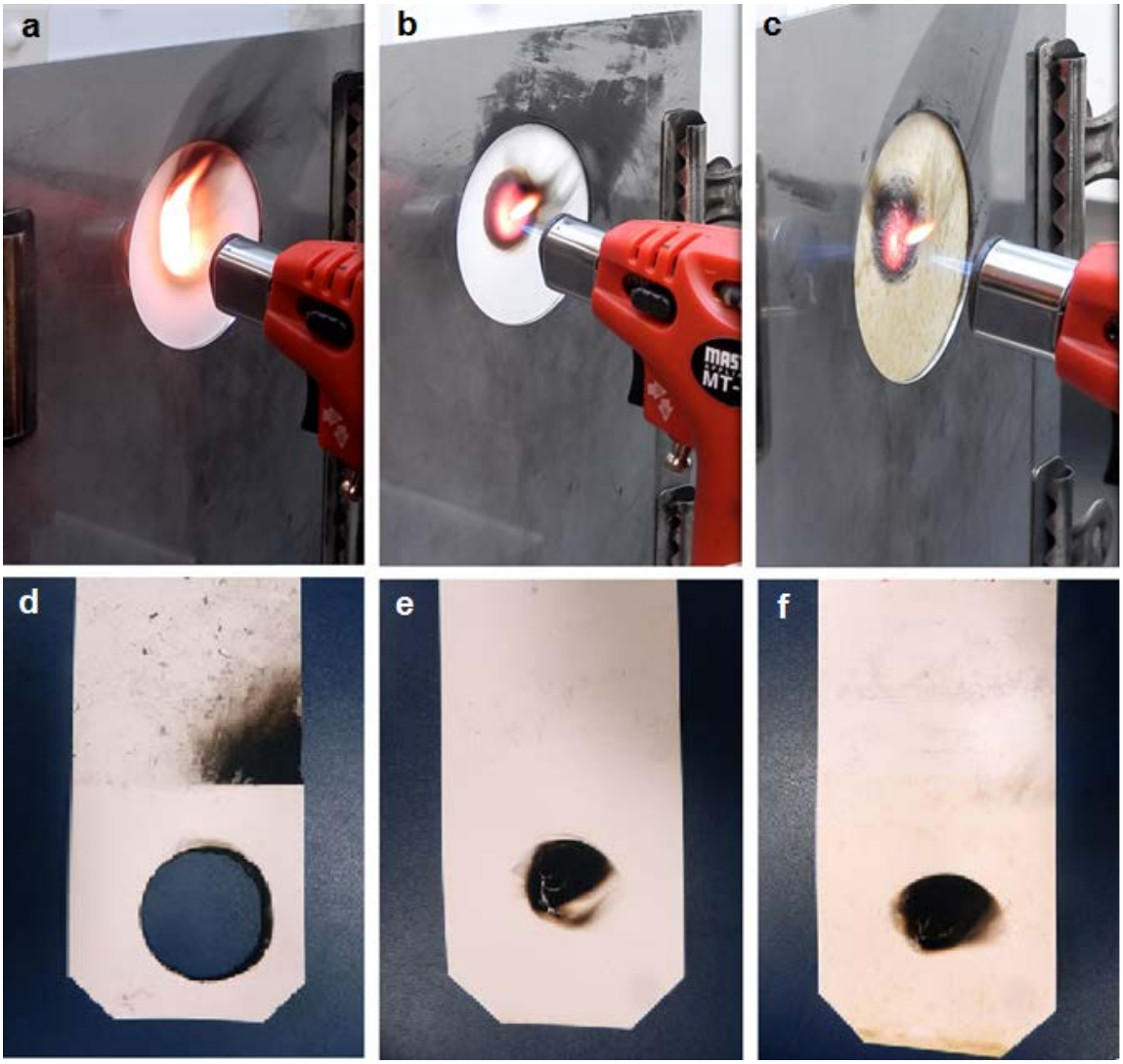

Figure 5.6. Pictures of flame-through torch test 5 sec after ignition of 3.2 mm thick polystyrene plates: control (a), 8 BL CH+tris/MMT film added (b), or 8 BL CH+tris/VMT film added (c). Pictures of the polystyrene plates after 10 sec flame-through torch test of the control (d), with a 3 BL CH+tris/MMT film added (e), or with a 2 BL CH+tris/VMT film added (f).

5.4 Conclusions

Layer-by-layer assembled coatings were deposited from solutions containing tris buffer in the polycation solution (and rinse) to greatly increase the thickness of the resultant films. Just 50 mM of added tris buffer increases the thickness and mass of an 8 bilayer chitosan/clay film by over an order of magnitude, achieving 3.9 μm with VMT clay. XPS analysis provides evidence of surface modification of the nanoclay by tris, which stabilizes the nanoplatelet stacks during deposition. This phenomenon is observed in both montmorrilonite and vermiculite clay sytems and is likely to work with other types of silicate nanoparticles. Furthermore, a variety of amine salts (e.g., hexylamine) were shown to produce the same (or greater) thickening effects. These films display impressive gas barrier and flame retardant properties with very few bilayers. For example, a 6 BL chitosan/vermiculite film assembled with 50 mM tris buffer has an oxygen permeability equivalent to SiO_x thin films. A 2 bilayer film renders a 3.2 mm thick polystyrene plate self-extinguishing in a flame-through test, while an 8 bilayer film is able to completely prevent ignition. This simple modification to the layer-by-layer assembly process provides an important tool for depositing functional mutilayer films much faster than traditional LbL assembly (due to fewer deposition steps needed).

6. CONCLUSIONS AND FUTURE WORK

6.1 Improving Layer-by-Layer Assembly for Superior Gas Barrier and Flame Retardant Thin Films

The goal of this dissertation was to investigate methods to improve layer-by-layer assembly to produce more effective multifunctional thin films in a more efficient manner. Through multiple methods, such as rinsing with ultrasonication in between deposition steps or utilizing amine salts, the quality of the assembled films was improved and the number of steps to achieve desirable properties was reduced. This work demonstrates the potential of layer-by-layer assembly as a commercially viable processing technique.

6.1.1 Maintaining Hand and Improving Fire Resistance of Cotton Fabric through Ultrasonication Rinsing of Multilayer Nanocoating (Section 3)

The effects of sonication during the rinsing step of layer-by-layer deposition were explored in an effort to produce soft, flame retardant cotton fabric. Multilayer nanocoatings of chitosan and poly(sodium phosphate) were applied to cotton fabric and acted as an intumescent flame retardant. Rinsing with ultrasonication reduced the weight required to pass a vertical flame test by half and produced a much softer fabric, as fiber bridging was largely eliminated. Incorporating sonication into layer-by-layer assembly is a simple modification that improves the coating performance of layer-by-layer films on complex substrates, while sacrificing none of its desirable qualities (e.g., soft hand). It is

believed that this procedure could be used with any type of fabric (e.g., nylon, polyester, etc.) to achieve similar improvement, making this a commercially viable treatment.

6.1.2 Thick Growing Multilayer Nanobrick Wall Thin Films: Super Gas Barrier with Very Few Layers (Section 4)

Thick-growing polymer/clay layer-by-layer films were assembled using a buffered rinsed step. These nanobrick wall films contained over 87 wt% clay and their thickness could be tailored by altering the buffer concentration. Despite the increase in thickness, the characteristic order of layer-by-layer films was maintained (monitored with TEM). The oxygen barrier of these films was extremely high, achieving an oxygen transmission rate of 0.009 $cc/m^2 \cdot day \cdot atm$ with only 6 bilayers. These easily fabricated multilayer nanocomposites provide an inexpensive, environmentally-benign alternative to current barrier layers. The reduction in required layers makes this technique more appealing for commercial production.

6.1.3 Exceptional Flame Resistance and Gas Barrier with Thick Multilayer Nanobrick Wall Thin Films (Section 5)

It was found that the incorporation of amine salts in the cationic solution and rinse greatly increases the thickness of thick-growing polymer/clay layer-by-layer films. Just 50 mM of added tris buffer increases the thickness and mass of an 8 BL chitosan/clay film by over an order of magnitude, achieving 3.9 μm with vermiculite clay. XPS analysis provides evidence of surface modification of the nanoclay by tris,

which potentially stabilizes the nanoplatelet stacks during deposition. This phenomenon is observed in both montmorillonite and vermiculite clay systems and is likely to work with other types of silicate nanoparticles. Furthermore, a variety of amine salts (e.g., hexylamine) were shown to produce the same (or greater) thickening. These films display impressive gas barrier and flame retardant properties with very few bilayers. A 6 bilayer chitosan/vermiculite film, assembled with 50 mM tris buffer, has an oxygen permeability equivalent to SiO_x thin films. Additionally, a two bilayer film renders a 3.2 mm thick polystyrene plate self-extinguishing in a flame-through test, while an eight bilayer film is able to completely prevent ignition. This simple modification to the layer-by-layer assembly process provides an important tool for depositing functional multilayer films much faster than traditional LbL assembly.

6.2 Future Studies

In the previous sections it was shown that layer-by-layer assembly can be improved to create higher quality films with fewer processing steps. There still remains a great deal of potential for bringing layer-by-layer assembly to commercial viability. Improvements in industrial-scale film application and improvements in the real-world application of the films are needed for these films to become practical alternatives to conventional thin films. Three-dimensional substrates pose a great challenge for industrial scale-up, and there are currently no good methods for applying layer-by-layer films to such substrates (e.g., open-celled polyurethane foam). Additionally, these films suffer from poor chemical durability, especially in basic conditions, which makes them

unsuitable for a wide variety of applications. Finally, the thickening mechanism presented in sections 4 and 5 has unexplored potential to create free-standing films for a variety of applications.

6.2.1 Large Scale Through-Flow Layer-by-Layer Coater

Previous work on scaling the production of layer-by-layer films have involved two dimensional substrates, such as plastic sheeting or woven mats,[169] or thin substrates, such as light-weight cotton fabric.[16, 170] These substrates are ideal for steady-state processing due to prior advancements in the textile and sheeting industries.[6] However, there has been no method proposed to apply layer-by-layer films to complex 3-dimensional substrates, such as polyurethane foam, at an industrial scale.[6] These substrates pose a unique challenge to coat, as the film must penetrate the entirety of the substrate for properties to be effectively applied.[7, 53, 171]

It is possible to coat these 3-D substrates by alternately pumping polyelectrolyte solutions through the void volume of the substrate, keeping the substrate stationary. The pore surfaces of the substrate are put in contact with the solutions when the substrate is filled with the solution. A rendering of a machine capable of performing this is shown in Figure 6.4. This method of applying multilayer films has the added advantage of causing no damage to the substrate. Current research methods requires squeezing, wringing, or smashing the substrate to rinse it thoroughly.[7, 53] Preliminary results with open-celled polyurethane foam show that the rinsing using flowing water removes 98% as much excess solution as hand rinsing and wringing. Air drying can be accomplished in a

closed space to remove almost all retained solutions or rinse water. This method, though a batch process, is nearly infinitely-scalable, which makes it a viable method for applying nanofilms on an industrial scale.

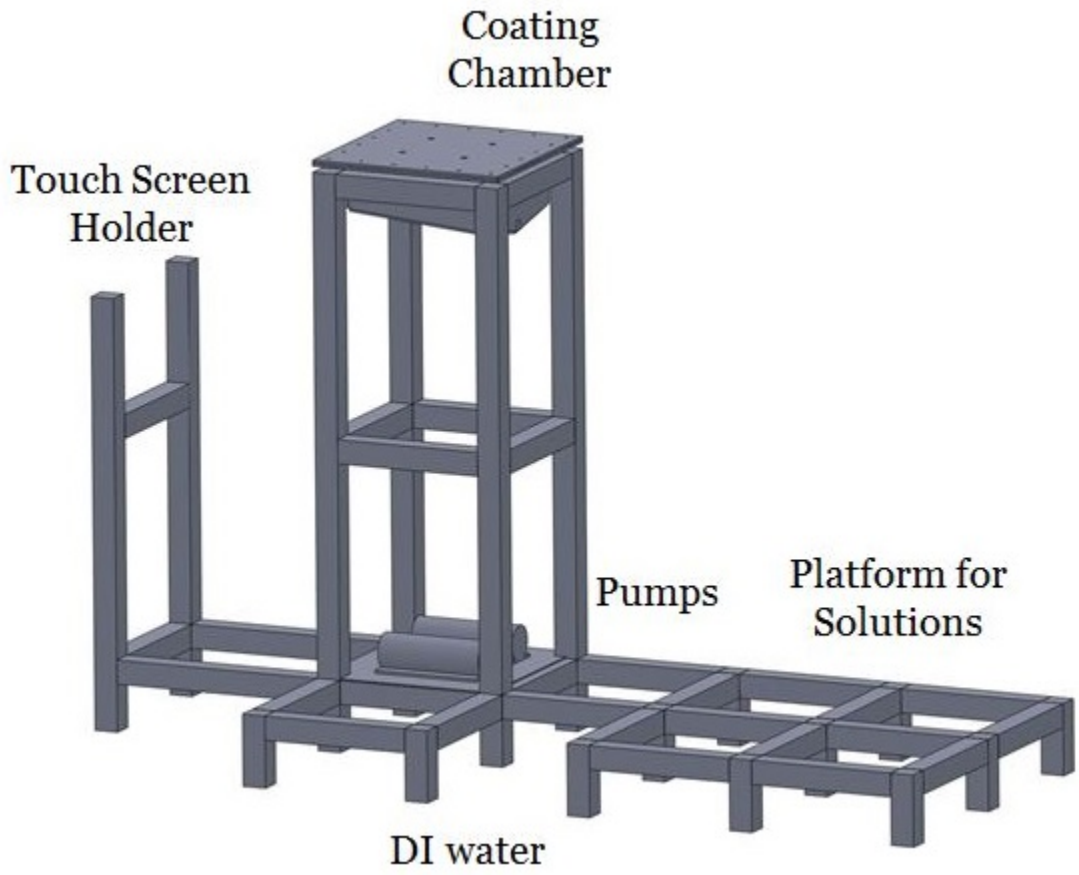

Figure 6.1. Rendering of a large-scale through-flow layer-by-layer coater. The substrate is held stationary in the coating chamber.

6.2.2 Leak Detection for Chemically and Mechanically Durable Gas Barrier Thin Films

Sections 4 and 5 describe nanoclay-based layer-by-layer films which are excellent barriers to oxygen. Previous work has described layer-by-layer films composed of polymer and graphene oxide (GO), which are also capable of blocking oxygen.[9, 114] Graphene oxide is a multi-functional organic platelet which is readily dispersible in water,[172-173] and can be easily reduced to conductive reduced graphene oxide (rGO).[174-175] Previous research has shown that rGO can be assembled into impermeable, conductive films via layer-by-layer assembly.[114] From this work, it is reasonable to assume that LbL films from poly(vinylamine) (PVAm) and rGO might have excellent gas barrier and act as a semiconductor. PVAm is readily crosslinkable,[176-177] with glutaraldehyde quickly reacting with the primary amines of PVAm to generate Schiff base crosslinks.[177-178] These Schiff bases are readily reduced to relatively stable secondary amines with sodium borohydride.[178-179] Preliminary results show that crosslinked PVAm / rGO LbL films are not removed from the substrate when gently abraded during exposure to strong acids, oxidizing agents, reducing agents, organic solvents, or brine. With conventional gas detection methods, small leaks in LbL films are very slow to be detected due to their low permeability.[180-181] As the electrical resistance of PVAm / rGO films responds dramatically to small flaws in the film, small pinholes can be detected immediately. Preliminary tests show that even defects which do not penetrate the entire film can be readily detected. Additionally, the two-dimensional nature of the rGO-based films allows for the location of the leak to be detected using two

separate resistivity meters and basic correlative software. A table of raw data for electrical resistance as a function of leak location is shown in Table 6.1.

Table 6.1. Point-to-point increase in electrical resistance of PVAm / rGO as a function of scratch location. The electrical resistance is normalized against the unscratched film.

	Change in Resistance Between Points			
Scratch Location	2-4	4-6	6-8	8-2
2-8	1%	1%	2%	12%
4-6	3%	21%	2%	2%
2-8	2%	3%	2%	9%
4-6	2%	17%	2%	2%
Full Length 8	0%	0%	45%	41%

6.2.3 Free-Standing Thick Growing Graphene Oxide Nanobrick Wall Thin Films

As described in section 6.2.2, graphene oxide (GO) is an extremely versatile organic nanoplatelet that has shown promise as a component in LbL assembly.[114, 172-173, 175] These GO-based films have extremely high electrical capacitance,[14] low gas barrier,[9, 114] and high modulus, but are unsuitable for scale-up into bulk materials due to their extreme thinness (< 6 nm/bilayer).[14, 114] Preliminary results show that tris buffer has a thickening effect on GO-based films in a similar manner to clay-based films,[3, 54] as shown in Figure 6.5. Chitosan (CH) is an ideal choice for these films due to its low toxicity and cost.[182] Preliminary results show that CH / GO films deposited from 50 mM tris solutions are over 10 times thicker than conventional GO-based LbL films.[9, 14, 114, 183-184] Given recent advancements in large-scale steady-state LbL coaters, it should be

possible to create free-standing graphene oxide-based LbL films which can be used for a wide variety of applications, such as supercapacitors,[183-184] biomedical materials,[185-186] or ultra-high strength composites.[185, 187-188] Incorporating amine-salts could realize the first mass-produced free-standing LbL-based material.

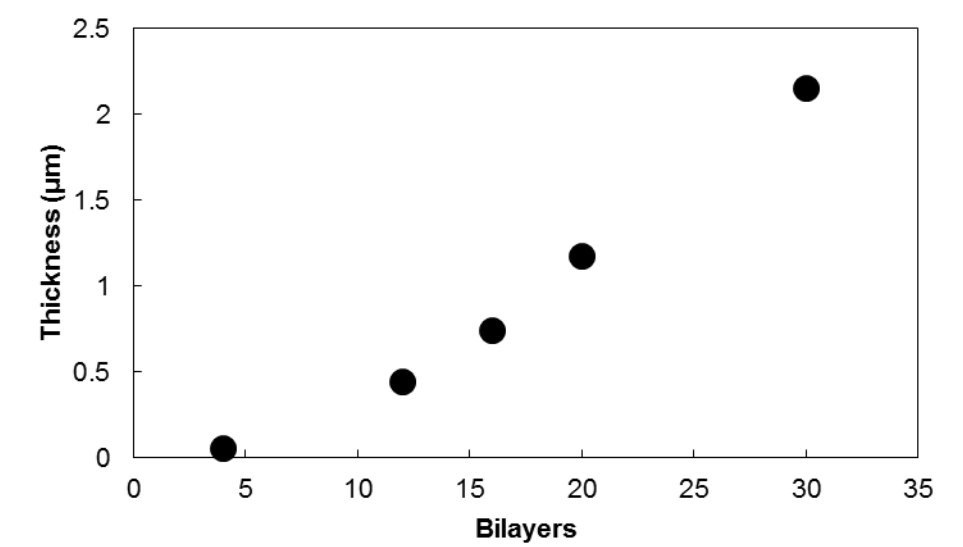

Figure 6.2. Film thickness as a function of bilayers deposited for CH+tris/GO thin films.

REFERENCES

1. Decher, G.; Schlenoff, J., *Multilayer Thin Films*. Wiley-VCH: Weinheim, Germany, **2012**; Vol. 1.

2. Decher, G.; Hong, J. D.; Schmitt, J., Buildup of ultrathin multilayer films by a self-assembly process: III. Consecutively alternating adsorption of anionic and cationic polyelectrolytes on charged surfaces. *Thin Solid Films* **1992,** *210/211*, 831-835.

3. Guin, T.; Krecker, M.; Hagen, D. A.; Grunlan, J. C., Thick growing multilayer nanobrick wall thin films: Super gas barrier with very few layers. *Langmuir* **2014,** *30* (24), 7057-60.

4. Joshi, M.; Khanna, R.; Shekhar, R.; Jha, K., Chitosan nanocoating on cotton textile substrate using layer-by-layer self-assembly technique. *Journal of Applied Polymer Science* **2011,** *119* (5), 2793-2799.

5. Bertrand, P.; Jonas, A.; Laschewsky, A.; Legras, R., Ultrathin polymer coatings by complexation of polyelectrolytes at interfaces: suitable materials, structure and properties. *Macromolecular Rapid Communications* **2000,** *21* (7), 319-348.

6. Richardson, J. J.; Bjornmalm, M.; Caruso, F., Multilayer assembly. Technology-driven layer-by-layer assembly of nanofilms. *Science* **2015,** *348* (6233), aaa2491.

7. Cain, A. A.; Nolen, C. R.; Li, Y.-C.; Davis, R.; Grunlan, J. C., Phosphorous-filled nanobrick wall multilayer thin film eliminates polyurethane melt dripping and reduces heat release associated with fire. *Polymer Degradation and Stability* **2013,** *98* (12), 2645-2652.

8. Yang, Y.-H.; Bolling, L.; Haile, M.; Grunlan, J. C., Improving oxygen barrier and reducing moisture sensitivity of weak polyelectrolyte multilayer thin films with crosslinking. *RSC Advances* **2012,** *2* (32), 12355.

9. Yang, Y. H.; Bolling, L.; Priolo, M. A.; Grunlan, J. C., Super gas barrier and selectivity of graphene oxide-polymer multilayer thin films. *Advanced Materials* **2013,** *25* (4), 503-8.

10. Dubas, S. T.; Kumlangdudsana, P.; Potiyaraj, P., Layer-by-layer deposition of antimicrobial silver nanoparticles on textile fibers. *Colloids and Surfaces A: Physicochemical and Engineering Aspects* **2006,** *289* (1-3), 105-109.

11. Dawidczyk, T. J.; Walton, M. D.; Jang, W.-S.; Grunlan, J. C., Layer-by-layer assembly of UV-resistant poly(3,4-ethylenedioxythiophene) thin films. *Langmuir* **2008,** *24*, 8314-8318.

12. Eshaghi, A.; Mojab, M., Fabrication of antireflective antifogging nano-porous silica thin film on glass substrate by layer-by-layer assembly method. *Journal of Non-Crystalline Solids* **2014,** *405*, 148-152.

13. Nuraje, N.; Asmatulu, R.; Cohen, R. E.; Rubner, M. F., Durable antifog films from layer-by-layer molecularly blended hydrophilic polysaccharides. *Langmuir* **2011,** *27* (2), 782-91.

14. Sarker, A. K.; Hong, J.-D., Electrochemical reduction of ultrathin graphene oxide/polyaniline films for supercapacitor electrodes with a high specific capacitance. *Colloids and Surfaces A: Physicochemical and Engineering Aspects* **2013,** *436*, 967-974.

15. Priolo, M. A.; Gamboa, D.; Holder, K. M.; Grunlan, J. C., Super gas barrier of transparent polymer-clay multilayer ultrathin films. *Nano Letters* **2010,** *10* (12), 4970-4.

16. Mateos, A. J.; Cain, A. A.; Grunlan, J. C., Large-scale continuous immersion system for layer-by-layer deposition of flame retardant and conductive nanocoatings on fabric. *Industrial & Engineering Chemistry Research* **2014,** *53* (15), 6409-6416.

17. Xiang, F.; Givens, T. M.; Grunlan, J. C., Fast spray deposition of super gas barrier polyelectrolyte multilayer thin films. *Industrial & Engineering Chemistry Research* **2015,** *54* (19), 5254-5260.

18. Borges, J.; Mano, J. F., Molecular interactions driving the layer-by-layer assembly of multilayers. *Chemical Reviews* **2014,** *114* (18), 8883-942.

19. Li, Y. C.; Mannen, S.; Morgan, A. B.; Chang, S.; Yang, Y. H.; Condon, B.; Grunlan, J. C., Intumescent all-polymer multilayer nanocoating capable of extinguishing flame on fabric. *Advanced Materials* **2011,** *23* (34), 3926-31.

20. Cole, R. Process for the Flame-Retardant Treatment of Textiles. 5942006, **1999**.

21. Sabic Coated Films. http://sfs.sabic.eu/product/lexan-film/coated-films/ (accessed March 28).

22. Reporter, D. M. Drive for the mist-free windscreen: New coating could make scraping ice from the glass a thing of the past, say scientists. http://www.dailymail.co.uk/sciencetech/article-2288268/Drive-mist-free-windscreen-New-coating-make-scraping-ice-glass-thing-past-say-scientists.html (accessed March 28).

23. Rocha, J. Innovation Spotlight: Svaya Molecular Layer Deposition. http://www.nsti.org/news/entry.html?id=144 (accessed March 28).

24. Laufer, G.; Kirkland, C.; Cain, A. A.; Grunlan, J. C., Oxygen barrier of multilayer thin films comprised of polysaccharides and clay. *Carbohydrate Polymers* **2013,** *95* (1), 299-302.

25. Priolo, M. A.; Holder, K. M.; Greenlee, S. M.; Grunlan, J. C., Transparency, gas barrier, and moisture resistance of large-aspect-ratio vermiculite nanobrick wall thin films. *ACs Applied Materials & Interfaces* **2012,** *4* (10), 5529-33.

26. Guin, T.; Krecker, M.; Milhorn, A.; Grunlan, J. C., Maintaining hand and improving fire resistance of cotton fabric through ultrasonication rinsing of multilayer nanocoating. *Cellulose* **2014,** *21* (4), 3023-3030.

27. Iler, R. K., Multilayers of Colloidal Particles. *Journal Of Colloid And Interface Science* **1966,** *21*, 569-594.

28. DeLongchamp, D. M.; Kastantin, M.; Hammond, P. T., High-contrast electrochromism from layer-by-layer polymer films. *Chemistry of Materials* **2003,** *15*, 1576-1586.

29. Shukla, A.; Fuller, R. C.; Hammond, P. T., Design of multi-drug release coatings targeting infection and inflammation. *Journal of Controlled Release* **2011,** *155* (2), 159-66.

30. Ogawa, T.; Ding, B.; Sone, Y.; Shiratori, S., Super-hydrophobic surfaces of layer-by-layer structured film-coated electrospun nanofibrous membranes. *Nanotechnology* **2007,** *18* (16), 165607.

31. Dotzauer, D. M.; Dai, J. H.; Sun, L.; Bruening, M. L., Catalytic membranes prepared using layer-by-layer adsorption of polyelectrolyte/metal nanoparticle films in porous supports. *Nano Letters* **2006,** *6* (10), 2268-2272.

32. Dubas, S. T.; Schlenoff, J. B., Factors controlling the growth of polyelectrolyte multilayers. *Macromolecules* **1999,** *32* (24), 8153-8160.

33. Hagen, D. A.; Saucier, L.; Grunlan, J. C., Controlling effective aspect ratio and packing of clay with pH for improved gas barrier in nanobrick wall thin films. *ACS Applied Materials & Interfaces* **2014,** *6* (24), 22914-9.

34. Findenig, G.; Kargl, R.; Stana-Kleinschek, K.; Ribitsch, V., Interaction and structure in polyelectrolyte/clay multilayers: a QCM-D study. *Langmuir* **2013,** *29* (27), 8544-53.

35. Tan, H. L.; McMurdo, M. J.; Pan, G. Q.; Van Patten, P. G., Temperature dependence of polyelectrolyte multilayer assembly. *Langmuir* **2003,** *19* (22), 9311-9314.

36. Yang, Y. H.; Malek, F. A.; Grunlan, J. C., Influence of deposition time on layer-by-layer growth of clay-based thin films. *Industrial & Engineering Chemistry Research* **2010,** *49* (18), 8501-8509.

37. Nolte, A. J.; Treat, N. D.; Cohen, R. E.; Rubner, M. F., Effect of relative humidity on the Young's modulus of polyelectrolyte multilayer films and related nonionic polymers. *Macromolecules* **2008,** *41* (15), 5793-5798.

38. Gamboa, D.; Priolo, M. A.; Ham, A.; Grunlan, J. C., Note: Influence of rinsing and drying routines on growth of multilayer thin films using automated deposition system. *The Review Of Scientific Instruments* **2010,** *81* (3), 036103.

39. Israelachvili, Y. K. J., Effect of pH and Salt on the Adsorption and Interactions of an Amphoteric Polyelectrolyte. *Macromolecules* **1992,** *25*, 5081-5088.

40. Losche, M.; Schmitt, J.; Decher, G.; Bouwman, W. G.; Kjaer, K., Detailed structure of molecularly thin polyelectrolyte multilayer films on solid substrates as revealed by neutron reflectometry. *Macromolecules* **1998,** *31*, 8893-8906.

41. Zhang, H.; Wang, D.; Wang, Z.; Zhang, X., Hydrogen bonded layer-by-layer assembly of poly(2-vinylpyridine) and poly(acrylic acid): Influence of molecular weight on the formation of microporous film by post-base treatment. *European Polymer Journal* **2007,** *43* (7), 2784-2791.

42. Liang, Z.; Dzienis, K. L.; Xu, J.; Wang, Q., Covalent layer-by-layer assembly of conjugated polymers and CdSe nanoparticles: Multilayer structure and photovoltaic properties. *Advanced Functional Materials* **2006,** *16* (4), 542-548.

43. Shimazaki, Y.; Mitsuishi, M.; Ito, S.; Yamamoto, M., Preparation of the layer-by-layer deposited ultrathin film based on the charge-transfer interaction. *Langmuir* **1997,** *13*, 1385-1387.

44. Altman, M.; Shukla, A. D.; Zubkov, T.; Evmenenko, G.; Dutta, P.; Boom, M. E. v. d., Controlling structure from the bottom-up: structural and optical properties of layer-by-layer assembled palladium coordination-based multilayers. *JACS* **2006,** *128*, 7374-7382.

45. Xiang, F.; Ward, S. M.; Givens, T. M.; Grunlan, J. C., Structural tailoring of hydrogen-bonded poly(acrylic acid)/poly(ethylene oxide) multilayer thin films for reduced gas permeability. *Soft Matter* **2015,** *11* (5), 1001-7.

46. Holder, K. M.; Priolo, M. A.; Secrist, K. E.; Greenlee, S. M.; Nolte, A. J.; Grunlan, J. C., Humidity-responsive gas barrier of hydrogen-bonded polymer–clay multilayer thin films. *The Journal of Physical Chemistry C* **2012,** *116* (37), 19851-19856.

47. Caruso, F.; Trau, D.; Mohwald, H.; Renneberg, R., Enzyme encapsulation in layer-by-layer engineered polymer multilayer capsules. *Langmuir* **2000,** *16* (4), 1485-1488.

48. Zhang, Y.; He, H.; Gao, C.; Wu, J., Covalent layer-by-layer functionalization of multiwalled carbon nanotubes by click chemistry. *Langmuir* **2009,** *25* (10), 5814-24.

49. Buck, M. E.; Zhang, J.; Lynn, D. M., Layer-by-layer assembly of reactive ultrathin films mediated by click-type reactions of poly(2-alkenyl azlactone)s. *Advanced Materials* **2007,** *19* (22), 3951-3955.

50. Hammond, P. T., Building biomedical materials layer-by-layer. *Materials Today* **2012,** *15* (5), 196-206.

51. Roberts, A. P.; Henry, B. M.; Sutton, A. P.; Grovenor, C. R. M.; Briggs, G. A. D.; Miyamoto, T.; Kano, M.; Tsukahara, Y.; Yanaka, M., Gas permeation in silicon-oxide/polymer (SiOx/PET) barrier films: role of the oxide lattice, nano-defects and macro-defects. *Journal of Membrane Science* **2002,** *208*, 75-88.

52. Wohl, B. M.; Engbersen, J. F., Responsive layer-by-layer materials for drug delivery. *Journal of Controlled Release* **2012,** *158* (1), 2-14.

53. Laufer, G.; Kirkland, C.; Cain, A. A.; Grunlan, J. C., Clay-chitosan nanobrick walls: completely renewable gas barrier and flame-retardant nanocoatings. *ACS Applied Materials & Interfaces* **2012,** *4* (3), 1643-9.

54. Apaydin, K.; Laachachi, A.; Ball, V.; Jimenez, M.; Bourbigot, S.; Toniazzo, V.; Ruch, D., Polyallylamine–montmorillonite as super flame retardant coating assemblies by layer-by layer deposition on polyamide. *Polymer Degradation and Stability* **2013,** *98* (2), 627-634.

55. Jang, W.-S.; Rawson, I.; Grunlan, J. C., Layer-by-layer assembly of thin film oxygen barrier. *Thin Solid Films* **2008,** *516* (15), 4819-4825.

56. Priolo, M. A.; Holder, K. M.; Greenlee, S. M.; Stevens, B. E.; Grunlan, J. C., Precisely tuning the clay spacing in nanobrick wall gas barrier thin films. *Chemistry of Materials* **2013,** *25* (9), 1649-1655.

57. Cussler, E. L.; Hughes, S. E.; III, W. J. W.; Aris, R., Barrier membranes. *Journal of Membrane Science* **1988,** *38*, 161-174.

58. Hagen, D. A.; Foster, B.; Stevens, B.; Grunlan, J. C., Shift-time polyelectrolyte multilayer assembly: fast film growth and high gas barrier with fewer layers by adjusting deposition time. *ACS Macro Letters* **2014,** *3* (7), 663-666.

59. Cui, M.; Ng, W. S.; Wang, X.; Darmawan, P.; Lee, P. S., Enhanced electrochromism with rapid growth layer-by-layer assembly of polyelectrolyte complexes. *Advanced Functional Materials* **2015,** *25* (3), 401-408.

60. Kamal, M.; Jinnah, I.; Utracki, L., Permeability of oxygen and water vapor through polyethylene/polyamide films. *Polymer Engineering & Science* **1984,** *24*, 1337-1347.

61. Kumar, R. S.; Aucha, M.; Oua, E.; Ewaldb, G.; Jina, C. S., low moisture permeation measurement through polymer substrates for organic light emitting devices. *Thin Solid Films* **2002,** *417*, 120-126.

62. Li, N. N.; Fane, A. G.; Ho, W. S. W.; Matsuura, T., *Advanced Membrane Technology and Applications*. Wiley: **2011**.

63. Fick, A., V. On liquid diffusion. *Philosophical Magazine* **1855**.

64. George, S. C.; Thomas, S., Transport phenomena through polymeric systems *Progress in Polymer Science* **2001,** *26*, 985-1017.

65. Parkinson, C. R.; Walker, M.; McConville, C. F., Reaction of atomic oxygen with a Pt() surface: chemical and structural determination using XPS, CAICISS and LEED. *Surface Science* **2003,** *545* (1-2), 19-33.

66. Boehm, H. P., Surface oxides on carbon and their analysis: a critical assessment. *Carbon* **2002,** *40*, 145-149.

67. Alba, S.; Ohashi, M.; Huang, S.-Y. w., Rapid determination of oxygen permeability of polymer membranes. *Industrial & Engineering Chemistry Fundamentals* **1968,** *7* (3), 497.

68. Graham, T., Liquid diffusion applied to analysis. *Philosophical Transactions of the Royal Society of London* **1861,** *151*, 183-224.

69. Graham, T., On the molecular mobility of gases. *Philisophical Transactions of the Royal Society of London* **1863,** *153*, 385-405.

70. Kerkhof, P. J. A. M., New light on some old problems: Revisiting the stefan tube, Graham's law, and the Bosanquet equation. *Industrial & Engineering Chemistry Research* **1997,** *36*, 915-922.

71. Malek, K.; Coppens, M.-O., Effects of surface roughness on self- and transport diffusion in porous media in the knudsen regime. *Physical Review Letters* **2001,** *87* (12).

72. Xiap, J.; Weis, J., Diffusion mechanism of hydrocarbons in zeolites. *Chemical Engineering Science* **1992,** *47* (5), 1123-1141.

73. Koresh, J. E.; Soffer, A., Mechanism of permeation through molecular-sieve carbon membrane *JACS* **1986,** *82*, 2057-2063.

74. Gilron, J.; Soffer, A., Knudsen diffusion in microporous carbon membranes with molecular sieving character. *Journal of Membrane Science* **2002,** *209*, 339-352.

75. Alentiev, A. Y.; Yampolskii, Y. P., Free volume model and tradeoff relations of gas permeability and selectivity in glassy polymers. *Journal of Membrane Science* **2000,** *165*, 201-216.

76. Chrambach, A.; Aldroubi, A., Relative efficiency of molecular sieving in solutions of four polymers. *Electrophoresis* **1993,** *14*, 18-22.

77. Acharya, N. K.; Yadav, P. K.; Vijay, Y. K., Study of temperature dependent gas permeability for polycarbonate membrane. *Indian Journal of Pure & Applied Physics* **2004,** *42*, 179-181.

78. Krishna, R., Problems and pitfalls in the use of the fick formulation for intraparticle diffusion. *Chemical Engineering Science* **1993,** *48*, 845-861.

79. Stuhr, U.; Steinbinder, D.; Wipf, H.; Frick, B., Hydrogen diffusion in f.c.c. TiHx and YHx: Two distinct examples for diffusion in a concentrated lattice gas. *Europhysics Letter* **1992,** *20* (2), 117.

80. Freeman, B. D., Basis of permeability/selectivity tradeoff relations in polymeric gas separation membranes. *Macromolecules* **1999,** *32*, 375-380.

81. Zielinski, J. M.; Duda, J. L., Predicting polymer/solvent diffusion coefficients using free-volume theory. *AIChE Journal* **2004,** *38* (3), 405-415.

82. Park, J. Y.; Paul, D. R., Correlation and prediction of gas permeability in glassy polymer membrane materials via a modified free volume based group contribution method. *Journal of Membrane Science* **1997,** *126*, 23-29.

83. Hull, D.; Clyne, T., *An Introduction to Composite Materials*. Cambridge University Press: Cambridge, MA, **1996**.

84. Majumdar, A., Microscale transport phenomena. In *Handbook of heat transfer*, Rohsenow WM; JR, H.; YI, C., Eds. McGraw-Hill: New York, **1998**, pp 1-8.

85. Young, R. J.; Kinloch, I. A.; Gong, L.; Novoselov, K. S., The mechanics of graphene nanocomposites: A review. *Composites Science and Technology* **2012,** *72* (12), 1459-1476.

86. Kiliaris, P.; Papaspyrides, C. D., Polymer/layered silicate (clay) nanocomposites: An overview of flame retardancy. *Progress in Polymer Science* **2010,** *35* (7), 902-958.

87. M, V. E. Polymer-clay nanocomposites—the importance of particle dimensions. TU Delft, **2001**.

88. Favier, V.; Chanzy, H.; Cavaille, J. Y., Polymer nanocomposites reinforced by cellulose whiskers. *Macromolecules* **1995,** *28*, 6356-6367.

89. Auad, M. L.; Contos, V. S.; Nutt, S.; Aranguren, M. I.; Marcovich, N. E., Characterization of nanocellulose- reinforced shape memory polyurethanes. *Polymer International* **2008,** *57* (4), 651-659.

90. Usuki, A.; Kojima, Y.; Kawasumi, M.; Okada, A.; Fukushima, Y.; Kurauchi, T.; Kamigaito, O., Synthesis of nylon 6-clay hybrid. *Journal of Materials Research* **1993,** *8* (5).

91. Han, Z.; Fina, A., Thermal conductivity of carbon nanotubes and their polymer nanocomposites: A review. *Progress in Polymer Science* **2011,** *36* (7), 914-944.

92. Tripathi, S. K., Inorganic/organic hybrid nanocomposite and its device applications. *Solid State Phenomena* **2013,** *201*, 65-101.

93. Azizian-Kalandaragh, Y.; Khodayari, A., Ultrasound-assisted preparation of CdSe nanocrystals in the presence of Polyvinyl alcohol as a capping agent. *Materials Science in Semiconductor Processing* **2010,** *13* (4), 225-230.

94. Panayotidou, E.; Kroustalli, A.; Baklavaridis, A.; Zuburtikudis, I.; Achilias, D. S.; Deligianni, D., Biopolyester-based nanocomposites: Structural, thermo-mechanical and biocompatibility characteristics of poly(3-hydroxybutyrate)/montmorillonite clay nanohybrids. *Journal of Applied Polymer Science* **2014**, 41628-41639.

95. Sabetzadeh, M.; Bagheri, R.; Masoomi, M., Effect of organomodified montmorillonite concentration on tensile and flow properties of low-density polyethylene-thermoplastic corn starch blends. *Journal of Thermoplastic Composite Materials* **2012,** *27* (8), 1022-1036.

96. Wang, S., Preparation and characterization of flame retardant ABS/montmorillonite nanocomposite. *Applied Clay Science* **2004,** *25* (1-2), 49-55.

97. Das, A.; Stöckelhuber, K. W.; Jurk, R.; Saphiannikova, M.; Fritzsche, J.; Lorenz, H.; Klüppel, M.; Heinrich, G., Modified and unmodified multiwalled carbon nanotubes in high performance solution-styrene–butadiene and butadiene rubber blends. *Polymer* **2008,** *49* (24), 5276-5283.

98. Giannelis, E. P., Polymer-Layered Silicate Nanocomposites: Synthesis, Properties and Applications. *Applied Organometallic Chemistry* **1998,** *12*, 675-680.

99. Kim, S. W.; Cha, S.-H., Thermal, mechanical, and gas barrier properties of ethylene-vinyl alcohol copolymer-based nanocomposites for food packaging films: Effects of nanoclay loading. *Journal of Applied Polymer Science* **2014,** *131* (11), 40289-40301.

100. Aldana, D.; Villa, E.; De Dios Hernández, M.; Sánchez, G.; Cruz, Q.; Gallardo, S.; Castillo, H.; Casarrubias, L., Barrier properties of polylactic acid in cellulose based packages using montmorillonite as filler. *Polymers* **2014,** *6* (9), 2386-2403.

101. Anadão, P., Polymer/ clay nanocomposites: concepts, researches, applications and trends for the future. Ebrahimi, F., Ed. InTech: **2012**.

102. Muller, P.; Kapin, E.; Fekete, E., Effects of preparation methods on the structure and mechanical properties of wet conditioned starch/montmorillonite nanocomposite films. *Carbohydrate Polymers* **2014,** *113*, 569-76.

103. Apaydin, K.; Laachachi, A.; Ball, V.; Jimenez, M.; Bourbigot, S.; Toniazzo, V.; Ruch, D., Intumescent coating of (polyallylamine-polyphosphates) deposited on polyamide fabrics via layer-by-layer technique. *Polymer Degradation and Stability* **2014,** *106*, 158-164.

104. Priolo, M. A.; Holder, K. M.; Guin, T.; Grunlan, J. C., Recent advances in gas barrier thin films via layer-by-layer assembly of polymers and platelets. *Macromolecular Rapid Communication* **2015,** *36* (10), 866-79.

105. Takahashi, S.; Goldberg, H. A.; Feeney, C. A.; Karim, D. P.; Farrell, M.; O'Leary, K.; Paul, D. R., Gas barrier properties of butyl rubber/vermiculite nanocomposite coatings. *Polymer* **2006,** *47*, 3083-3093.

106. Chang, J.-H.; An, Y. U.; Sur, G. S., Poly(lactic acid) nanocomposites with various organoclays. I. Thermomechanical properties, morphology,and gas permeability. *Journal of Polymer Science Part B: Polymer Physics* **2003,** *41*, 94-103.

107. Nielsen, L. E., Models for the permeability of filled polymer systems. *Journal of Macromolecular Science* **1967,** *A1*, 929.

108. Derocher, J.; Gettelfinger, B.; Wang, J.; Nuxoll, E.; Cussler, E., Barrier membranes with different sizes of aligned flakes. *Journal of Membrane Science* **2005,** *254* (1-2), 21-30.

109. Lape, N. K.; Nuxoll, E. E.; Cussler, E. L., Polydisperse flakes in barrier films. *Journal of Membrane Science* **2004,** *236* (1-2), 29-37.

110. Koch, C. A.; Akhave, J. R.; Bharadwaj, R. K. Layer by layer assembled nanocomposite barrier coatings. **2004**.

111. Levasalmi, J. M.; McCarthy, T. J., Poly(4-methyl-1-pentene)-supported polyelectrolyte multilayer films: Preparation and gas permeability. *Macromolecules* **1997,** *30* (6), 1752-1757.

112. Priolo, M. A.; Gamboa, D.; Grunlan, J. C., Transparent clay−polymer nano brick wall assemblies with tailorable oxygen barrier. *ACS Applied Materials & Interfaces* **2010,** *2* (1), 312-320.

113. Tzeng, P.; Lugo, E. L.; Mai, G. D.; Wilhite, B. A.; Grunlan, J. C., Super hydrogen and helium barrier with polyelectolyte nanobrick wall thin film. *Macromolecular Rapid Communications* **2015,** *36* (1), 96-101.

114. Stevens, B.; Dessiatova, E.; Hagen, D. A.; Todd, A. D.; Bielawski, C. W.; Grunlan, J. C., Low-temperature thermal reduction of graphene oxide nanobrick walls: unique combination of high gas barrier and low resistivity in fully organic polyelectrolyte multilayer thin films. *ACS Applied Materials & Interfaces* **2014,** *6* (13), 9942-5.

115. Stroeve, P.; Vasquez, V.; Coelho, M. A. N.; Rabolt, J. F., Gas transfer in supported films made by molecular self-assembly of ionic polymers. *Thin Solid Films* **1996,** *284*, 708-712.

116. Kim, D.; Tzeng, P.; Barnett, K. J.; Yang, Y. H.; Wilhite, B. A.; Grunlan, J. C., Highly size-selective ionically crosslinked multilayer polymer films for light gas separation. *Advanced Materials* **2014,** *26* (5), 746-51.

117. Ji, Q.; Honma, I.; Paek, S. M.; Akada, M.; Hill, J. P.; Vinu, A.; Ariga, K., Layer-by-layer films of graphene and ionic liquids for highly selective gas sensing. *Angewandte Chemie* **2010,** *49* (50), 9737-9.

118. Hilado, C., *Flammability Handbook for Plastics*. 5 ed.; Technomic Publishing AG: United States, **1998**.

119. Camino, G.; Costa, L.; Cortemiglia, M. P. L. d., Overview of fire retardant mechanisms. *Polymer Degradation and Stability* **1991,** *33*, 131-154.

120. Camino, G.; Costa, L., Performance and mechanisms of fire retardants in polymers: A review. *Polymer Degradation and Stability*, **1988,** *20*, 271-294.

121. Bolland, J. L.; Gee, G., Kinetic studies in the chemistry of rubber and related materials: II.The kinetics of oxidation of unconjugated olefins. *Transactions of the Faraday Society* **1945**, 244-251.

122. Bolland, J. L.; Gee, G., Kinetic studies in the chemistry of rubber and related materials: iii. thermochemistry and mechanisms of olefin oxidation. *Transactions of the Faraday Society* **1945**, 244-251.

123. Walters, R. N.; Lyon, R. E., Molar group contributions to polymer flammability. *Journal of Applied Polymer Science* **2002,** *87*, 548-563.

124. Krevelen, D. W. v., Some basic aspects of flame resistance in polymeric materials. *Polymer* **1975,** *16*, 615-620.

125. Horrocks, A. R., Flame retardant challenges for textiles and fibres: New chemistry versus innovatory solutions. *Polymer Degradation and Stability* **2011,** *96* (3), 377-392.

126. Li, Y.-C.; Schulz, J.; Mannen, S.; Delhom, C.; Condon, B.; Chang, S.; Zammarano, M.; Grunlan, J. C., Flame retardant behavior of polyelectrolyte-clay thin film assemblies on cotton fabric. *ACS Nano* **2010,** *6*, 3325-3337.

127. Kandola, B. K., Flame retardancy design for textiles. In *Fire Retardancy of Polymeric Materials*, B., C. A. W. A., Ed. Taylor and Francis Group CRC Press,: **2010**, pp 725-762.

128. Morgan, A. B.; Gilman, J. W., An overview of flame retardancy of polymeric materials: application, technology, and future directions. *Fire and Materials* **2013,** *37* (4), 259-279.

129. Hindersinn, R. R., Historical aspects of polymer fire retardance. *American Chemical Society Symposium Series* **1990,** *415*.

130. Wojciechowska, R.; Wojciechowski, W.; Kamihski, J., Thermal decompositions of ammonium and potassium alums. *Journal of Thermal Analysis* **1988,** *33*, 503-509.

131. Momoh, M.; Eboatu, A. N.; Kaliel, M.; Abdulrahman, F. W., Effect of flame-retardant treatment on the thermal behavior of cotton fabric. *Textile Research Journal* **1990,** *60*, 557-560.

132. Shen, D.; Xiao, R.; Gu, S.; Zhang, H., The overview of thermal decomposition of cellulose in lignocellulosic biomass. **2013**.

133. Shen, D. K.; Gu, S., The mechanism for thermal decomposition of cellulose and its main products. *Bioresource Technology* **2009,** *100* (24), 6496-504.

134. Hema, S.; N. M., R.; S. S. J., S., Effect of preparatory textile treatments on physical properties of cotton fabric. *Annals of Agricultural Biological Research* **2014,** *19*, 793-796.

135. Laufer, G.; Kirkland, C.; Morgan, A. B.; Grunlan, J. C., Intumescent multilayer nanocoating, made with renewable polyelectrolytes, for flame-retardant cotton. *Biomacromolecules* **2012,** *13* (9), 2843-8.

136. Gaan, S.; Sun, G., Effect of phosphorus and nitrogen on flame retardant cellulose: A study of phosphorus compounds. *Journal of Analytical and Applied Pyrolysis* **2007,** *78* (2), 371-377.

137. Kandola, B. K.; Horrocks, A. R., Complex char formation in flame-retarded fibre-intumescent combinations-II. Thermal analytical studies. *Polymer Degradation and Stability* **1996,** *54*, 289-303.

138. Aenishanslin, R.; Guth, P. H.; Maeder, A.; Nachbur, H., A new chemical approach to durable flame retardant cotton fabrics. *Textile Research Journal* **1969,** *39*, 375-381.

139. Weil, E. D., *Proceedings of 2nd Conference: Advances in Flame Retardant Polymers: Business Communications* **1991**.

140. Nguyen, T.-M.; Chang, S.; Condon, B.; Smith, J., Fire self-extinguishing cotton fabric: development of piperazine derivatives containing phosphorous-sulfur-nitrogen and their flame retardant and thermal behaviors. *Materials Sciences and Applications* **2014,** *05* (11), 789-802.

141. Alongi, J.; Ciobanu, M.; Malucelli, G., Novel flame retardant finishing systems for cotton fabrics based on phosphorus-containing compounds and silica derived from sol–gel processes. *Carbohydrate Polymers* **2011,** *85* (3), 599-608.

142. Li, Y. C.; Schulz, J.; Grunlan, J. C., Polyelectrolyte/nanosilicate thin-film assemblies: influence of pH on growth, mechanical behavior, and flammability. *ACS Applied Materials & Interfaces* **2009,** *1* (10), 2338-47.

143. Lin, Z.; Renneckar, S.; Hindman, D. P., Nanocomposite-based lignocellulosic fibers 1. Thermal stability of modified fibers with clay-polyelectrolyte multilayers. *Cellulose* **2007,** *15* (2), 333-346.

144. Alongi, J.; Carosio, F.; Malucelli, G., Layer by layer complex architectures based on ammonium polyphosphate, chitosan and silica on polyester-cotton blends: flammability and combustion behaviour. *Cellulose* **2012,** *19* (3), 1041-1050.

145. Carosio, F.; Alongi, J.; Malucelli, G., Layer by Layer ammonium polyphosphate-based coatings for flame retardancy of polyester–cotton blends. *Carbohydrate Polymers* **2012,** *88* (4), 1460-1469.

146. Zhang, T.; Yan, H.; Wang, L.; Fang, Z., Controlled formation of self-extinguishing intumescent coating on ramie fabric via layer-by-layer assembly. *Industrial & Engineering Chemistry Research* **2013,** *52* (18), 6138-6146.

147. Picart, C.; Lavalle, P.; Hubert, P.; Cuisinier, F. J. G.; Decher, G.; Schaaf, P.; Voege, J.-C., Buildup mechanism for poly(L-lysine)/hyaluronic acid films onto a solid surface. *Langmuir* **2001,** *17*, 7414-7424.

148. Abdelkebir, K.; Gaudière, F.; Morin-Grognet, S.; Coquerel, G.; Labat, B.; Atmani, H.; Ladam, G., Evidence of different growth regimes coexisting within biomimetic Layer-by-layer films. *Soft Matter* **2011,** *7* (19), 9197.

149. Kawabata, S.; Niwa, M.; Yamashita, Y., Recent developments in the evaluation technology of fiber and textiles: toward the engineered design of textile performance. *Journal of Applied Polymer Science* **2002,** *83*, 687–702.

150. Kawabata, S.; Niwa, M.; Wang, F., Objective hand measurement of nonwoven fabrics. *Textile Research Journal* **1994,** *64*, 597-610.

151. Beech, S., *Textile Terms and Definitions*. 8 ed.; The Textile Institution: Manchester, UK, **1988**.

152. El-Sabbagh, A.; Taha, I., Characterization of the draping behavior of jute woven fabrics for applications of natural-fiber/epoxy composites. *Journal of Applied Polymer Science* **2013,** *130* (3), 1453-1465.

153. Mohamed, A. L.; Er-Rafik, M.; Moller, M., Supercritical carbon dioxide assisted silicon based finishing of cellulosic fabric: a novel approach. *Carbohydrate Polymers* **2013,** *98* (1), 1095-107.

154. Graff, G. L.; Burrows, P. E.; Williford, R. R.; Praino, R. F., Barrier Layer Technology for Flexible Displays. In *Flexible Flat Panels*, Crawford, G. P., Ed. John Wiley & Son, Ltd: Chichester and Hoboken, NJ, **2005**, pp 57-77.

155. Inc., P. P. Oxygen Transmission Rate. http://www.polyprint.com/flexographic-otr.html (accessed March 4).

156. Affinito, J. D.; Gross, M. E.; Coronado, C. A.; Graff, G. L.; Greenwell, E. N.; Martin, P. M., A new method for fabricating transparent barrier layers. *Thin Solid Films* **1996,** *291*, 63-67.

157. Mathieson, A., Mg-vermculite: A refinement and re-examination of the crystal structure of the 14.36 A phase. *American Mineralogist* **1958,** *43*, 216-227.

158. Zare, Y.; Garmabi, H., Thickness, modulus and strength of interphase in clay/polymer nanocomposites. *Applied Clay Science* **2015,** *105-106*, 66-70.

159. Michel, M.; Toniazzo, V.; Ruch, D.; Ball, V., Deposition mechanisms in layer-by-layer or step-by-step deposition methods: from elastic and impermeable films to soft membranes with ion exchange properties. *ISRN Materials Science* **2012,** *2012*, 1-13.

160. Hagen, D. A.; Box, C.; Greenlee, S.; Xiang, F.; Regev, O.; Grunlan, J. C., High gas barrier imparted by similarly charged multilayers in nanobrick wall thin films. *RSC Advances* **2014,** *4* (35), 18354.

161. Priolo, M. A.; Holder, K. M.; Gamboa, D.; Grunlan, J. C., Influence of clay concentration on the gas barrier of clay-polymer nanobrick wall thin film assemblies. *Langmuir* **2011,** *27* (19), 12106-14.

162. Geng, F.; Ma, R.; Ebina, Y.; Yamauchi, Y.; Miyamoto, N.; Sasaki, T., Gigantic swelling of inorganic layered materials: a bridge to molecularly thin two-dimensional nanosheets. *Journal of the American Chemical Society* **2014,** *136* (14), 5491-500.

163. Walker, G. F., Macroscopic swelling of vermiculite crystals in water. *Nature* **1960,** *187*, 312-313.

164. Graf, R. B.; Wahl, F. M.; Grim, R. E., Phase transformations in silica-alumina-magnesia mixtures as examined by continuous X-ray diffraction: Talc-kaolinite compositions. *The American Mineralogist* **1962,** *47*, 1273-1283.

165. Tertre, E.; Delville, A.; Prêt, D.; Hubert, F.; Ferrage, E., Cation diffusion in the interlayer space of swelling clay minerals – A combined macroscopic and microscopic study. *Geochimica et Cosmochimica Acta* **2015,** *149*, 251-267.

166. Le Pluart, L.; Duchet, J.; Sautereau, H.; Gérard, J. F., Surface modifications of montmorillonite for tailored interfaces in nanocomposites. *The Journal of Adhesion* **2002,** *78* (7), 645-662.

167. Lin, J.-J.; Wei, J.-C.; Juang, T.-Y.; Tsai, W.-C., Preparation of protein-silicate hybrids from polyamine intercalation of layered montmorillonite. *Langmuir* **2007,** *23*, 1995-1999.

168. Hong, P.-Z.; Li, S.-D.; Ou, C.-Y.; Li, C.-P.; Yang, L.; Zhang, C.-H., Thermogravimetric analysis of chitosan. *Journal of Applied Polymer Science* **2007,** *105* (2), 547-551.

169. Morton, S. W.; Herlihy, K. P.; Shopsowitz, K. E.; Deng, Z. J.; Chu, K. S.; Bowerman, C. J.; Desimone, J. M.; Hammond, P. T., Scalable manufacture of built-to-order nanomedicine: spray-assisted layer-by-layer functionalization of PRINT nanoparticles. *Advanced Materials* **2013,** *25* (34), 4707-13.

170. Chang, S.; Slopek, R. P.; Condon, B.; Grunlan, J. C., Surface coating for flame-retardant behavior of cotton fabric using a continuous layer-by-layer process. *Industrial & Engineering Chemistry Research* **2014,** *53* (10), 3805-3812.

171. Laufer, G.; Kirkland, C.; Morgan, A. B.; Grunlan, J. C., Exceptionally flame retardant sulfur-based multilayer nanocoating for polyurethane prepared from aqueous polyelectrolyte solutions. *ACS Macro Letters* **2013,** *2* (5), 361-365.

172. Becerril, H. A.; Mao, J.; Liu, Z.; Stoltenberg, R. M.; Bao, Z.; Chen, Y., Evaluation of solution-processed reduced graphene oxide films as transparent conductors. *ACS Nano* **2008,** *2*, 463–470.

173. Compton, O. C.; Nguyen, S. T., Graphene oxide, highly reduced graphene oxide, and graphene: versatile building blocks for carbon-based materials. *Small* **2010,** *6* (6), 711-23.

174. Dreyer, D. R.; Park, S.; Bielawski, C. W.; Ruoff, R. S., The chemistry of graphene oxide. *Chemical Society Review* **2010,** *39* (1), 228-40.

175. Pei, S.; Cheng, H.-M., The reduction of graphene oxide. *Carbon* **2012,** *50* (9), 3210-3228.

176. Thaiboonrod, S.; Milani, A. H.; Saunders, B. R., Doubly crosslinked poly(vinyl amine) microgels: hydrogels of covalently inter-linked cationic microgel particles. *Journal of Material Chemistry B* **2014,** *2* (1), 110-119.

177. Pelton, R., Polyvinylamine: a tool for engineering interfaces. *Langmuir* **2014,** *30* (51), 15373-82.

178. Johnson, T. J. A., Glutaraldehyde crosslinking: Fast and slow modes. *Biocatalyst Design For Stability And Specificity* **1993,** *1*, 283-295.

179. Billman, J. H.; Diesing, A. C., Reduction of schiff bases with sodium borohydride. *Journal of Organic Chemistry* **1956,** *22*, 1068-1070.

180. Burkhart, C. W. Gas separation chamber and portable leak detection system US 4459844 A, **1984**.

181. Mayer, D. W.; Demorest, R. L.; Bode, J. Method for measuring gas leakage from sealed packages. US 6460405 B1, **2000**.

182. Bailey, S. E.; Olin, T. J.; Bricka, R. M.; Adrian, D. D., A review of potentially low-cost sorbent for heavy metals. *Water Research* **1999,** *33* (11), 2469-2479.

183. Zhao, X.; Zhang, Q.; Hao, Y.; Li, Y.; Fang, Y.; Chen, D., Alternate multilayer films of poly(vinyl alcohol) and exfoliated graphene oxide fabricated via a facial layer-by-layer assembly. *Macromolecules* **2010,** *43* (22), 9411-9416.

184. Gao, Z.; Yang, W.; Wang, J.; Yan, H.; Yao, Y.; Ma, J.; Wang, B.; Zhang, M.; Liu, L., Electrochemical synthesis of layer-by-layer reduced graphene oxide sheets/polyaniline nanofibers composite and its electrochemical performance. *Electrochimica Acta* **2013,** *91*, 185-194.

185. Wang, X.; Bai, H.; Yao, Z.; Liu, A.; Shi, G., Electrically conductive and mechanically strong biomimetic chitosan/reduced graphene oxide composite films. *Journal of Materials Chemistry* **2010,** *20* (41), 9032.

186. Bai, H.; Li, C.; Wang, X.; Shi, G., A pH-sensitive graphene oxide composite hydrogel. *Chemical Communications* **2010,** *46* (14), 2376-8.

187. Putz, K. W.; Compton, O. C.; Palmeri, M. J.; Nguyen, S. T.; Brinson, L. C., High-nanofiller-content graphene oxide-polymer nanocomposites via vacuum-assisted self-assembly. *Advanced Functional Materials* **2010,** *20* (19), 3322-3329.

188. Han, D.; Yan, L.; Chen, W.; Li, W., Preparation of chitosan/graphene oxide composite film with enhanced mechanical strength in the wet state. *Carbohydrate Polymers* **2011,** *83* (2), 653-658.

189. Meredith, P.; Sarna, T., The physical and chemical properties of eumelanin. *Pigment Cell Research* **2006,** *19* (6), 572-94.

190. Kim, B. G.; Kim, S.; Lee, H.; Choi, J. W., Wisdom from the human eye: a synthetic melanin radical scavenger for improved cycle life of Li–O_2battery. *Chemistry of Materials* **2014,** *26* (16), 4757-4764.

191. Jacques, S. L., Corrigendum: Optical properties of biological tissues: a review. *Physics in Medicine and Biology* **2013,** *58* (14), 5007-5008.

192. Shanmuganathan, K.; Cho, J. H.; Iyer, P.; Baranowitz, S.; Ellison, C. J., Thermooxidative stabilization of polymers using natural and synthetic melanins. *Macromolecules* **2011,** *44* (24), 9499-9507.

193. Bellono, N. W.; Oancea, E. V., Ion transport in pigmentation. *Archives Of Biochemistry And Biophysics* **2014,** *563*, 35-41.

194. Dezidério, S. N.; Brunello, C. A.; da Silva, M. I. N.; Cotta, M. A.; Graeff, C. F. O., Thin films of synthetic melanin. *Journal of Non-Crystalline Solids* **2004,** *338-340*, 634-638.

195. Pitts, D. G.; Cullen, A. P.; Hacker, P. D., Ocular effects of ultraviolet radiation from 295-365 nm. *Investigative Ophthalmogy and Visual Science* **2003,** *16*, 932-939.

196. Picart, C.; Lavalle, P.; Hubert, P.; Cuisinier, F. J. G.; Decher, G.; Schaaf, P.; Voegel, J.-C., Buildup mechanism for poly(l-lysine)/hyaluronic acid films onto a solid surface. *Langmuir* **2001,** *17*, 7414-7424.

197. Wünsche, J.; Cicoira, F.; Graeff, C. F. O.; Santato, C., Eumelanin thin films: solution-processing, growth, and charge transport properties. *Journal of Materials Chemistry B* **2013,** *1* (31), 3836.

198. Gandini, S.; Autier, P.; Boniol, M., Reviews on sun exposure and artificial light and melanoma. *Progress In Biophysics And Molecular Biology* **2011,** *107* (3), 362-6.

199. Hill, H. Z.; Li, W.; Xin, P.; Mitchell, D. L., Melanin: A two edged sword? *Pigment Cell Research* **1997,** *10*, 158-161.

200. Stark, K. B.; Gallas, J. M.; Zajac, G. W.; Eisner, M.; Golab, J. T., Spectroscopic study and simulation from recent structural models for eumelanin: II. Oligomers. *Journal of Physical Chemistry B 2* **2003,** *107*, 11558-11562.

201. Wu, J.; Zhang, L.; Wang, Y.; Long, Y.; Gao, H.; Zhang, X.; Zhao, N.; Cai, Y.; Xu, J., Mussel-inspired chemistry for robust and surface-modifiable multilayer films. *Langmuir* **2011,** *27* (22), 13684-91.

202. Alemu, D.; Wei, H.-Y.; Ho, K.-C.; Chu, C.-W., Highly conductive PEDOT:PSS electrode by simple film treatment with methanol for ITO-free polymer solar cells. *Energy & Environmental Science* **2012,** *5* (11), 9662.

APPENDIX: WATER-BASED MELANIN THIN FILMS WITH BROADBAND UV ABSORPTION[4]

Introduction

Melanin is widely available biocompatible polymer with many useful properties, such as broadband UV absorption,[189-191] anti-oxidant behavior,[192] photoelectric behavior,[189] and free-radical scavenging.[192] In nature, melanin is responsible for the brown-black coloring in human pigmentation that protects the skin, hair and eyes from the harmful effects of UV radiation. [189,190, 193] Historically, melanin has been very difficult to adapt for broad use in materials applications because it is insoluble in all common solvents and usually exists as granular aggregates.[189, 192] In an effort to expand its utility, recent research has focused on producing synthetic melanin, which is soluble in organic solvents.[192] Melanin thin films can now be produced by spin coating or drop casting.[194] A particularly useful synthetic melanin has been produced that is dispersible in mildly basic water,[192] allowing melanin to be processed without organic solvents.

In this work, thin films of water-soluble synthetic melanin and poly(allylamine hydrochloride) (PAH) were fabricated via layer-by-layer assembly in ambient conditions from dilute aqueous solutions to produce extremely thin, well-adhered films with broad UV-protection capability. This appears to be the first time melanin has been deposited as a durable thin film from water using already-prepared melanin. These coatings absorb

---

[4] Reprinted with permission from "Water-Based Melanin Thin Films With Broadband UV Absorption" by Guin, et. al, 2015. *ACS Macro Letters,* 4, 335-338, Copyright 2015 by ACS.

more than 63% of the UV light that is most damaging to human eyes (265-275 nm),[195] with a thickness of just 108 nm. Additionally, these films are shown to reduce UV damage to a thin conductive film of poly(3,4-ethylenedioxythiophene):poly(styrene sulfonate) (PEDOT:PSS). This novel method of producing melanin thin films could be useful for a number of applications requiring UV protection (e.g., eyewear, organic electronics, etc.).

Experimental

Water-soluble melanin was produced by oxidative polymerization of L-dopa. 33.8 g of L-dopa (AK Scientific, Inc., Union City, CA) and 41.6 g of benzoyl peroxide were mixed together in 4.5 L of anhydrous DMSO (Chem-Impex International, Inc., Wood Dale, IL), which was purified using activated alumina. The solution was quickly sealed and stirred at room temperature, gradually turning pink and then black over 2 hours. The reaction was stopped after 28 days and the solution was concentrated by evaporating excess DMSO at 100 ^{o}C using a rotary evaporator. Subsequently, melanin was precipitated by drop-wise addition of the concentrated solution into a large quantity of acetonitrile (Alfa Aesar, Heysham, Lancashire, UK) under vigorous stirring. The resulting precipitate was retrieved by centrifugation (3600 rpm, 10 min). Finally, synthetic melanin was dried under vacuum at room temperature for 2 days and then at 70 ^{o}C for 1 day until a constant weight was reached. The black powder was obtained with 85% yield.

Anionic melanin solution used for layer-by-layer assembly was prepared by adding 0.1 wt% synthetic melanin to 0.001 M NaOH (Sigma Aldrich, Milwaukee, WI), and sonicating in a 10L Branson 5510 ultrasonic cleaner for 30 min. The melanin solution for spin coating was prepared by adding 10 wt% melanin to 1 M NaOH and sonicating for 30 min. After solvation, the pH of the melanin solution was adjusted to pH 10 with 1 M NaOH and the solution was used immediately (the pH of the solution was not stable after 24 hours). Cationic poly(allylamine hydrochloride) (PAH) solution was prepared by adding 0.1 wt% PAH (120-200 kDa, Polysciences, Inc., Warrington, PA) for LbL assembly, or 10 wt% for spin coating, into 18 MΩ deionized (DI) water and adjusting the pH to 10 using 1 M NaOH. LbL assembled films were constructed by alternately dipping a prepared substrate into PAH and melanin solutions, beginning with the PAH solution. The first two depositions were 5 min, while subsequent depositions were 1 min each. In between deposition, films were rinsed thoroughly with DI water and dried with a stream of filtered air. After the desired number of bilayers was deposited, the films were dried for 30 min at 70˚C to remove excess moisture.

Thickness of the film was measured on (1 0 0) silicon wafers that were cleaned with a 10 min plasma treatment, using a PDC-32G plasma cleaner (Harrick Plasma, Ithaca, NY), with both a P-6 profilometer (KLA-Tencor, Milpitas, CA) and an alpha-SE elliposometer (J.A. Woollam Co., Inc., Lincoln, NE). Mass of the films was measured on Ti/Au crystals using a Maxtek Research Quartz Crystal Microbalance (QCM) from Infinicon (East Syracuse, NY), with a frequency range of 3.8-6 MHz. The UV absorption and roughness of the films and was measured on fused quartz slides

(Structure Probe, Inc., West Chester, PA) which had been cleaned using 30 min 4:1 piranha treatment (*caution! Piranha solution reacts violently with organic materials).* AFM images were taken using a Bruker Dimension Icon AFM (Billerica, MA) in intermittent tapping mode. Area roughness (Ra) of each film was calculated using a 20 × 20 μm height image.

The UV absorption of the films was measured using a USB2000 UV-Vis spectrometer (Ocean Optics, Dunedin, FL) from 200 to 900 nm. UV protection of the LbL films was measured on poly(3,4-ethylenedioxythiophene):poly(styrene sulfonate) (PEDOT:PSS) (Clevious PH 1000, Heraeus, West Conshohocken, PA), which had been spin coated on glass slides. The glass slides were spin coated with a 1.3 wt% PEDOT:PSS solution for 60 sec at 3000 RPM using a WS-650 spin coater (Laurell Technologies, North Wales, PA) and then annealed with methanol at 70 ˚C. LbL assembled films were then deposited on top of the ~50 nm thick PEDOT:PSS and two leads, 16 mm apart, were connected to the coated slide using clamps and silver adhesive (Electron Microscopy Sciences, Hatfield, PA). The slides were exposed to a 400 W mercury lamp and the resistance was measured using a Keithley 2000 Multimeter (Cleveland, OH). The temperature of the slide was kept at 65°C using a 12 W fan.

Results and Discussion

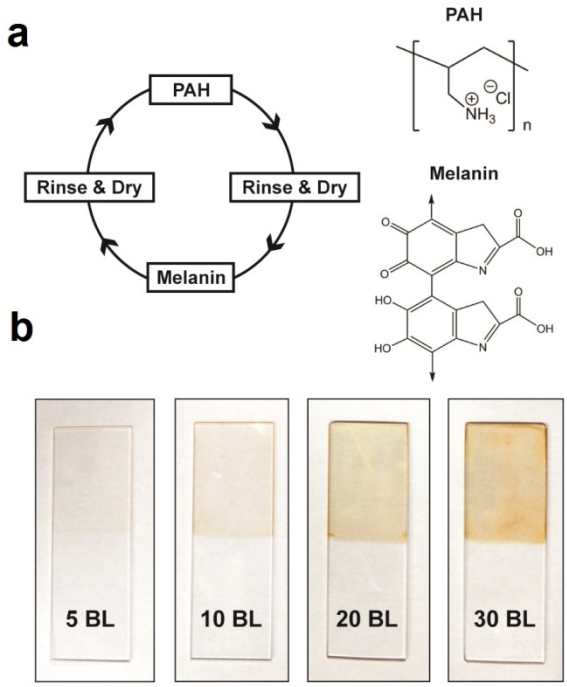

Figure A.1. (a) Schematic of the layer-by-layer (LbL) deposition process and chemical structures of deposited polyelectrolytes. (b) Photographs of different numbers of melanin/PAH bilayers (BL) deposited on quartz.

Melanin-containing multilayer films (shown in Figure A.1) were initially grown on silicon wafers and thickness was measured using ellipsometry and profilometry, as shown in Figure A.2(a). There is excellent agreement between these two measurement techniques. The melanin-PAH multilayer films grew linearly, depositing 1.7 nm per bilayer. The mass of the films was determined after each deposition step using a quartz

crystal microbalance (QCM), as shown in Figure A.2(b), and the concentration of each component was calculated as described previously.[7, 15] PAH/melanin multilayer films contain 37 wt% melanin and the melanin concentration is independent of the number of bilayers deposited. This is a significant increase over previous work, where only 5 wt% melanin was melt blended with common thermoplastic polymers that exhibited some visible melanin aggregation.[192]

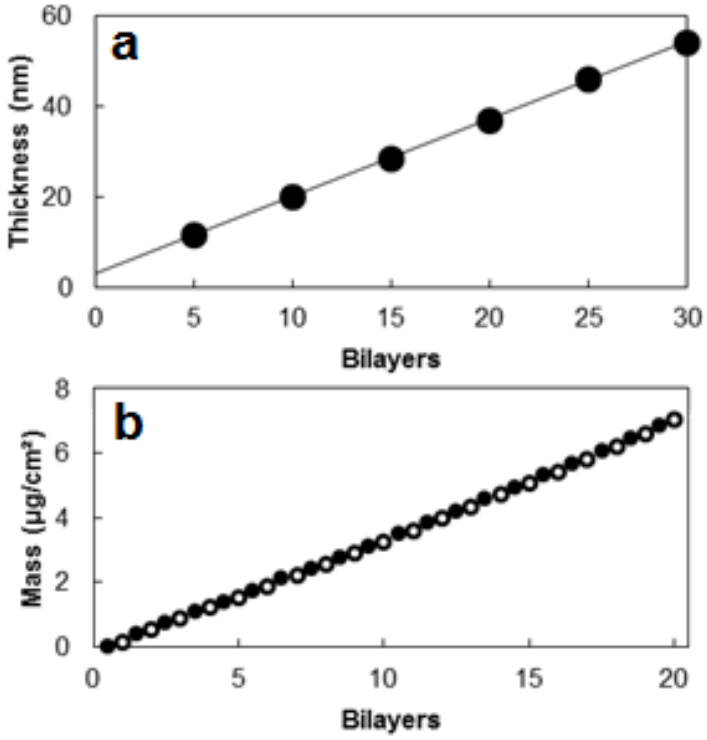

Figure A.2. (a) Thickness of melanin-PAH multilayer films as a function of the number of bilayers deposited. (b) Mass deposited as a function of the number of layers deposited (filled points: PAH, open points: melanin).

Figure A.3 shows the surface topography of these films in atomic force microscope (AFM) images. A five bilayer film deposited on quartz is composed of small islets on top of a thinner film (Figure A.3(a)), which is likely an artifact of "island-growth" in the beginning stages of deposition. As the film grows, the roughness increases only modestly (R_a (5 BL) = 3.4 nm and R_a (30 BL) = 9.3 nm), suggesting that the film deposits in a uniform and coherent manner between 5 and 30 BL (rather than as semi-solvated aggregates).[196] Previous work on melanin thin films spin coated from DMSO reported a surface roughness less than 0.4 nm at a film thickness of 30 nm.[197] It is believed that the low surface roughness of the spin-coated melanin film is due to self-arrangement of the melanin during solvent evaporation.[197] The electrostatic forces between the PAH and the melanin in the layer-by-layer assembled films likely prevent the melanin from rearranging into a smoother film, thereby locking in the island topography of the initial bilayers.

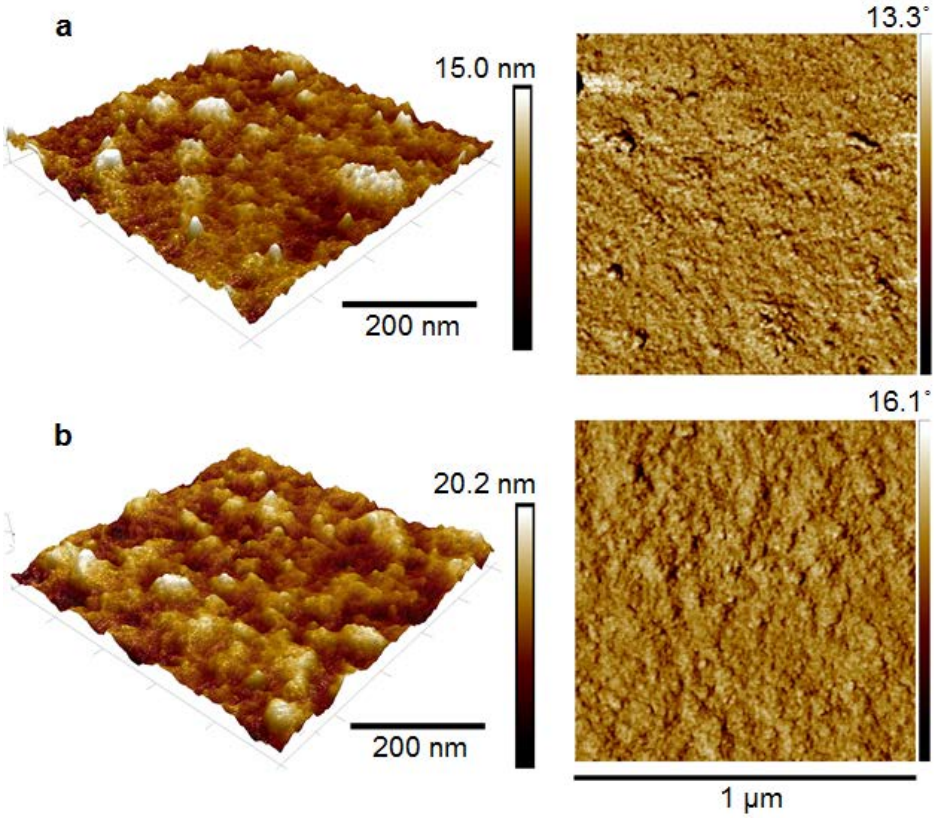

Figure A.3. AFM 3D height and phase images of (a) 5 BL and (b) 30 BL PAH/melanin multilayer films deposited on quartz.

Melanin multilayer films on quartz display broadband UV–vis light absorption from 200 - 700 nm, as shown in Figure A.4(a). Vertebrates use melanin to prevent eye damage from short wavelength UV light, particularly from 265–275 nm,[193, 195, 198-199] and a quartz substrate coated with a 30 BL melanin-containing multilayer film on both sides absorbed 63% of the light in this range. As a comparison, neat melanin and PAH were spin coated onto quartz from water. The multilayer films have optical properties very similar to natural melanin, displaying a broad absorbance of UV and visible light, which

decreases slightly at higher wavelengths (Figure A.4(a)).[189, 191, 200] Spin-coated melanin films display an additional peak at 280 nm, which is most likely due to the quinone in the melanin backbone (Figure A.1(a)) reverting to a catechol under ambient conditions.[201] It is interesting to note that the backbone quinone melanin in the multilayer film did not revert back to a catechol in dry conditions, which may be due to interactions between the amine of the PAH and the quinone.

The absorbance spectrum of the melanin multilayer film is atypical of an organic chromophore and would typically be associated with scattering effects due to aggregated particles in the film.[189] It should be noted that melanin is known to display this broadband absorption curve even when well-solvated and, combined with the nature of the deposition method, is consistent with well-dispersed melanin in the multilayer film.[200] Figure A.4(b) shows that the absorbance of the PAH/melanin films at various wavelengths of UV light is directly proportional to their thickness. This is further evidence that the melanin concentration of the film remains constant with increasing bilayers. Despite the multilayer film being only 37 wt% melanin, as determined by QCM, the total absorbance of the film is remarkably similar to a spin coated film composed entirely of melanin of similar thickness (Fig. 4(b)). As the UV absorbance of the film is primarily derived from the melanin content, it is possible that the total melanin content is similar between the spin coated and LbL films, despite the additional PAH in the LbL film. It is well established that the conformation of the polyelectrolytes in LbL-assembled films allows for very dense films, exceeding the densities of the individual components.[12, 17, 24]

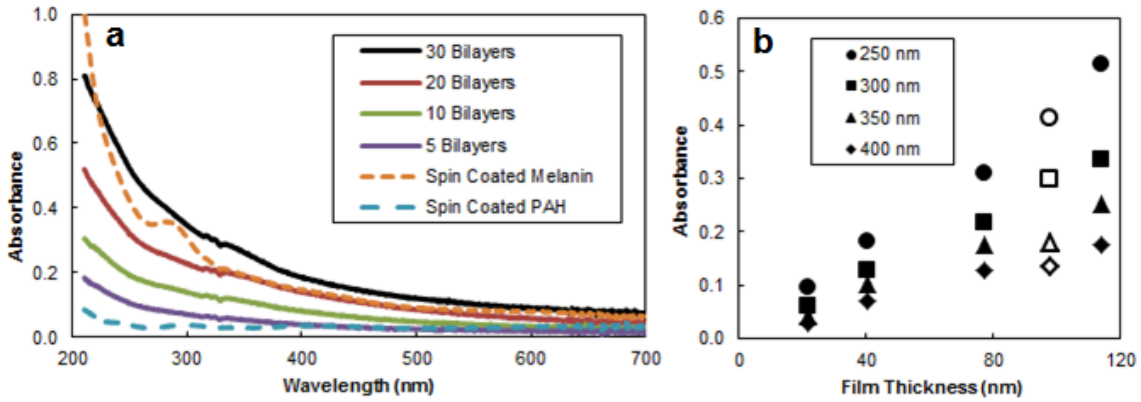

Figure A.4. (a) Absorbance spectra of varying bilayers of PAH/melanin multilayer films, along with 98 nm spin coatings of the constituent polyelectrolytes on fused quartz. (b) Absorbance of the multilayer films (filled points) and spin-coated pure melanin films (open points) as a function of film thickness.

UV absorbance and anti-oxidant properties of melanin are well-established,[189] so PAH/melanin multilayer thin films were deposited on spin coated PEDOT:PSS films to impart UV protection. PEDOT:PSS films were exposed to a 400 W mercury arc lamp, which degraded the film over time. The increase in electrical resistance was used to monitor PEDOT degradation, as shown in Figure A.5. Uncoated PEDOT:PSS quickly degrades in UV light,[11, 202] becoming 80% more resistive after 1 hour of exposure (Figure A.5(a)). The degradation of the film initially increased rapidly, but approached steady state after 10 min, after which the resistance increased linearly with time. This increase in resistance of the PEDOT:PSS is due to over-oxidation, which causes chain scission and reduces π transitions of the PEDOT.[202] The UV damage to the PEDOT was significantly reduced when the melanin multilayer film was added on top. With 30 bilayers, the longevity of the PEDOT increased by 550%. Figure A.5(b) shows the

decrease in UV damage is directly proportional to the thickness of the multilayer film. The melanin-based multilayer film itself is not conductive, but only marginally decreased the conductivity of the underlying PEDOT. These same nanocoatings could eventually be used as environmentally-friendly organic semiconductors, free radical scavengers, or anti-fouling layers.

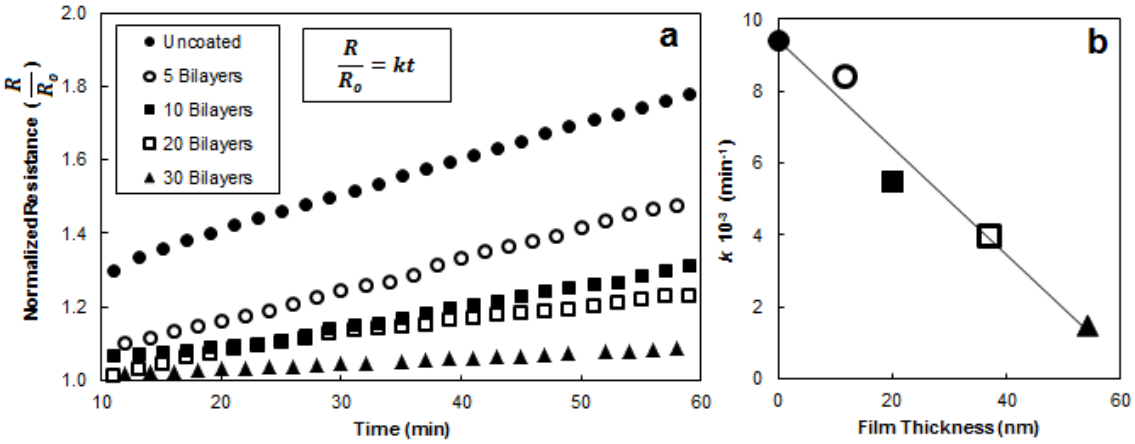

Figure A.5. (a) Resistance of spin-coated PEDOT:PSS films coated with PAH/melanin multilayer films as a function of time exposed to UV light, and (b) the associated slope of the resistance as a function of PAH/melanin multilayer film thickness.